Theses and Dissertations

August 2016

Large-Scale Urban Impervous Surfaces Estimation Through Incorporating Temporal and Spatial Information into Spectral Mixture Analysis

Wenliang Li
University of Wisconsin-Milwaukee

Recommended Citation

LARGE-SCALE URBAN IMPERVIOUS SURFACES

ESTIMATION THROUGH INCORPORATING

TEMPORAL AND SPATIAL INFORMATION

INTO SPECTRAL MIXTURE ANALYSIS

by

Wenliang Li

A Dissertation Submitted in

Partial Fulfillment of the

Requirements for the Degree of

Doctor of Philosophy

in Geography

at

The University of Wisconsin-Milwaukee

August 2016

ABSTRACT

LARGE-SCALE URBAN IMPERVIOUS SURFACES ESTIMATION THROUGH INCORPORATING TEMPORAL AND SPATIAL INFORMATION INTO SPECTRAL MIXTURE ANALYSIS

by

Wenliang Li

With rapid urbanization, impervious surfaces, a major component of urbanized areas, have increased concurrently. As a key indicator of environmental quality and urbanization intensity, an accurate estimation of impervious surfaces becomes essential. Numerous automated estimation approaches have been developed during the past decades. Among them, spectral mixture analysis (SMA) has been recognized as a powerful and widely employed technique. While SMA has proven valuable in impervious surface estimation, effects of temporal and spectral variability have not been successfully addressed. In particular, impervious surface estimation is likely to be sensitive to seasonal changes, majorly due to the shadowing effects of vegetation canopy in summer and the confusion between impervious surfaces and soil in winter. Moreover, endmember variability and multi-collinearity have adversely impacted the accurate estimation of impervious surface distribution with coarse resolution remote sensing imagery.

Therefore, the main goal of this research is to incorporate temporal and spatial information, as well as geostatistical approaches, into SMA for improving large-scale urban impervious surface estimation.

Specifically, three new approaches have been developed in this dissertation to improve the accuracy of large-scale impervious surface estimation. First, a phenology based temporal mixture analysis was developed to address seasonal sensitivity and spectral confusion issues with the multi-temporal MODIS NDVI data. Second, land use land cover information assisted temporal mixture analysis was proposed to handle the issue of endmember class variability through analyzing the spatial relationship between endmembers and surrounding environmental and socio-economic factors in support of the selection of an appropriate number and types of endmember classes. Third, a geostatistical temporal mixture analysis was developed to address endmember spectral variability by generating per-pixel spatial varied endmember spectra.

Analysis results suggest that, first, with the proposed phenology based temporal mixture analysis, a significant phenophase differences between impervious surfaces and soil can be extracted and employed in unmxing analysis, which can facilitate their discrimination and successfully address the issue of seasonal sensitivity and spectral confusion. Second, with the analyzed spatial distribution relationship between endmembers and environmental and socio-economic factors, endmember classes can be identified with clear physical meanings throughout the whole study area, which can effectively improve the unmixing analysis results. Third, the use of the spatially varying per-pixel endmember generated from the geostatistical approach can effectively consider the endmember spectra spatial variability, overcome the endmember within-class variability issue, and improve the accuracy of impervious surface estimates.

Major contributions of this research can be summarized as follows. First, instead of Landsat Thematic Mapper (TM) images, MODIS imageries with large geographic coverage and high temporal resolution have been successfully employed in this research, thus making timely and regional estimation of impervious surfaces possible. Second, this research proves that the incorporation of geographic knowledge (e.g. phonological knowledge, spatial interaction, and geostatistics) can effectively improve the spectral mixture analysis model, and therefore improve the estimation accuracy of urban impervious surfaces.

Dedicated to my parents,

my wife,

and my daughter

TABLE OF CONTENTS

LIST OF FIGURES

LIST OF TABLES

ACKNOWLEDGMENTS

My deepest thanks go to my advisor, Professor Changshan Wu, who has not only served as an excellent mentor for my academic work but also as a lifetime good friend. His expertise in remote sensing and GIS research, his generous friendly personality has influenced both my research and daily life. Without his encouragement and sincere help, I would not possible finish my Ph.D. work.

I also want to appreciate my committee members, Professor Mark Schwartz, Professor Woonsup Choi, Professor Alison Donnelly, and Professor Zengwang Xu for their valuable support to my dissertation work and my job search.

Moreover, I am also grateful to other faculty members in Geography, UW-Milwaukee who helped me during my time in UW-Milwaukee. Professor Linda McCarthy, Professor Glen Fredlund, Professor Ann Bonds, Professor Kristin Sziarto, Professor Rina Ghose, Prfessor Ryan Holifield, Professor Anna Mansson McGinty and Professor Hyejin Yoon. I would like to thank all the fellow graduate students in Geography UW-Milwaukee, Yang Song, Wei Xu, Hong Zhuo, Yingbin Deng, Haijian Liu, I-Hui Lin, Feng Pan, Yui Hashimoto, Minji Kim, So Hyung Lim, and Margaret Pettygrove.

My final thanks go to my family, my parents and parents in law, my twin brother, my wife Chang Liu, my daughter Nicole Li, and my closest friends, Rong Yu, Emma Hui Xiao, and Peng Li for their consistent support, encouragement, and invaluable friendship.

CHAPTER1 INTRODUCTION

1.1 Background

Since the second industrial revolution in the late 19th centuries, the world has experienced rapid urbanization. The percentage of people who reside in urban areas increased from 13.3% in 1900 to 29.4% in 1950, 51.6% in 2010, and it is expected to be over 67% in 2050 (United Nations 2012). Associated with the high speed of urbanization, large numbers of natural lands, such as agricultural land, forestland, and grassland, have been converted to industrial, residential, and commercial areas, which are mainly comprised by impervious surfaces. Impervious surfaces are generally defined as materials that water cannot infiltrate, and they can be found associated with two major types of land uses: building rooftops and transportation systems (e.g. roads, driveways, parking lots, and sidewalks) (Arnold and Gibbons 1996; Hu and Weng 2009; Schueler 1994).

As one of the major components of urban areas, impervious surfaces have been considered as an important index for analyzing urban growth pattern and quantifying the development of urban and suburban areas (Lu and Weng 2004; Rashed et al. 2001; Yang and Liu 2005; Yang 2006). Meanwhile, impervious surface has been widely applied in the corresponding socio-economic study areas, such as detailed population estimation, population distribution pattern analysis, and its impact on housing prices (Wu and Murray 2005; Yu and Wu 2004; Yu and Wu 2006). In addition to its role in quantifying urban extent and applications in socio-economic studies, impervious surfaces have also served as a key indicator for evaluating environmental quality. For instance, the increase of impervious surfaces influences surface and

underground water cycles, leads to the decrease of base flow, and the increase of surface runoff and flood frequency(Brabec et al. 2002; Brun and Band 2000; Weng 2001, 2007). Furthermore, the increase of impervious surfaces and corresponding surface runoff would influence surface pollutant transportation, and lead to associated water pollution (Arnold and Gibbons 1996; Gillies et al. 2003; Hurd and Civo 2004). In addition to the hydrological issues, impervious surfaces can alter local climate, and cause the corresponding urban heat island effect (Gluch et al. 2006; Imhoff et al. 2010; Yuan and Bauer 2007). Moreover, the reduction of natural habitats led by the increase of impervious surfaces can also lead to the reduction of biodiversity (Gillies et al. 2003; Goetz and Fiske 2008; Goetz et al. 2009). As the important role that urban impervious surfaces play, the accurate estimation and dynamic monitoring of impervious surfaces have become more and more important.

Numerous methods have been developed to estimate impervious surface areas at local and regional scales in past decades. Manual interpretation from air photographs is straightforward and the most accurate method. However, it is time-consuming and labor-intensive, and it is difficult to be conducted for a large geographical region. Since the launch of the first remote sensing satellite, satellite remote sensing data, with the advantages of large area coverage, regular revisit period, and multiple spectral bands, has become widely applied to monitor urban land use change and environmental quality (Bauer et al. 2004). Since then, traditional classification techniques, such as supervised and unsupervised classifications, have been applied to estimate the distribution of impervious surfaces from local to global scale. Although these approaches are straightforward, they only assign one land cover type to one pixel and ignore the spatial heterogeneity of urban areas. In reality, the spatial extent of a typical land use and land cover (LULC) type is usually smaller than the pixel size, and there may be a large

number of mixed pixels in an image due to the heterogeneity of land use combinations in urban environment. Therefore, information loss and reduced accuracy have been found associated with these hard classifications (Foody and Cox 1994). In order to address this issue, a vegetation–impervious surfaces–soil model (V-I-S) proposed by Ridd (1995) was applied to quantify the components of urban environment at the sub-pixel level with the assumption that the LULC types can be decomposed as the areal fractions of vegetation, impervious surfaces, and soil. Based on the conceptual V-I-S model, numerous automated methods have been proposed, and they can be grouped into three major types: (1) regression/decision tree (RT/DT); (2) artificial neural network (ANN); and (3) spectral mixture analysis (SMA).

DT/RT model is to construct the relationship between a dependent variable and independent variables by repeatedly splitting the data based on specific rules. ANN model is an adaptive system, which changes its structure through the learning process to model the complex relationships between input and output data. They are both considered as machine learning methods and also have been widely used for impervious surfaces estimation through constructing the empirical relationship with spatial and spectral characteristics offered by remote sensing data (Hu and Weng 2009; Lu et al. 2011; Lu and Weng 2009; Mohapatra and Wu 2010; Xian and Crane 2005; Yang et al. 2003a; Yang et al. 2003b; Yuan and Bauer 2007; Yuan et al. 2008). However, the estimation accuracy of both methods is highly dependent on the selection of the training data and test data, which is relatively subjective for the model construction and validation (Plaza et al. 2004; Somers et al. 2011). Furthermore, some ANN models, such as Multi-Layer Perceptron model, require both presence and absence data, true and false information, which make the data collection rather challenging.

Spectral mixture analysis is seen as one promising method for the estimation of impervious surfaces in recent years. It has also been applied in many fields, such as water quality assessment, climate change research, natural hazard risk assessment, vegetation mapping, etc. SMA assumes the spectra of a pixel as a linear/nonlinear combination of the spectra of comprised pure land cover types (also called endmembers), and the areal fraction of each land cover type can be examined through an inverse least squares deconvolution model. Due to the effectiveness of SMA in dealing with mixed pixels, it has been widely applied in many studies, especially for urban impervious surface estimations (Hu and Weng 2011; Lu and Weng 2006; Madhavan et al. 2001; Michishita et al. 2012; Phinn et al. 2002; Powell et al. 2007; Ward et al. 2000; Weng et al. 2009; Weng et al. 2008; Wu 2009; Wu 2004; Wu and Murray 2003).

Until now, medium resolution (e.g. Landsat TM/ETM+ and SPOT data) and high resolution (e.g. IKONOSand Quick bird) remote sensing imagery has been typically employed to estimate impervious surface distribution at the local scale (Demarchi et al. 2012; Huang and Townshend 2003; Weng and Hu 2008; Wu 2009; Wu and Murray 2003; Xu 2013; Yang et al. 2003a; Yang et al. 2003b; Yuan et al. 2005). Although relatively accurate results have been reported, these methods cannot be applied to a large geographic area due to the burdens of data acquisition, processing, and analysis (Elvidge et al. 2007; Knight and Voth 2011; Xian and Homer 2010). The other problem is associated with their low temporal resolutions. Medium- or high-resolution remote sensing imagery always has a low temporal resolution, and as a result, large-area land use land cover information can only be updated one or two times per decade. For example, the United States national land cover dataset (NLCD) is only produced once per decade by the United States Geological Survey (USGS), majorly due to the heavy burdens of data processing and low temporal resolutions of the Landsat TM/ETM+ imagery. Frequently updated

impervious surface information at the regional or global scales, however, is essential for many environmental studies, including regional and global land use land cover change modeling, impact analysis of land cover changes on water quantity and quality, and analysis of urbanization and regional climate, etc. (Sexton et al. 2013; Yang et al. 2010). Therefore, there is an urgent need of deriving fractional land cover information at an annual basis. The availability of the Moderate-resolution Imaging Spectroradiometer (MODIS) imagery made it possible for a timely estimation of impervious surface distribution over a large geographic area. With large geographic coverage and high temporal resolutions (e.g. daily), MODIS imagery can be employed for the studies at regional and global scales.

While MODIS imagery offers great potential for impervious surface estimation at a large geographic scale, there are two challenging problems. First, impervious surface estimation is likely to be sensitive to seasonal variations, majorly due to the shadowing effects of vegetation canopy in summer and the confusion between impervious surfaces and soil in winter. The other problem is associated with spectral variability and multi-collinearity of selected endmember spectra, which may also lead to unsatisfied estimation results. In summary, seasonal sensitivity and spectral variability of endmembers become the most profound error sources for impervious surface estimates, and it is essential to address these problems.

1.2 Problem Statement

The proposed research will be focusing on the issues of seasonal sensitivity and endmember spectral variability for improving the estimation accuracy of impervious surfaces.

Seasonal sensitivity refers to the variations of percent impervious surfaces area (%ISA) in

5

different seasons due to the impact of vegetation phenology including forestland, cropland, and pasture (Sung and Li 2012; Weng 2012; Weng et al. 2009; Wu and Yuan 2007). In particular, in spring, natural vegetation, such as forestland and grassland, is still at the early stage, the confusion of exposed bare soil and impervious surfaces can inevitably lead to inaccurate estimates. In fall, with degradation of forestland and grassland, the harvest of agricultural land, the exposed dry soil illustrate similar spectra with the bright impervious surfaces, the confusion between them would make impervious surfaces estimation to be less accurate (Weng et al. 2009). In winter, overestimation of impervious surfaces may also occur because of spectral confusions among bare soil, snow cover, and impervious surfaces. With the high vegetation abundance and increased spectral contrast between impervious surfaces and vegetation, the imagery in summer, therefore, becomes the preferred data source for the estimation of impervious surfaces in many studies (Lu and Weng 2006; Madhavan et al. 2001; Phinn et al. 2002; Powell et al. 2007; Ward et al. 2000; Weng et al. 2009; Weng et al. 2008; Wu 2009; Wu 2004; Wu and Murray 2003). However, since the remote sensing sensor can only reflect the upmost land cover layer, tree crowns and their shadows may obstruct underlying impervious surfaces, and thereby result in an underestimation. In conclusion, the estimation of impervious surface fractions based on a single date remote sensing data has become a challenging work.

The spectral variability of endmembers can be generally distinguished as within-class variability and between-class variability (Zhang et al. 2006). The first one refers to the relative spectral differences for a specific ground class, and the later one is associated with the spectral variations among different ground classes. In simple SMA, reflectance data has been used for the estimation of impervious surfaces. The reflectance spectra of a specific endmember may vary according to different specific conditions. For instance, soil spectra can be varied associated with

the variations of size, water content and composition in soil (Ben-Dor et al. 1999; Irons et al. 1989). Moreover, impervious surfaces illustrate much brightness variations because of the spectra differences ranging from low albedo to high albedo (Ben-Dor et al. 2001; Herold et al. 2004). In addition to the endmember within-class variability issue, the endmember between-class variability issues also bring difficulty for obtaining accurate estimation results. In particular, some pervious materials, such as bare soil, illustrate very similar spectral signatures when compared to those of impervious surfaces with the application of a single time image. Moreover, vegetation, such as forestland and agricultural land, may show rather similar reflectance spectra, majorly due to similar amount of chlorophyll content. In order to minimize the error caused by endmember spectral variability, reducing endmembers within-class variability and increasing endmembers between-class variability becomes an essential work.

In summary, the specific objectives of this proposed research include: (1) developing a temporal SMA method to address the seasonal sensitivity and spectral confusion issues associated with endmembers; (2) incorporating spatial information into SMA to identify the numbers and types of endmember combinations for mitigating spectral variability of image endmembers; (3) applying a geostatistic method in SMA to handle the endmember within-class variability issue.

1.3 Literature review

1.3.1 Seasonal sensitivity and endmember spectral variability

Due to the impact of seasonal sensitivity on impervious surface estimations, a number of studies have been carried out to find an optimal time through comparing the estimation accuracy

7

with different seasons.Wu and Yuan (2007) examined the accuracy of impervious surface estimation in April, July, October, and December in Franklin County, Ohio, U.S.A., using Landsat TM/ETM+ imagery, and found that the best estimation accuracy was achieved in the summer season (July). Weng et al. (2009) explored the seasonal impact using ASTER data in Indianapolis/Marion County, Indiana, and obtained the similar results that the fraction map examined from the summer image was more accurate than images from other seasons. In addition, he also reported that the winter image has the poorest performance due to the reduced spectral contrast among different ground classes and the high confusion between bare soil and impervious surfaces. Sung and Li (2012), however, argued that these studies were conducted in temperate regions, and for tropical and subtropical areas summer may not be the optimal season. Consequently, they conducted a comparative analysis in Austin, Texas, and found that winter imagery was with better accuracy. All the previous studies provide valuable references for selecting an optimal time for impervious surface estimation under different climates. However, their objectives were to select the best time for estimating impervious surfaces, and ignored seasonal sensitivity. In reality, no matter the summer in temperate regions or the winter in tropical areas, impervious surfaces still tend to be erroneously estimated, primarily due to the shadowing effects of vegetation canopy and spectral confusion between impervious surfaces and soil.

In addition to seasonal sensitivity issue, the spectral variability of endmembers has also been recognized as an important issue in the estimation of impervious surfaces, and several studies have been conducted for improving the estimation accuracy through reducing within-class variability or enhancing the between-class variability. One attempt was made by focusing on endmember spectral selection. Asner and Lobell (2000) introduced an autoSWIR approach to

8

highlight the variations among different land cover types through selecting the partial shortwave infrared (SWIR) spectrum region. Moreover, statistical approaches, such as principal component analysis (PCA) (Johnson et al. 1993; Miao et al. 2006), discrete cosine transform (DCT) (Li 2004), and residual analysis (Ball et al. 2007; Miao et al. 2006), have been proposed to select the best bands for spectral unmixing. Furthermore, a stable zone unmixing (SZU) technique was developed by Somers et al. (2010). In the SZU approach, the bands with the lowest within-class variation were selected according to the instability index (ISI), and were used for generating corresponding land cover fractions. Other techniques include spectral weighting, spectral transformation, and spectral transfer model. Chang and Ji (2006) developed a weighted spectral mixture analysis (WSMA) to reduce endmember variability, in which the spectral bands with the lowest endmember variability are assumed as more important, and a higher weight is assigned. WSMA has been demonstrated to perform better than the un-weighted SMA(Chang and Ji 2006). In order to upgrade WSMA, a two-step weighting SMA was developed by Somers et al. (2009) through considering the variations of the reflected energy associated with each band and endmember variability. In addition to the spectral weighting techniques, spectral transformation has also been developed for mitigating endmember variability.Wu (2004) proposed normalized spectral mixture analysis (NSMA) to reduce the within-class variation through normalizing the endmember spectra. This method was subsequently employed in geological applications (Zhang et al. 2005). In addition, a derivative spectral unmixing (DSU) was developed by Zhang et al. (2004) to highlight within-class variability along with reducing between-class variability through inputting the second-derivative endmember spectra in SMA. Although DSU is effective in solving the endmember variability issue, it also enhances high frequency noise. Thus, wavelet analysis, including the discrete wavelet and continuous wavelets techniques, has been proposed

9

(Li 2004). In the wavelet analysis, transformed spectral features, instead of original reflectance features, have been employed in SMA (Li 2004; Rivard et al. 2008). Further, soil modeling mixture analysis (SMMA) was proposed to decrease within-class moisture differences for soil (Lobell et al. 2002; Somers et al. 2009).

In addition to the aforementioned techniques for addressing endmember variability, the other approach is the trial-and-error technique, which considers all possible endmember combinations, and selects the best endmember set for each pixel. One widely applied approach is multiple endmember spectral mixture analysis (MESMA) proposed by Roberts et al. (1998). In MESMA, a spectra library with a wide range of endmember spectra is constructed, and different sets of endmember combinations, instead of a fixed endmember set in simple SMA, are allowed for each pixel. Thus, all possible endmember sets are considered and tested, and the best fit combination set is selected for each pixel. Generally, the lowest root mean square error (RMSE) is used as the selection criterion. In addition, some other selection techniques have been developed, such as the count-based approach (COB)(Roberts et al. 2003), endmember average RMSE (EAR) (Dennison and Roberts 2003), minimum average spectral angle (MASA) (Dennison et al. 2004), and Iterative endmember selection (IES) (Schaaf et al. 2011). Similar to MESMA, the endmember bundles approach proposed by Bateson and Curtiss (1996) is the other technique for mitigating endmember variability. Specifically, instead of using only one endmember spectra, a bundle of spectra for each endmember is collected and employed to construct endmember sets, and the minimum, mean, and maximum fractions for each land cover type are then extracted.

As a summary, although many studies have been conducted for addressing seasonal sensitivity and spectral variability issues, we are still facing a number of challenging problems.

10

To address these problems, temporal, spatial, and prior contextual information may be of significant help for better estimations of impervious surfaces.

1.3.2 Incorporating temporal information into SMA

Instead of using single-date imagery, MODIS NDVI data, with multi-temporal series and phenological information, may provide the potential to address the aforementioned issues. With two-year and four-year MODIS NDVI imagery, Knight and Voth (2011) developed temporal mixture analysis (TMA) approaches and found TMA with the two-year NDVI series performed better when compared to the four-year TMA and a sequential maximum angle convex cone approach. This attempt provides a new means for impervious surface estimation. However, with only two endmembers, impervious surfaces and deciduous forest, the resultant impervious surface estimates were with relatively low accuracy. Yang et al. (2012) applied multi-temporal imagery to examine impervious surfaces fractions in Japan, and conducted a comparative analysis with other SMA approaches. They found that the multi-temporal SMA technique performs the best. However, instead of using the one-year time-series data with integral phenological information, only six NDVI bands with the highest values were extracted as endmember spectra for SMA. As a result, although with multi-temporal NDVI imagery, only summer images were employed for SMA. Therefore, although a number of studies have been conducted to address the impact of seasonal sensitivity on impervious surface estimation, they have not been able to take advantage of phenological information derived from MODIS NDVI imagery, and more research in incorporating temporal information into SMA is needed.

1.3.3 Incorporating spatial information into SMA

The lack of using spatial information may be the other issue for the estimation of impervious surfaces. Although spatial information may have significant impact on mitigating endmember variability, it has rarely been considered. One exception is the work of Maselli (2001), who incorporated environmental factors in addressing spatial spectral variability using MODIS NDVI data. However, instead of using specific environmental factors, only NDVI has been considered as the important factor for reflecting the impact of environmental factors on vegetation. Actually, numerous environmental factors, such as elevation, slope, climate, water availability, etc. may have significant impact on the vegetation phonology, and they cannot be simply replaced by NDVI. Moreover, conventional multivariate regression analysis has been employed for examining the vegetation fractions. Although it is highly efficient and easily to be implemented, its ability of handling spectral mixing problems is questionable, and may lead to degraded estimation results. Therefore, how to incorporate spatial information into SMA becomes an important topic.

One attempt to incorporate spatial information into SMA was conducted in the endmember selection process. Instead of considering each pixel as independent of other pixels, the spatial relationships between the target pixel and its corresponding neighboring pixels have been examined by Roessner et al. (2001) for reducing the number of possibilities of endmember combination for each pixel. In addition, Plaza et al. (2002) took advantage of the mathematical morphology to develop an automated morphological endmember extraction approach, in which a set of spatial/spectral operations have been employed to extract endmember spectra. Furthermore, the spatial-spectral endmember extraction tool (SSEE) has been proposed by Rogge et al. (2007), with which the spatial characteristics were used to increase the spectral contrast and select endmembers with low contrast. Further, spatial constraints have been imposed to make the

12

selected endmembers to be more representative throughout the entire image. Moreover, Zortea and Plaza (2009) developed a novel approach to integrate the spatial and spectral information for the endmember extraction with the consideration of spectral similarity between target pixel and neighborhood pixels. The other attempt was made by Deng and Wu (In press)through developing a spatially adaptive spectral mixture analysis (SASMA) for improving the estimation accuracy. In SASMA, local spatial information has been incoporated into SMA to overcome the endmember variability problem for examining subpixel impervious surfaces fractions. In particular, spatial dependence, in which the spectral similarity is highly associated with the distance among pixels, has been considered as key point for local endmember selection, and spatially adaptive endmembers were extracted for spectral unmixing.

Although all proposed approaches have proven helpful for improving estimation accuracy, only the spatial correlation among neighborhood pixels and local spatial information have been considered. The impact of global spatial information such as relationships among ground land use land cover classes and corresponding environmental, social-economic factors and their impacts on endmembers variability have been ignored. Such information, however, may play an important role in quantifying the spatial distribution of endmembers and identifying the numbers and types of endmember combinations, and provides valuable information for addressing endmember variability.

1.3.4 Applying a geostatistic method in SMA

As discussed earlier, endmembers tend to illustrate spatial variability, majorly due to the impact of local environmental and socio-economic factors (e.g. topography, climate, economic

13

development, population density, etc.). However, in most studies, derived endmember spectra are often considered identical and applied to all the pixels in a remote sensing image. Therefore, endmember variability has become a profound error source and may severely affect the performance of an SMA model.

To derive spatially varying per-pixel endmember sets, MESMA is a major approach that employing a variety of endmember set combinations, and the one with the lowest error (e.g. RMSE) is chosen for spectral unmixing. Although widely applied, MESMA only employs pixel-based spectral information, and may be considered computational expensive. Recently, the SASMA proposed by Deng and Wu (2013) attempted to address endmember variability through deriving endmembers for a particular pixel through applying an inverse distance weighting (IDW) approach using all endmember candidates in a moving window. This approach, however, only employs the distance for generating weights, and the statistical meanings of the spatial variations of endmembers have been neglected. As a consequence, inappropriate endmembers may be selected and applied in SMA and result in erroneous estimations. As the powerful ability for generating localized information, the geostatistical technique may provide great support for handling the endmember variability issue. In particular, the ordinary kriging, a non-biased interpolation technique, can interpolate the value of a function at a given point by computing a weighted average of the known values of the function in the neighborhood of the point. In this case, per-pixel level endmember spectra can be generated and used in unmixing analysis for overcoming the endmember within-class variability.

CHAPTER2 PHENOLOGY BASED TEMPORAL MIXTURE ANALYSIS FOR ESTIMATING LARGE-SCALE IMPERVIOUS SURFACE DISTRIBUTIONS[1]

2.1 Introduction

Although urbanized areas only occupy a small proportion (3%) of the Earth's land surface (Grubler 1994), they constitute more than half of the world's population and are centres of political, economic, socio-cultural, scientific, and technological activity. Urban areas also provide high quality of life experiences, including education and employment opportunities, medical services, public transportation, sanitation, and social services (Wu 2010; Wu et al. 2011). Rapid urbanization, however, leads to challenging environmental and socio-economic problems on both local and global scales, such as alteration of local climate, reduction of biodiversity, increased soil erosion, degraded water quality, traffic congestion, public health deterioration, and resource depletion (Guttikunda et al. 2003; Lin and Ho 2003; Newman and Kenworthy 1999; Pauleit and Duhme 2000; Pielke 2005; Stevens, Dragicevic, and Rothley 2007; Van Metre and Mahler 2005; Zang et al. 2011; Zhou et al. 2004). Along with rapid urbanizsation, the prevalence of impervious surfaces, defined as materials that water cannot infiltrate (e.g., parking lots, building roofs, sidewalks), has increased concurrently. As one of the major biophysical compositions of urban areas, impervious surface area has been widely adopted as a key indicator of urbanization intensity and urban environmental quality (Arnold and Gibbons 1996; Jantz, Goetz, and Shelley 2004; Xian and Crane 2005). Due to the critical role of urban impervious

---

surfaces, knowledge of their quantity and spatial distribution is essential for urban planning and environmental management.

Numerous methods have been developed to estimate impervious surface area on local and regional scales. Manual interpretation from aerial photos is straightforward and the most accurate method. However, this manual approach is time-consuming and labour-intensive, which prevents its application to large geographical regions. Therefore, satellite remote-sensing techniques have been developed to map impervious surface areas due to their ability to cover large geographical areas, regular revisits,and improved spectral resolution (Bauer et al. 2004). With the availability of satellite remote sensing imagery at different spatial resolutions, unsupervised (e.g., ISODATA) and supervised (e.g., maximum likelihood, artificial neural network, classification tree) classification methods have been used to estimate impervious surface distributions from local to global scales. Although these approaches have been widely applied with some success, they neglect the spatial heterogeneity of urban areas, assigning only one land cover type to each pixel. Therefore, information loss and reduced accuracy are associated with these hard classifications (Foody and Cox 1994). To address these issues, sub-pixel analysis methods have been developed over the past several decades, including regression modelling, spectral mixture analysis (SMA), artificial neural networks (ANNs), regression trees (RTs), and random forests (RFs) (Bauer et al. 2004; Lee and Lathrop 2006; Lu and Weng 2004; Wu 2004; Wu and Murray 2003; Yuan, Wu, and Bauer 2008). Among these methods, SMA has been particularly widely employed, as it provides a physical-based means to addressing mixed pixels(Lu and Weng 2006; Madhavan et al. 2001; Phinn et al. 2002; Powell et al. 2007; Ward, Phinn, and Murray 2000; Weng and Hu 2008; Weng, Hu, and Liu 2009; Wu and Murray 2003; Wu 2004; Wu 2009; Yang et al. 2009). A number of studies have been conducted to improve the accuracy of impervious surface

estimation based on SMA. Wu and Murray (2003) developed a four-endmember SMA, with which the percent impervious surface area was derived as the summation of the percent of low- and high-albedo materials. Wu (2004)proposed normalized spectral mixture analysis (NSMA) to address the brightness variation and shade issues for the impervious surface estimation. In addition, Roberts et al. (1998) and Powell et al. (2007) presented multiple endmember spectral mixture analysis (MESMA) to improve the estimation accuracy in a complex urban environment by considering variations at the pixel level and allowing different sets of endmember combinations for each pixel (Powell et al. 2007). Yang, Matsushita, and Fukushima (2010) developed a pre-screened and normalized multiple endmember spectral mixture analysis (PNMESMA) by incorporating NSMA into MESMA, resulting in higher accuracy.

Until now, medium-resolution (e.g., Landsat TM/ETM+ and SPOT data) and high-resolution (e.g., IKONOS and Quick Bird) remote sensing imagery has been typically applied to estimate impervious surface distribution on a local scale (e.g., a city)(Huang and Townshend 2003; Weng and Hu 2008; Wu and Murray 2003; Wu 2009; Yang, Huang, et al. 2003; Yang, Xian, et al. 2003; Yuan et al. 2005; Goodwin, Coops, and Stone 2005; Demarchi et al. 2012). Although reasonably accurate results have been reported, these methods cannot be applied to a large geographic area due to the burdens of data acquisition, processing, and analysis (Elvidge et al. 2007; Xian and Homer 2010; Knight and Voth 2011). Additionally, these methods suffer from low temporal resolutions. Medium- or high-resolution remote sensing imagery has a low temporal resolution, and as a result, large-area land use or land cover information can only be updated infrequently. For example, the United States National Land Cover Dataset (NLCD) is only produced once per decade by the United States Geological Survey (USGS), mostly due to the heavy burden of data processing and the low temporal resolutions of high quality Landsat

TM/ETM+ imagery due to weather conditions such as could cover and atmospheric effects. Frequently updated impervious surface information at regional or global scales, however, is required for many environmental studies, such as regional and global land use/land cover change modelling, impact analysis of land cover changes on water quantity and quality, and analysis of urbanisation and regional climate (Sexton et al. 2013). The availability of Moderate-Resolution Imaging Spectroradiometer (MODIS) imagery enables the timely estimation of impervious surface distribution over a large geographic area. With a coarse spatial resolution (e.g., 250 m, 500 m, and 1000 m) but a high temporal resolution (e.g., daily), MODIS imagery can be employed for studies on regional and global scales.

Although applying SMA to MODIS imagery provides great potential for large-scale impervious surface estimation, some problems remain. In particular, impervious surface estimation is likely to be sensitive to seasonal changes, mostly due to the shadowing effects of vegetation canopy in summer and confusion between impervious surfaces and soil in winter. In summer, tree crowns and their shadows may obstruct underlying impervious surfaces, resulting in an underestimation. In winter, inaccurate estimation of impervious surfaces may occur because of spectral confusion among bare soil, snow cover, and impervious surfaces. Wu and Yuan (2007) examined the accuracy of impervious surface estimation in April, July, October, and December in Franklin County, Ohio, U.S.A. using Landsat TM/ETM+ imagery and found that the best estimation accuracy was achieved in the summer (July). Weng, Hu, and Liu (2009) explored the seasonal impact using ASTER data in Indianapolis/Marion County, Indiana, U.S.A. and obtained similar results. Sung and Li (2012), however, noted that these studies were conducted in temperate regions and argued that summer may not be the optimal season for tropical and subtropical areas. Consequently, they conducted a comparative analysis in Austin,

18

Texas, U.S.A. and found that winter imagery yielded better accuracy. All previous studies provide valuable references for selecting an optimal time for impervious surface estimation under different climates. However, their objectives were to select the best time for estimating impervious surfaces, ignoring seasonal sensitivity. In reality, even if summer data are used in temperate regions and winter data are used in tropical areas, impervious surfaces still tend to be erroneously estimated, primarily due to the shadowing effects of vegetation canopy and spectral confusion between impervious surfaces and soil.

Instead of using single-date imagery, the use of MODIS NDVI data, with multi-temporal series and phenological information, may be best suited to address the aforementioned issues. Using two-year and four-year MODIS NDVI imagery, Knight and Voth (2011) developed temporal mixture analysis (TMA) approaches and found that TMA with the two-year NDVI series performed better than the four-year TMA and a sequential maximum angle convex cone approach. This result provides a new means for impervious surface estimation. However, with only two endmembers, impervious surfaces and deciduous forest, the resultant impervious surface estimates had low accuracy. Yang et al. (2012) applied multi-temporal imagery to examine impervious surface fractions in Japan and conducted a comparative analysis with other SMA approaches. They found that the multi-temporal SMA technique performs best. However, instead of using the one-year time-series data with integral phenological information, only six NDVI bands with the highest values were extracted as endmember spectra for SMA. As a result, only summer images were employed for SMA, despite the use of multi-temporal NDVI imagery. Therefore, although a number of studies have been conducted to address the impact of seasonal sensitivity on impervious surface estimation, the phenological information derived from MODIS

19

NDVI imagery has yet to be taken advantage of, and further efforts to incorporate temporal information into SMA are warranted.

In this study, we proposed phenology-based temporal mixture analysis (PTMA) and phenology-based multi-endmember temporal mixture analysis (PMETMA) to address the challenges associated with seasonal sensitivity and spectral confusion. Additionally, the performances of these two phenology-based methods were compared with those of TMA methods applied to summer and winter seasons. This chapter is organized as follows: Section 2.2 introduces the study area and data sources. Section 2.3 develops the PTMA and PMETMA methods for impervious surface estimation. Comparative analyses of PTMA, PMETMA, Summer TMA, and Winter TMA are reported in Section 2.4. Finally, a discussion and conclusions are provided in Sections 2.5 and 2.6, respectively.

2.2 Study area and data

The State of Wisconsin, U.S.A. was chosen as the study area in this research. Wisconsin is situated in the north-central part of the United States and along the west side of Lake Michigan, with latitudes between $42°37'$ and $47°05'$ N and longitudes between $86°46'$ and $92°53'$ W (see Figure1). It has a geographical area of 169,639 km^2, covering 72 counties. Almost 68% of the population of Wisconsin resides in urban areas, including Madison (the state capital), Green Bay, and Milwaukee (the most populated city). Wisconsin has experienced rapid population growth and urbanisation over the past several decades. The population of Wisconsin increased from 4.89 million in 1990 to 5.71 million in 2011, an increase of approximately 16%, and this trend is likely to continue in the near future. This rapid urbanization has caused a number of challenging issues, including environmental pollution and traffic congestion.

Therefore, an accurate and timely estimation of impervious surfaces in Wisconsin is essential.
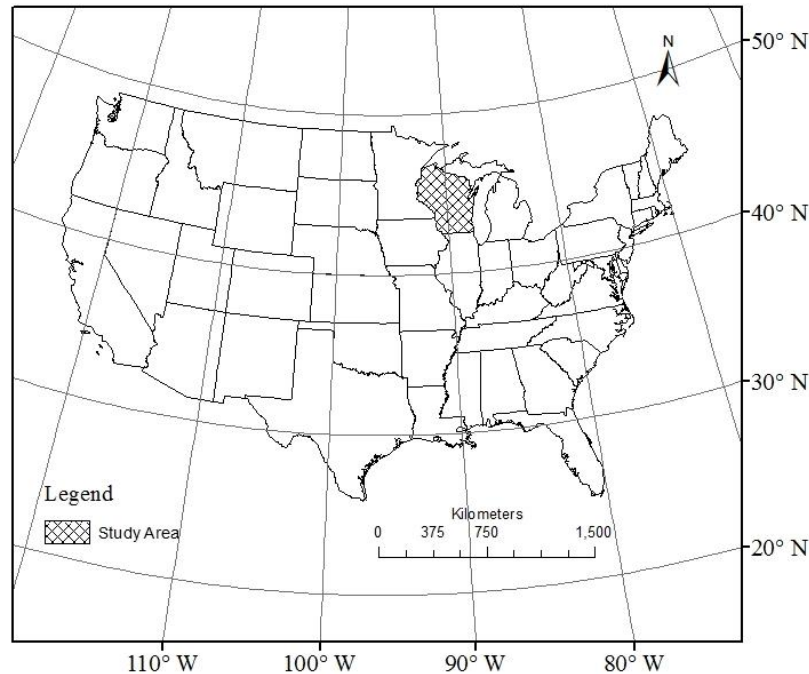
Figure 1Study area: the State of Wisconsin, U.S.A.

In this study, MODIS NDVI images in 2006 (product of MOD13Q1, 2 images per month), with 250-m spatial resolution and 0.5-pixel positional accuracy were obtained from the United States Geographical Survey (USGS) website (www.usgs.gov). Further, the EVI standardized anomaly evaluation method developed by Samanta et al. (2012) was applied to detect MODIS NDVI anomalies. As a result, the early November image was identified and removed from further analysis due to heavy cloud cover and suboptimal quality, and the NDVI time-series image with 22 bands (except the one in early November) were employed for estimating large-scale impervious surface abundance. These images were stacked together to construct a single image with 22 layers using ERDAS Imagine 9.3 software. Additionally, the National Land Cover Data (NLCD) 2006 Percent Developed Imperviousness data were obtained

from the Multi-Resolution Land Characteristics Consortium (MRLC) website (http://www.mrlc.gov/nlcd06_data.php) and employed as the reference data for accuracy assessment. NLCD 2006 data was derived using Landsat ETM+ and TM imagery acquired from 02/11/2005 to 10/03/2007 (Fry et al. 2012). Although the imagery acquisition dates do not match perfectly with those of the MODIS data, we assume that no significant changes have taken place in Wisconsin during this two-year period, and therefore NLCD 2006 data can serve as reference information for accuracy assessment.

2.3 Methodology

2.3.1 Phenology-based temporal mixture analysis (PTMA)

To address seasonal sensitivity and spectral confusion issues, we developed a phenology-based temporal mixture analysis (PTMA) method using multi-temporal NDVI data with integral phenological information for deriving impervious surfaces fractions. In particular, two steps were carried out, 1) endmember selection and 2) fully constrained linear spectral unmixing, to derive impervious surface abundance information. For multi-temporal MODIS NDVI data, endmember selection is the first and most important step. To reduce noise whitening and guide image endmember selection, maximum noise fraction (MNF) transformation (Green et al. 1988) was applied. MNF transformation orders components according to signal-to-noise ratios (SNRs), with the majority of spectral information provided by the first several components. In this study, the first three MNF components (see Figure 2) were employed to identify the endmember type, number, and spectra. Through careful visual examination, we identified five endmembers, including impervious surfaces, agriculture (soil), pasture, evergreen forest, and deciduous forest,

22

and the NDVI spectra of these endmembers are shown in Figure 3. For agricultural lands, bare soil is usually exposed in fall and winter (with low NDVI values) and occupied by green vegetation (e.g. crops) in spring and summer (with high NDVI values). These endmember spectra illustrate representative phenological signatures with different phenophases (including dormancy, green up, maturity, and senescence). Specifically, evergreen forest only experiences the maturity phenophase, with relatively high NDVI values for the entire year. Agricultural land (soil), deciduous forest, and pasture experience integral phenophases with different timing, including dormancy with low NDVI values in winter, green up with increasing NDVI values in spring, maturity with high NDVI values in summer, and senescence with decreasing NDVI values in fall. Impervious surfaces only experience dormancy, with low NDVI values throughout the whole year. These significantly varied phenological signatures were used as endmember spectra for impervious surface estimations.

With the selected endmember signatures, a fully constrained linear spectral unmixing was conducted, with which the NDVI spectra of a mixed pixel can be linearly modelled by the NDVI spectra of all identified endmembers and the areal fractions of each land cover type can be derived accordingly. The formulation of the fully constrained linear spectral unmixing is as follows:

$$NDVI_b = \sum_{i=1}^{N} f_i \times NDVI_{i,b} + e_b \tag{2.1}$$

$$\sum_{i=1}^{N} f_i = 1 \tag{2.2}$$

$$f_i \geq 0 \tag{2.3}$$

where $NDVI_b$ is the value of NDVI for each band b in the MODIS NDVI image, N is the number of endmembers, f_i is the estimated fraction for endmember i, $NDVI_{i,b}$ is the NDVI value of

endmember *i* in band *b*, and e_b is the residual. The model fitness can be assessed using the root mean square error (RMSE) (see equation 2.4):

$$RMS = \left(\frac{\sum_{b=1}^{M} e_b^2}{M}\right)^{1/2}$$

(2.4)

where *M* is the number of bands in the remote sensing image.
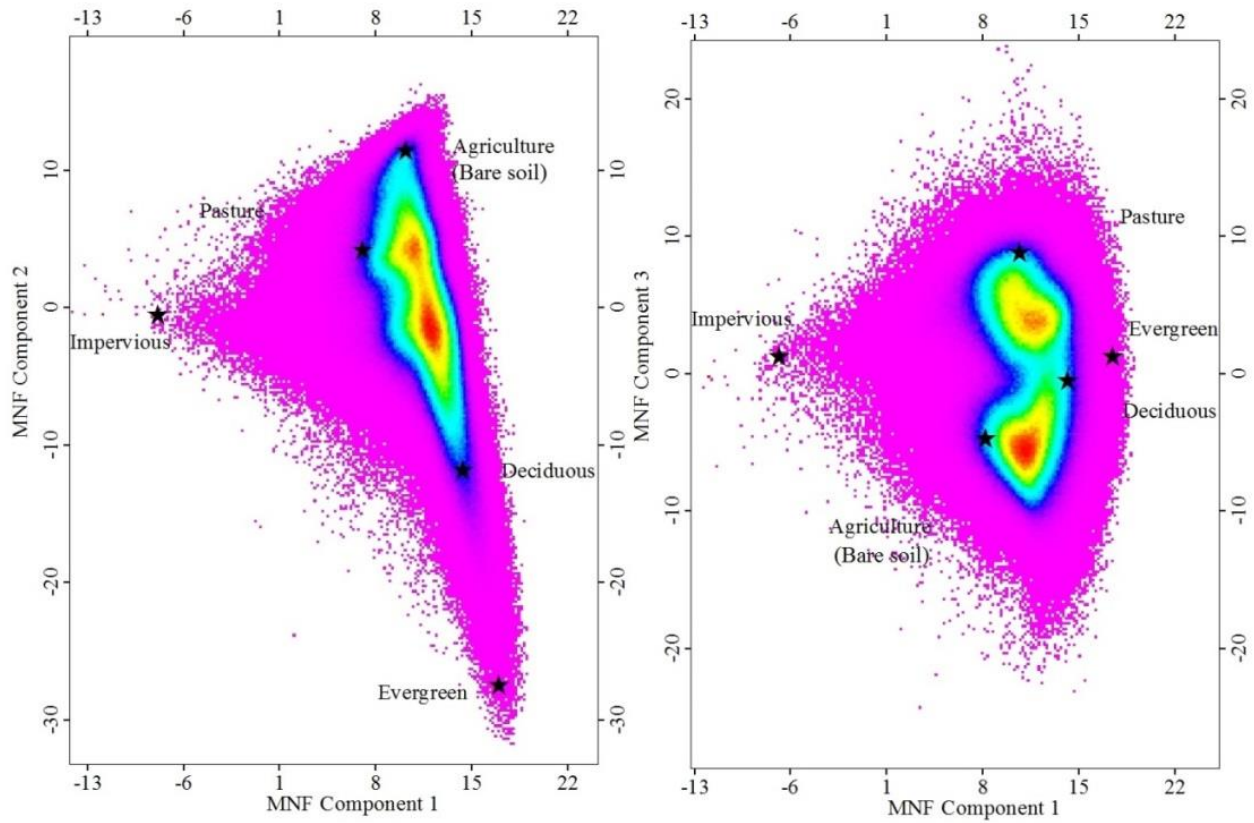
Figure 2 Two-dimensional feature space plots using the first three MNF components
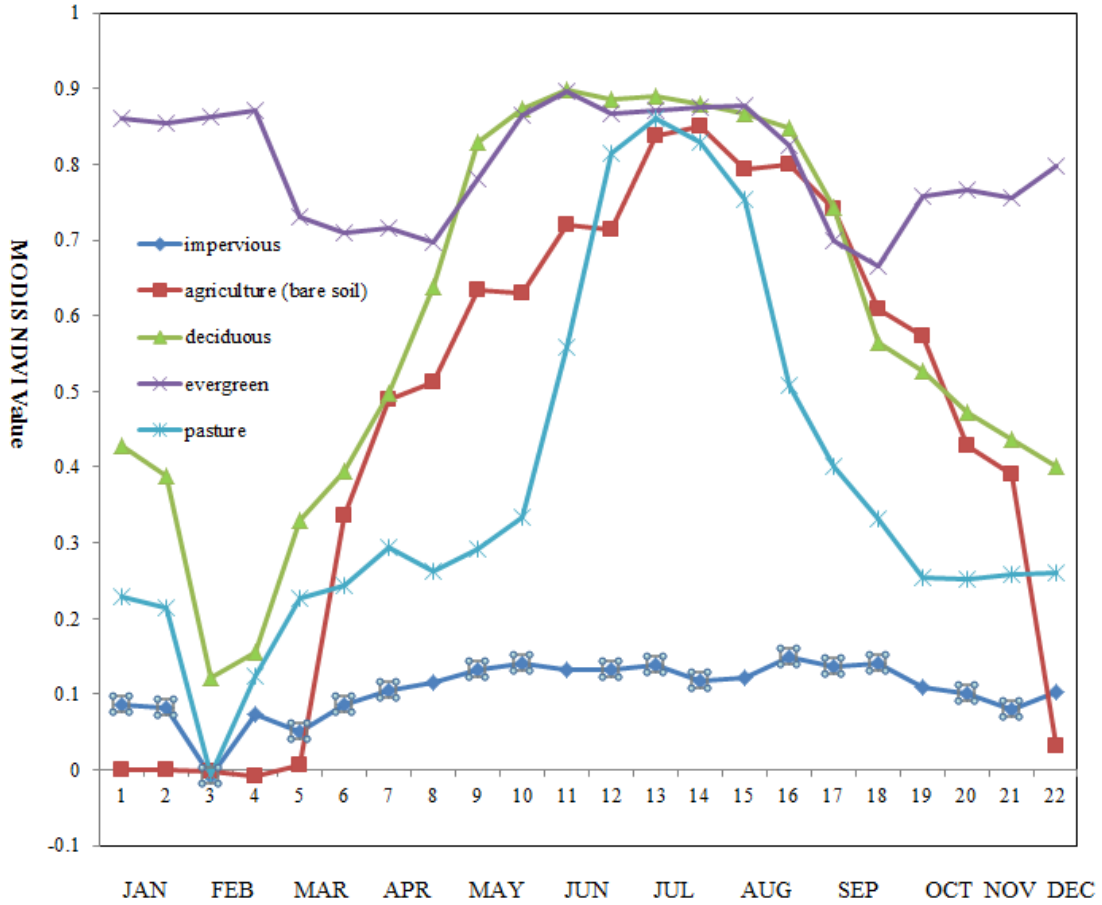
Figure 3 Endmember NDVI spectra of impervious surfaces, agriculture (bare soil), deciduous forest, evergreen forest, and pasture

2.3.2 Phenology-based multiple-endmember temporal mixture analysis (PMETMA)

PTMA only employs a fixed set of endmembers and does not consider the variability of endmember type and number or their within-class spectral variations (Pu et al. 2008). Therefore, in addition to PTMA, we also developed phenology-based multiple-endmember temporal mixture analysis (PMETMA) to mitigate the issues associated with endmember variability. PMETMA allows the use of different sets of endmember combinations for each pixel. It tests all corresponding combination models and selects the one with the best fit. As a result, it effectively reduces the estimation error (Demarchi et al. 2012; Franke et al. 2009; Rosso, Ustin, and

Hastings 2005). In this study, the bundles endmember selection approach was employed to reduce within-class endmember variability, and for each bundle, five endmembers were selected from the vertices of the 2-D scatter plot (see Figure 4).
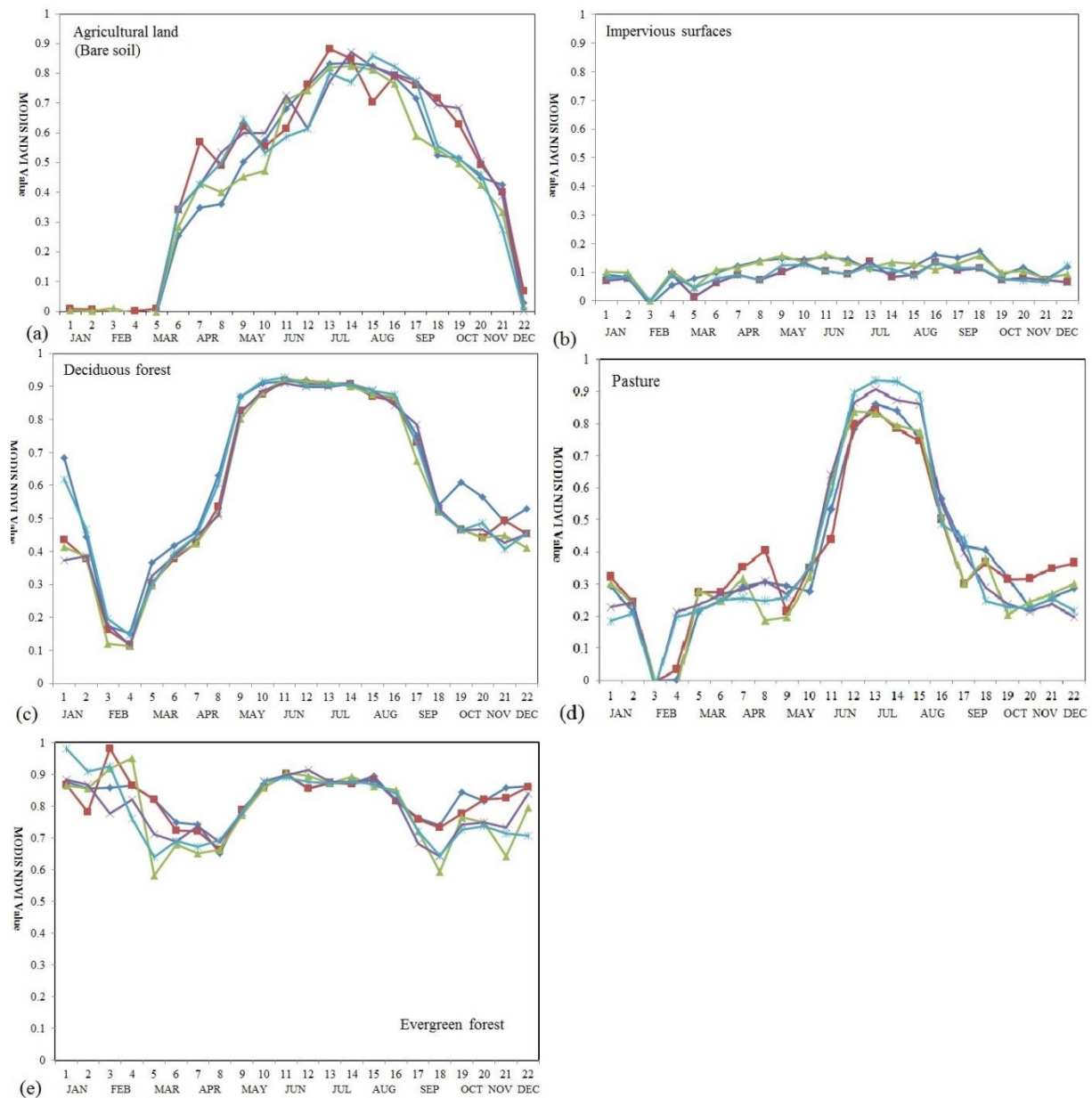
Figure 4 Endmember bundle spectra of (a) Agricultural land (bare soil), (b) Impervious surfaces, (c) Deciduous forest, (d) Pasture, and (e) Evergreen forest

With PMETMA, RMSE cannot be employed as the single criterion for examining model fitness, as lower RMSE values are likely to be achieved with a larger number of endmembers. To address this problem, the threshold INCR$_{rel}$ developed by Demarchi et al. (2012)was employed to select the model with the best performance. INCR$_{rel}$ is calculated based on the change in RMSE, giving preference to a model that employs a lower number of endmembers. The lowest RMSE was selected from the 2-EM, 3-EM, 4-EM, and 5-EM model sets, and the increase in RMSE from the 5-EM model to the 4-EM model, the 4-EM model to the 3-EM model, and the 3-EM to the 2-EM model set can be calculated as follows:

$$INCR_{rel} = \frac{RMS_{(n-EM)} - RMS_{(n+1-EM)}}{RMS_{(n+1-EM)}} \tag{2.5}$$

Where n is the total number of endmembers in each combination model set, RMS$_{(n-EM)}$ is the lowest RMSE from all n-EM combination model sets, and RMS$_{(n+1-EM)}$ is the lowest RMSE from all n+1-EM combination model sets. The n-EM combination model set is chosen as the best fit model set for spectral unmixing if the INCR$_{rel}$ value is higher than the threshold value; otherwise, the n+1-EM model set will be selected. In this study, an empirical threshold of 90% was chosen based on guidance provided by Demarchi et al. (2012).

2.3.3 Temporal mixture analysis with summer and winter imagery

In addition to the proposed PTMA and PMETMA techniques, we also developed two other TMA methods with multi-temporal NDVI imagery for the summer and winter seasons for comparative purposes. In Summer TMA, proposed by Yang et al. (2012), the NDVI values were rearranged, and six maximum NDVI time-series values were selected for extracting impervious

surfaces fractions. Similarly, Winter TMA was developed by applying the six lowest NDVI time-series values. These two TMA methods were developed to examine the seasonal differences of impervious surface estimations.

2.3.4 Accuracy assessment

Using the fractional impervious surface estimates obtained via the aforementioned models, PTMA, PMETMA, Summer TMA, and Winter TMA, we conducted accuracy assessment through a pixel-by-pixel comparison with the National Land Cover Data (NLCD) 2006 Percent Developed Imperviousness data. Three indices were utilised to evaluate the accuracy for the impervious surface estimation results: the root mean square error (RMSE, Equation 2.6), systematic error (SE, Equation 2.7), and mean average error (MAE, Equation 2.8).

$$RMSE = \sqrt{\frac{\sum_{i=1}^{N}(\hat{I}_i - I_i)^2}{N}} \tag{2.6}$$

$$SE = \frac{\sum_{i=1}^{N}(\hat{I}_i - I_i)}{N} \tag{2.7}$$

$$MAE = \frac{\sum_{i=1}^{N}|I_i - \hat{I}_i|}{N} \tag{2.8}$$

Where $\hat{I}_i$ is the estimated impervious surface fraction value for pixel i, I_i is the reference impervious surface fraction value for pixel i, and N is the total number of pixels. Specifically, *RMSE* and *MAE* quantify relative estimation errors of impervious surface fractions for the whole study area, and *SE* reflects the estimation bias (over- or underestimation).

2.4 Results

2.4.1 Phenology-based methods

The two developed phenology-based temporal mixture analysis methods, PTMA and PMETMA were used to derive the resultant impervious surface maps, as illustrated in Figures5a and 5b. A similar impervious surface distribution pattern is obtained using these two methods. Specifically, reasonably high impervious surface fractions can be found in major metropolitan areas, including Milwaukee (the most populated city), Madison (the state capital), and Green Bay. Furthermore, medium-sized cities, such as La Crosse and Stevens Point, feature lower fractions of impervious surfaces. Finally, the majority of Wisconsin, especially northwest Wisconsin, has very low fractions of impervious surfaces, as these areas are mostly covered by forest and grassland.

In addition to the visual examination, we also performed a quantitative analysis of the estimation accuracy for the whole study area, developed areas (%ISA of at least 30%), and less developed areas (%ISA of less than 30%). The 30% of %ISA threshold is selected based on the definition of developed lands of the NLCD (http://www.epa.gov/mrlc/definitions.html). Three accuracy measures, RMSE, SE, and MAE, were calculated accordingly (see Table 1).The results show that, in general, the performances of these phenology-based TMA methods are satisfactory, with an RMSE of approximately 7-8%, SE of 2-4%, and MAE of 3-4%. Both models performed much better in less developed areas (an MAE of 3-4%) than developed areas (an MAE of 12%). Moreover, they tend to overestimate impervious surface fractions in less developed regions (2%-4%), and underestimate impervious surface fractions in developed regions (-7% to -9%). In addition to the above comparisons, a scatterplot was generated to illustrate the relationship

between the estimated and "true" impervious surface fractions using 120 stratified randomly selected samples (see Figure 6). Visual examination of Figure 6 indicates that PTMA and PMETMA provide comparable and satisfactory performances, with slopes close to one (e.g., 0.7488 and 0.7775) and intersects near zero (0.0491 and 0.0402). Moreover, fairly high values of R^2 were achieved (0.7623 for PTMA and 0.7587 for PMETMA).

Although the performances of PTMA and PMETMA are comparable, there are some small differences. PMETMA performs much better in less-developed regions, with a lower MAE value (3.23% versus 3.90%) but a slightly higher RMSE value (7.51% versus 7.07%). In addition, the estimation bias of PMETMA is lower than that of PTMA, with an SE of 2.13% (versus 3.25%) for the entire study area, -7.46% (versus -8.17%) for developed areas, and 2.32% (versus 3.43%) for less-developed areas. These results indicate that the estimation errors caused by endmember variability are somewhat reduced with PMETMA, especially for less-developed regions.
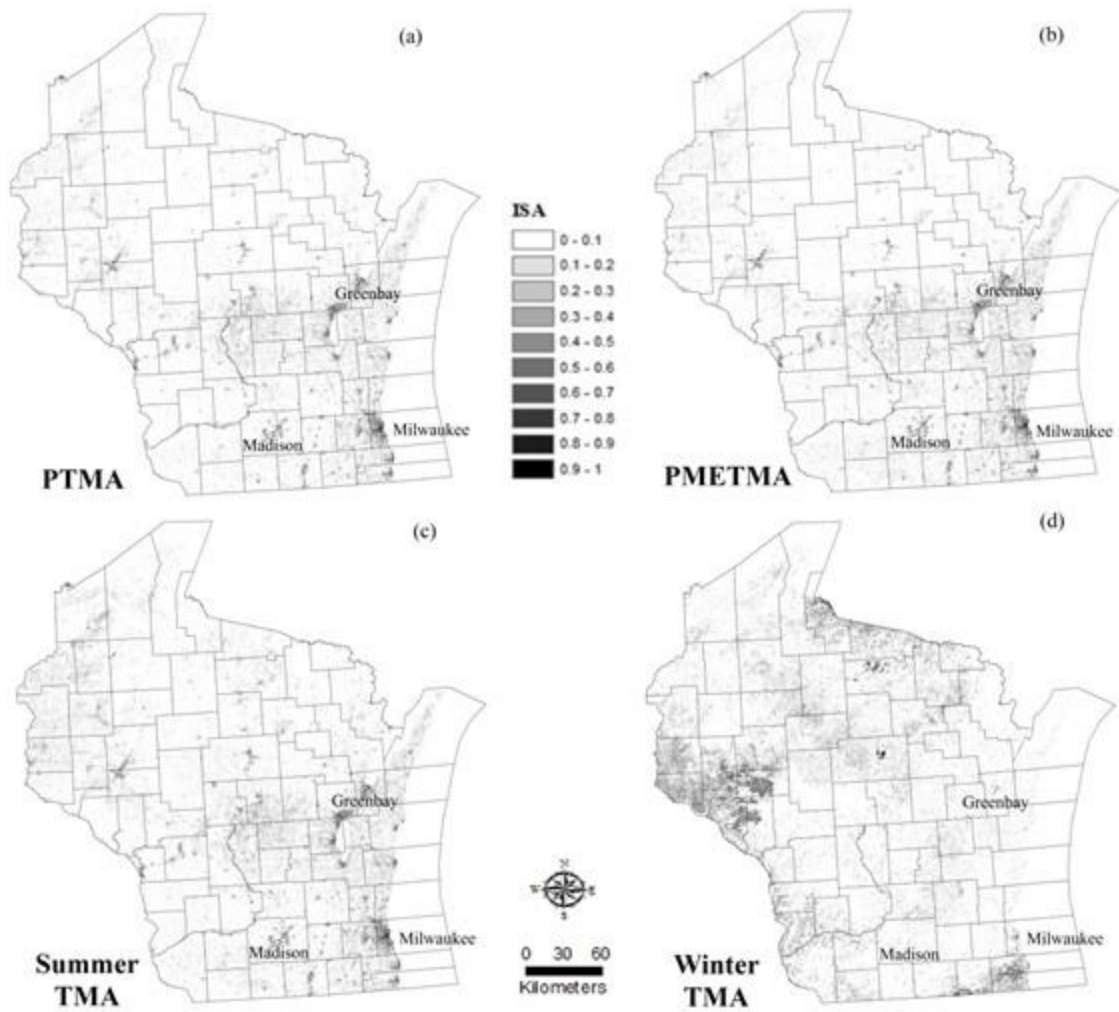
Figure 5 Impervious surface fraction maps generated from (a) PTMA, (b) PMETMA, (c) Summer TMA, and (d) Winter TMA

Table 1 Accuracy assessment of impervious surface estimation with PTMA, PMETMA, Summer TMA, and Winter TMA

		RMSE	SE	MAE
PTMA	Overall	7.27	3.25	4.03
	Developed	15.41	-8.17	12.15
	Less developed	7.07	3.43	3.90
PMETMA	Overall	7.54	2.13	3.36
	Developed	15.62	-7.46	12.16
	Less developed	7.51	2.32	3.23
Summer TMA	Overall	10.01	4.91	6.16
	Developed	14.52	-5.69	11.13
	Less developed	8.62	5.08	5.40
Winter TMA	Overall	15.52	4.98	7.56
	Developed	39.25	-35.27	36.45
	Less developed	13.96	5.62	6.94
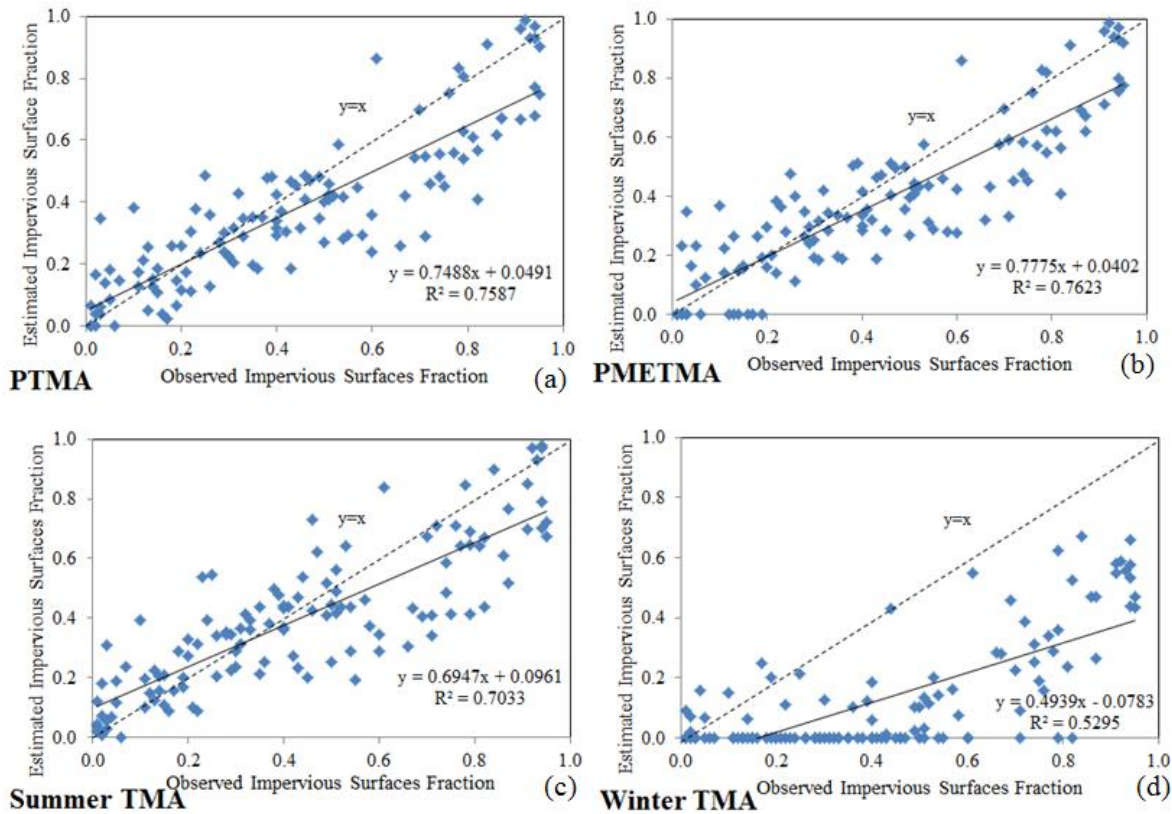
Figure 6 Accuracy assessment of the impervious surface estimation by (a) PTMA, (b) PMETMA, (c) Summer TMA, and (d) Winter TMA

.

2.4.2 Summer TMA and Winter TMA

For comparison, Summer TMA (Yang et al. 2012)and Winter TMA were implemented, and the results are reported in Figures 5 and 6 and Table 1. As illustrated in Figure 5c and Table 1, Summer TMA's overall performance is worse than that of the phenology-based TMA models, with much higher RMSE (10.01%), SE (4.91%), and MAE (6.16%). In particular, obvious overestimations can be found in less-developed areas, as indicated by the relatively high values of SE (5.08%), RMSE (8.62%), and MAE (5.40%). For developed regions, however, Summer TMA performed slightly better than the phenology-based models. Specifically, the underestimation of impervious surface areas is less severe, with an SE of -5.69%, when compared to PTMA (-8.17%) and PMETMA (-7.46%). Moreover, a comparable but slightly worse accuracy can also be observed between the estimated and the "true" impervious surface fractions (Figure 6c). These results indicate that Summer TMA is an effective alternative for estimating impervious surface areas.

In contrast, the performance of Winter TMA is significantly worse than that of the other three TMA methods. In particular, there is an obvious underestimation in developed regions (SE = -35.27%) and overestimation in less-developed areas (SE=5.62%), and the resultant impervious surface map (Figure 5d) is unacceptable. This conclusion can also be reached by reviewing the scatterplot of the estimated and the "true" impervious surface fractions (Figure 6d). The poor performance of Winter TMA is not unexpected, as significant confusion exists between bare soil and impervious surfaces with only winter NDVI series. The implementation of Winter TMA is only for comparison purposes, and it should not be applied to estimate impervious surfaces for Wisconsin.

2.5 Discussion

Seasonal variations of vegetation and spectral confusion between impervious surfaces and bare soil may prohibit an accurate estimation of impervious surface abundance at the regional or national scales (Sung and Li 2012; Weng 2012; Weng, Hu, and Liu 2009; Wu and Yuan 2007). When using remote sensing imagery for a single season, impervious surface abundance information may be sensitive to seasonal variations and therefore tends to be erroneously estimated. In particular, impervious surfaces may be obstructed by tree canopy in summer and frequently confused with soil in winter. The developed phenology-based methods, PTMA and PMETMA, partially address the seasonal variability problem by adopting one-year multi-temporal NDVI data with four integral phenological phases (i.e., dormancy, green-up, maturity, senescence). Specifically, urban impervious surfaces only experience the dormancy phenophase, with low NDVI values throughout the year. Bare soil experiences dormancy in winter, with low NDVI values; green-up in spring, with elevated NDVI values associated with the growth of vegetation (e.g., agricultural lands); maturity in summer, with high NDVI values; and senescence in autumn, with decreasing NDVI values due to the harvest (e.g., agricultural lands). Consequently, the significant phenophase difference between impervious surfaces and soil facilitates their discrimination with phenology-based approaches.

The results also indicate that, compared to phenology-based TMA models, summer TMA performs slightly better in developed areas but worse in less-developed areas (see Table 1). A possible explanation may be that, with Summer TMA, any materials with low NDVI values in summer are considered impervious surfaces. These materials, however, may include shade, non-photosynthetic vegetation, bare soil, etc. In less-developed areas, therefore, significant overestimation of impervious surfaces occurred (e.g., SE = 5.08). Such overestimation, however,

may help mitigate the underestimation problem in developed areas, resulting in better estimation accuracy, with a better SE value (e.g., -5.69%). For both phenology-based TMA and Summer TMA methods, a clear underestimation exists in developed areas, and overestimation exists in less-developed areas. One possible cause could be associated with the fully constrained spectral mixture analysis model. With this model, the fractions of all land covers should be positive and sum to one. Although the estimation results from the fully constrained model have clear physical meanings, overestimation in less-developed areas and underestimation in developed areas may exist.

When compared to PTMA, the performance of PMETMA is similar in developed areas but much better in less-developed areas. This result is consistent with the findings of Powell et al. (2007), who found that multiple endmember spectral mixture analysis (MESMA) performs better in less-developed areas than in urban areas. This difference may be due to the significant heterogeneous spectral variations of manmade materials in urban areas, causing the models with multiple endmembers to be less efficient than when applied to less-developed areas.

2.6 Conclusions and future research

In this study, phenology-based TMA techniques, PTMA and PMETMA, were developed to estimate subpixel impervious surface fractions in the State of Wisconsin, U.S.A. In particular, one-year-continuous NDVI series with integral phenological stages were employed to reduce seasonal sensitivity and spectral confusion of land covers. The estimated results were compared to those obtained using TMA techniques applied only to summer and winter seasons (i.e., Summer TMA and Winter TMA). The estimation accuracy of these models was assessed using the National Land Cover Data (NLCD) 2006 Percent Developed Imperviousness data as

reference, and comparative analyses were conducted among PTMA, PMETMA, Summer TMA, and Winter TMA models. The results suggest several major conclusions.

First, both phenology-based models, PTMA and PMETMA, are able to estimate the percent impervious surface areas well. In particular, these two models feature an MAE of approximately 3.3-4.0% for the entire study area, 12.2% for developed areas, and 3.2-3.9% for less-developed areas. Moreover, a slight overestimation for less-developed areas (2.3-3.4%) and an underestimation for developed areas (-8.2 to -7.5%) were found using these phenology-based models. Second, a comparative analysis between these two models indicates that PMETMA performs better than PTMA. In particular, PMETMA performs significantly better in less-developed areas, with relatively lower SE and MAE, and slightly better or similar to PTMA in developed areas. Third, compared to Summer TMA and Winter TMA models, phenology-based models provide better estimation accuracy. Summer TMA is effective in developed areas but achieved consistent overestimation and higher estimation error for the whole study area and the less developed areas. The performance of Winter TMA is unacceptable, with significant estimation errors for the entire study area.

Although the performances of the developed phenology-based TMA models are satisfactory in estimating large-scale urban imperviousness, their ability to separate urban impervious surfaces and bare soil remains unknown, mostly due to the unavailability of bare soil reference data for a large geographic area. Therefore, one future research direction may be the collection of actual bare soil ground data for the further validation of the PTMA and PMETMA approaches. In addition, although the phenology-based TMA and METMA perform fairly well in this study, an obvious underestimation exists in developed areas for both approaches. Therefore, another research direction could involve improving the impervious surface estimation in

developed areas by incorporating spatial information into the unmixing analysis. Such information may be of significant help in mitigating endmember variability and improving estimation accuracy.

CHAPER3 INCORPORATING LAND USE LAND COVER PROBABILITY INFORMATION INTO ENDMEMBER CLASS SELECTIONS FOR TEMPORAL MIXTURE ANALYSIS[2]

3.1 Introduction

Spectral mixture analysis (SMA) is a promising method for estimating fractional land covers within a remote sensing image pixel. As a physical based approach, SMA has proven effective in addressing mixed pixel problem and been successfully applied in urban analysis (Weng and Hu, 2008; Wu and Murray, 2003; Wu, 2004), vegetation mapping (Liu and Yang, 2013; Small, 2001; Small and Lu, 2006; Song, 2005), geological mapping (Bedini, 2009; Johnson et al., 1993; Ramsey and Christense, 1998; Sunshine and Pieters, 1993), natural hazard risk assessment(Jia et al., 2006; Eckmann et al., 2010), etc..SMA assumes the spectra of a pixel as a linear/nonlinear combination of the spectra of comprised pure land cover types (also called endmember classes), and the areal fraction of each endmember class can be estimated through an inversion model such as the inverse least squares deconvolution method.For successful applications of SMA, an important step is the selection of the number, type, and spectral signatures of endmember classes(Tompkins et al., 1997; Elmore et al., 2000). Within these, the choice of appropriate spectral signatures has been extensively studied in the past decades (Somers et al.,2011). In particular, Asner and Lobell (2000)introduced an autoSWIR approach to extract endmembers through highlighting the variations among different land cover types. In addition to band selection, spectral transformations have also been applied in SMA. Wu (2004) proposed a normalized spectral mixture analysis (NSMA) to reduce within-class brightness variations of the reflectance spectra. Zhang et al., (2004) developed a derivative spectral

---

unmixing (DSU) method to highlight between-class variability while reducing within-class variability, with which spectral unmixing was implemented with the second derivative endmember spectra. Further, wavelet analysis techniques, including discrete wavelets and continuous wavelets, were proposed by Li (2004).In addition to the spectral transformation method, spectral weighting is another alternative. Instead of considering all bands as equally important, the weighted spectral mixture analysis (WSMA) (Chang and Ji (2006)) assumes that the spectral bands with the lowest endmember variability are more important, thereby assigned higher weights accordingly. Further, Somers et al. (2009a) found that the traditional SMA generally overlooked the correlation of error variance and reflectance energy, and then developed a two-step WSMA through taking the variations of the reflected energy into consideration. Moreover, Somers et al. (2010) developed a stable zone unmixing (SZU) technique to select spectral bands with the lowest within-class variations in SMA for generating corresponding land cover fractions. In addition, the multiple endmember spectral mixture analysis (MESMA) method was also proposed to address endmember variability (Roberts et al., 1998). With MESMA, a spectra library with a wide range of endmembers is constructed, and different sets of endmember combinations, instead of a fixed endmember set, are employed to derive the fractional land covers for each pixel. Recently, Deng and Wu (2013)developed a spatially adaptive spectral mixture analysis (SASMA) to mitigate endmember variability through only including spatially adjacent endmember candidates into consideration.

Besides the selection of an appropriate endmember sets, the choices of type and number of endmember classes also play an essential role in SMA and a few studies have examined this issue (Somers et al., 2009b). One early attempt was made by Smith et al., (1990), who proposed a three-endmember model: vegetation-soil-shade (V-S-S) model for mapping vegetation cover

fractions in a desert environment. Furthermore, Ridd (1995)proposed a vegetation-impervious surface-soil (V-I-S) model for characterizing urban environments. Moreover, Small (2001)considered that urban environments are composed by vegetation, low-albedo materials, and high-albedo materials, and developed another three-endmember model (V-L-H) for urban applications. Wu and Murray (2003) developed a four-endmember model: vegetation-low albedo-high albedo-soil (V-L-H-S) model to characterize the urban environments of Columbus, Ohio, United States. Zhang et al., (2014) applied the V-L-H model in high-density urban areas, and the V-L-H-S model in low-density urban areas. In addition to these models with a fixed endmember set for each pixel, MESMA has taken the endmember class types and number into consideration, and chosen the optimal endmember class types based on a set of error terms (Dennison and Roberts 2003).

While these models provide valuable references in selecting endmember classes for parameterizing biophysical compositions, several problems remain. Specifically, endmember classes are typically identified from vertices of n-dimensional scatter plots and then applied to the entire study area. This approach applies the same endmember class set to each individual pixel for the whole image, and neglects their spatial distributions. Consequently, if a non-existing endmember class is included in the unmixing process, the estimated abundance for this endmember class is usually over zero, thereby inevitably generating large over-estimation errors. On the contrary, if an endmember class is mistakenly ignored, the resultant abundance of that class is zero, thereby leading to severe under-estimation errors. While MESMA has taken the selections of endmember class types and number into consideration, it neglects the spatial associations of land use land covers, and only employs pixel-wise estimation errors (e.g. root mean square error (RMSE)) as the criteria.

To address this problem, in this study, we proposed to automatically select endmember classes for SMA through incorporating land use land cover probability information derived from socio-economic and environmental drivers. A logistic regression model is typically applied to estimate the distribution probability of a land use land cover (LULC) type through analyzing the relationships among LULCs and their socio-economic and environmental factors, such as distance to the nearest city, distance to water, elevation, slope, etc. For instance, urban infrastructures are likely to be found in areas with flat or gentle slopes and with convenient access to transportation networks; vegetation may be found near to lakes and river streams. This logistic regression analysis has been applied in explaining the process of urbanization, and simulating future urban development scenarios (Verburg et al., 2004; Li and Wu 2013; Li et al.,2014). Such analysis, therefore, may provide a physical means of explaining the existence and spatial distribution of endmember classes, and its successful applications in land use studies suggest that it might be a better alternative for addressing the endmember class selection issue in SMA. In this study, we incorporated LULC probability information into the selections of endmember class type and number, and further inputted to spectral unmixing for better deriving impervious surface estimates. This proposed model includes three consecutive steps, including 1) quantifying the distribution probability of each endmember class using a logistic regression analysis, 2) identifying whether each endmember class exists or not in a particular pixel using a classification tree method, and 3) estimating fractional land covers using temporal mixture analysis (TMA). TMA is a variant of SMA, with which NDVI values, instead of the original reflectance spectra, are employed for spectral unmixing (Knight and Voth 2011; Yang et al., 2012, 2014; Li and Wu, 2014). One major advantage of TMA is the incorporation of NDVI time series profiles into spectral unmixing. With NDVI time series profiles, different phenophases

41

(green up, maturity, senescence, and dormancy) of green vegetation can be identified and the significant amount of phenological information can be of great help for distinguishing one land cover type from another, thereby effectively addressing the issues of endmember variability. For instance, impervious surfaces only experience the dormancy phenological stage during the entire year with very low NDVI values. Bare soil, on the other hand, is with very low NDVI values in fall and winter (e.g. dormancy), but with relatively high NDVI values in spring and summer due to the growth of vegetation. Therefore, NDVI time series profiles are essential for distinguishing impervious surfaces and bare soil. Further, NDVI time series profiles can also help estimating the percent of impervious surfaces due to its close relation to vegetation fractions. Therefore, TMA, instead of SMA, has been employed in this study for estimating large-scale impervious surface distribution. The rest of the paper is organized as follows. The study area and data are introduced in Section 3.2. Details of the proposed TMA approach, as well as comparative analysis and accuracy assessment, are described in Section 3.3. Results of this study are reported in Section 3.4. Finally, discussion and conclusions are provided in Sections 3.5 and 3.6.

3.2 Study area and data

The State of Wisconsin, located in the north-central part of the United States of America, was chosen as the study area. Wisconsin is within the longitudes of 86°46′-92°53′ W and latitudes of 42°37′ - 47°05′ N (see Figure 7), with a geographic area of 169,639 square kilometers that covering 72 counties. The total population of Wisconsin was 5.68 million in 2010, and the majority of the population resides in the southeastern part of the state. Approximately 68% of the population in Wisconsin resides in urbanized areas, including Milwaukee, Madison, and

Green Bay, etc. Wisconsin has experienced fast population growth and urbanization in the past decades. The population has increased almost 16%, from 4.89 million in 1990 to 5.68 million in 2010, and it is expected that the growth trend will continue in the future. This rapid urbanization has caused challenging issues, including environmental pollution, traffic congestion, etc. As impervious surfaces are served as one of the major components of urban areas and widely considered as a key indicator of urbanization intensity and environmental quality, accurate estimates of impervious surfaces are essential for Wisconsin.
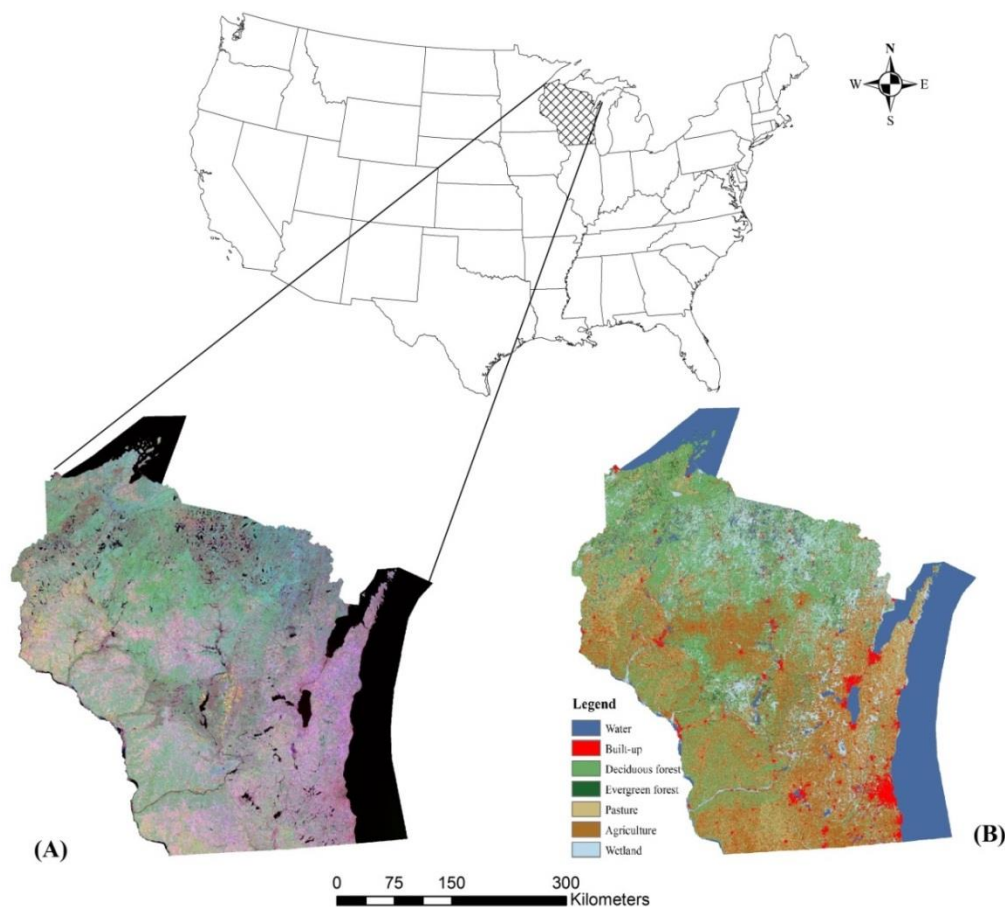
Figure 7 Study area: the State of Wisconsin, U.S.A. (A: stacked MODIS products; B: Land use land cover data from NLCD2006)

To carry out the proposed TMA approach for estimating urban impervious surface distribution, 22 Moderate-resolution Imaging Spectroradiometer (MODIS) NDVI images acquired in 2006 (Two images per month, product of MOD13Q1, late November data was excluded due to its suboptimal quality), with a spatial resolution of 250 m and a positional accuracy of 0.5 pixel, were collected from the United States Geological Survey (USGS) website (www.usgs.gov). In order to identify LULC type and assess the estimation accuracy, the 2006 National Land Cover Data (NLCD) land cover and percent developed Imperviousness data obtained from the Multi-Resolution Land Characteristics Consortium (MRLC) website (http://www.mrlc.gov/nlcd06_data.php) were employed as reference data. NLCD 2006 data was generated using Landsat TM and ETM+ remote sensing data collected between 2 November 2005 and 10 March 2007. While the data collected dates are not fully consistent with the MODIS images, we consider little change has been taken place in Wisconsin during those periods. Thus, NLCD 2006 data are qualified as the reference data for identifying LULC types and evaluating estimation accuracy. In addition to remote sensing data, digital elevation data (DEM) and hydrological data (e.g. rivers, lakes) were collected from United States Geological Survey (USGS) website (www.usgs.gov). Further, transportation networks (e.g. Highway, railway), and georeferenced city and village data were obtained from the American Geographical Society Library at the University of Wisconsin-Milwaukee. All the data were re-projected to the Universal Transverse Mercator (UTM) projection with a datum of World Geodetic System (WGS) 84.

3.3 Methodology

The flowchart of the proposed method can be found in Figure8. Before implementing the proposed land use/land cover probability incorporated TMA, potential endmember classes have to be identified. In order to reduce noise and facilitate endmember selection, a maximum noise fraction (MNF) transformation was employed (Green et al., 1988). Specifically, MNF transformation was conducted with the help of the ENVI program, a commercial remote sensing image processing software. Spectral feature spaces were generated using the first several MNF components, and endmembers were identified from the vertices of those scatterplots. In this study, five potential endmember classes, including impervious surfaces, deciduous forest, pasture, evergreen forest, and agricultural land, were chosen according to the scatterplots of the first three MNF components (see Figure9)
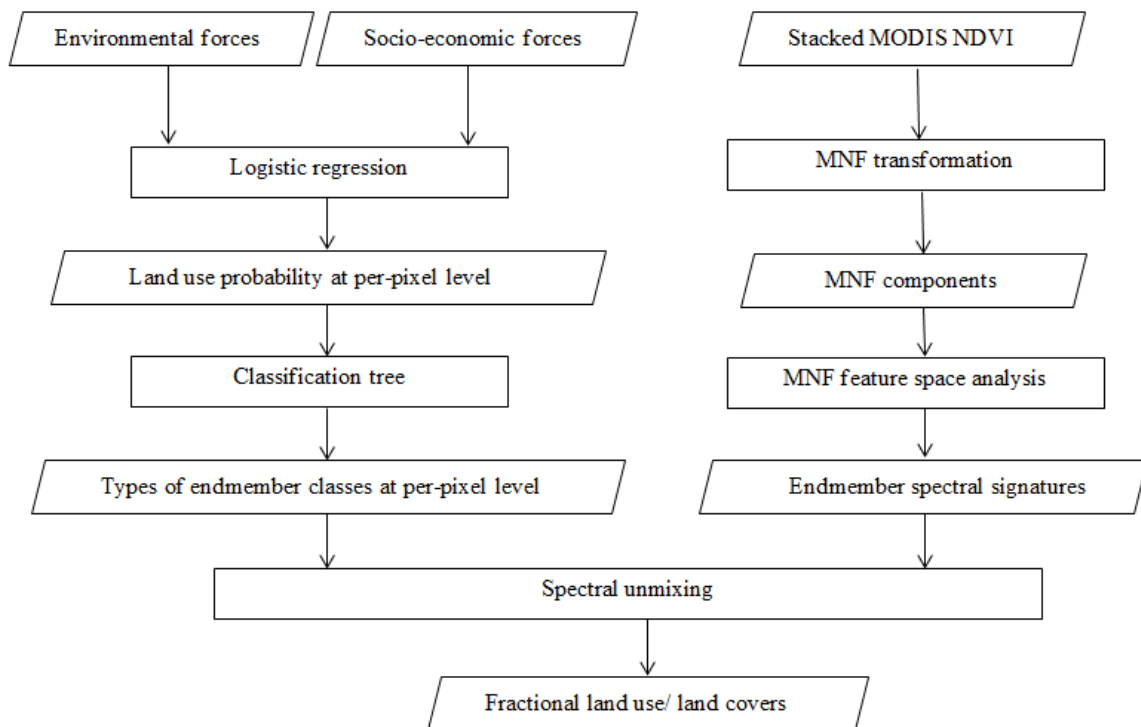
Figure 8 Flowchart of the proposed land use/land cover probability incorporated TMA approach

45
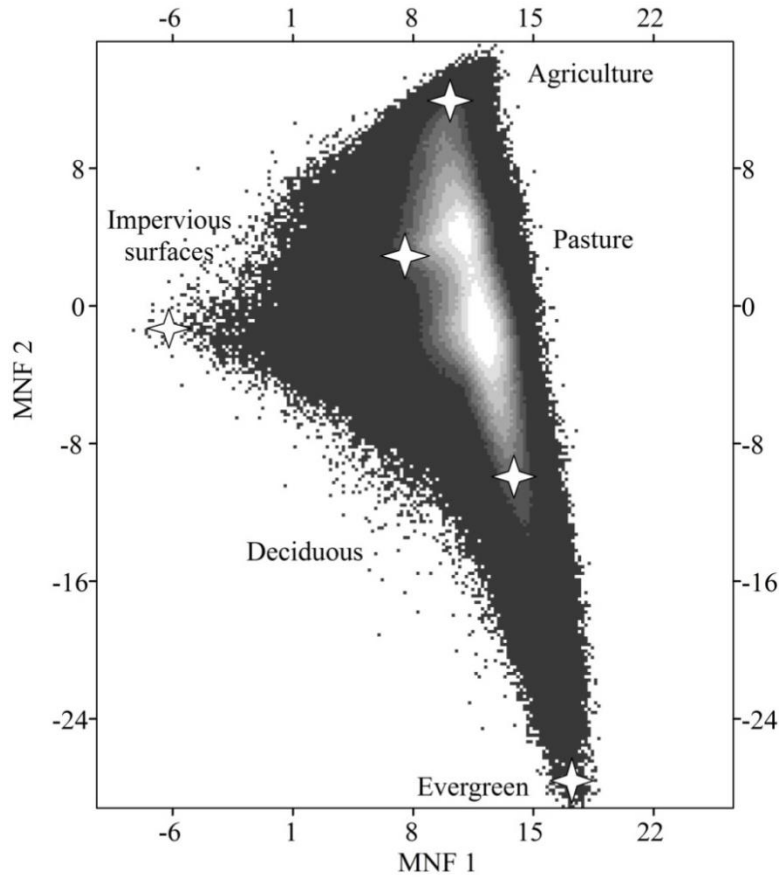
Figure 9 Spectral feature spaces of MNF components

3.3.1 Endmember class probability estimation using logistic regression analysis

In order to generate the endmember class probability for each individual pixel, a logistic regression analysis was employed in this study. The logistic regression model has the ability to uncover the complicated interrelationship between the spatial distribution of LULCs and their determinants, and has been widely employed for deriving land use distribution probability and explaining the causes and effects of LULC change dynamics through incorporating terrain, distances and other physical and socio-economic factors (Overmars et al., 2003; Verburg et al., 2004; Dendoncker et al., 2007). In this study, five LULC types (identified from NLCD2006),

namely agricultural land, deciduous forest, built-up (impervious surfaces), evergreen forest, and pasture, were chosen as the potential endmember class types. Eight driving factors, including elevation, slope, distance to the nearest city, distance to the nearest lake, distance to the nearest railway, distance to the nearest river, distance to the nearest village, and distance to the nearest road, were selected to examine the probability of each endmember class. The relationship between the probability of the existence of an endmember class and its driving forces can be modeled as follows.

$$Log\left(\frac{P_k}{1-P_k}\right) = \alpha_0 + \alpha_1 X_{1,k} + \alpha_2 X_{2,k} + \cdots + \alpha_n X_{n,k} \qquad (3.1)$$

where P_k is the probability that endmember class k exists in a pixel; $X_{j,k}$ is the jth driving factors for the class k, α_j is the regression coefficient of the jth driving factor, and n is the total number of driving factors. To collect samples of each endmember class for constructing the regression model, the NLCD 2006 data was utilized. Specifically, the spatial distribution map of all endmember classes were extracted from NLCD2006and then 2000 samples were randomly selected for each endmember class using ArcGIS. To assess the fitness of the regression model, the relative operating characteristic (ROC) was applied (Pontius Jr and Schneider 2001). The ROC value ranges from 0 to 1. The higher the ROC value, the better the spatial distribution of a specific endmember class explained by the selected driving factors.

3.3.2 Endmember class types and number selection using classification tree model

With the knowledge of the spatial distribution probabilities of all endmember classes produced from the logistic regression model, a classification tree approach was utilized to

automatically identify whether an endmember class exists in each pixel. As an established model for image classification, classification tree can generate interpretable results by incorporating categorical data and continuous data without the need of rigorous statistical assumptions of the data. It can uncover the relationship between a categorical variable (e.g. whether the built-up endmember class exists in a pixel or not) and independent variables (e.g. the probabilities of the existence of an endmember class type). The classification results were produced through splitting all the data with the interactions between the categorical variable and the independent variables. The classification tree was conducted using SEE5 (or C5.0), a commercial program, with 200 samples randomly selected for each endmember class type. SEE5 was employed to generate a decision tree proposed by Quinlan (1993)(https://www.rulequest.com/see5-info.html). Specifically, all samples were randomly collected from the spatial distribution map of five land use land covers based on NLCD2006 data.

3.3.3Temporal mixture analysis

With the identified endmember classes fo reach pixel, a fully constrained linear TMA was applied to extract the areal fractions of all land cover types using multi-temporal MODIS NDVI data. With TMA, the multi-temporal NDVI data, instead of the original reflectance spectra, was employed for spectral unmixing. The spectral signatures of five endmembers, including impervious surfaces, deciduous forest, pasture, evergreen forest, and agricultural land were chosen according to the scatterplots of the first three MNF components. With the selections of the types, number, and spectral signatures of endmember classes, fractional land covers can be modeled using TMA as follows.

48

$$NDVI_b = \sum_{i=1}^{N} f_i \times NDVI_{i,b} + e_b \quad\quad\quad\quad (3.2)$$

Subject to $\quad \sum_{i=1}^{N} f_i = 1$ and $f_i \geq 0$ $\quad\quad\quad\quad\quad\quad\quad\quad (3.3)$

Where $NDVI_b$ is the NDVI value for band b, N is the number of endmembers, f_i is the fraction of endmember i, $NDVI_{i,b}$ is the NDVI value of endmember i in band b, and e_b is the residual. In order to assess the model fitness, the e_b and RMS were applied.

$$RMS = \left(\frac{\sum_{b=1}^{M} e_b^2}{M}\right)^{1/2} \quad\quad\quad\quad\quad\quad\quad (3.4)$$

Where M is the number of bands of the remote sensing image.

3.3.4 Comparative Analysis and Accuracy assessment

To evaluate the performance of the proposed TMA model, comparative analysis with a simple TMA and multiple endmember TMA (METMA) techniques was conducted. With the simple TMA, all five endmember classes were adopted, and the spectra of each endmember class were obtained using the same approach described in the previous section. In terms of the METMA, different endmember combination sets were allowed for each pixel. In particular, the bundles selection method has been utilized for identifying endmember spectra and the root mean square error (RMSE) has been employed for examining endmember number at each pixel. As a lower RMSE is always associated with a larger number of endmembers, the indicator proposed by Demarchi et al. (2012) was applied to select endmember combination models in METMA (Li and Wu 2014). To quantitatively assess the performances of the proposed TMA method, an accuracy assessment was conducted through comparing with the National LandCover Data

(NLCD) 2006 Percent Developed Imperviousness data. This dataset was derived from Landsat TM/ETM+ imagery with a spatial resolution of 30 m. With the help of NLCD 2006 Percent Impervious surfaces data, a computer based pixel-by-pixel comparison has been conducted for quantitative analysis of the estimation accuracy. Two widely used error measurement indices, systematic error (SE) and mean absolute error (MAE), were utilized to assess the accuracy of the impervious surfaces fractions estimated by the proposed TMA method. Specifically, MAE reflects the relative estimated errors of impervious surface abundances, and SE measures the bias, an overall tendency of over- or under-estimation. These indices can be calculated using the following equations (Equations 3.5and 3.6).

$$SE = \frac{\sum_{i=1}^{N}(\widehat{I_i} - I_i)}{N} \tag{3.5}$$

$$MAE = \frac{\sum_{i=1}^{N}|I_i - \widehat{I_i}|}{N} \tag{3.6}$$

Where $\widehat{I_i}$ is the modelled impervious surface fraction value for pixel i, $I_i$is the reference impervious surface fraction value for pixel i, and N is the total number of pixels.These two accuracy metrics were calculated for the entire study area, developed areas (with ISA% equals and over 30%), and less developed areas (with ISA% less than 30%).

3.4 Results

3.4.1 Endmember class probability estimation

The distribution probabilities of all endmember classes, including agricultural lands, deciduous forest, built-up, evergreen forest, and pasture, were estimated using the logistic regression analysis. Table 2 reports the coefficients of each LULC drivers employed in the

logistic regression analysis, as well as the ROC value. Taken the built-up endmember class as an example (see Table 2), it appears that higher probability of built-up areas is associated with lower elevation, relatively higher slope, closer to the nearest city, lake, river, village, and road, and farther away from railway. On the contrary, higher probability of evergreen forest endmember class is positively correlated with areas with lower elevation, lower slope, longer distance to cities, villages, and roads, and closer to railway and rivers. The ROC values for all the logistic regression models were over 0.65, indicating that these driving factors have effectively explained the spatial distributions of these LULC types. The resultant distribution probabilities of these endmember classes are reported in Figure 10 It illustrates that the spatial patterns of endmember class probabilities reasonably reflect the actual LULC patterns of Wisconsin. As an example, built-up areas (Figure 10B) were mainly found in the southeastern Wisconsin and forests (deciduous and evergreen) (Figure 10C and 10D) were located in the northern Wisconsin.

Table 2 Results of logistic regression analysis for each endmember class

Driving factors	Agricultural land	Deciduous forest	Built up	Evergreen forest	Pasture
Elevation (m)	0.00064894	0.00813792	-0.00231551	-0.00107184	-0.00018148
Slope (degree)	-0.14955313	0.32144669	0.00207563	-0.22212906	-0.03614778
DisCity (m)	-0.00002835	0.00002630	-0.00002211	0.00001151	-0.00003098
DisLake (m)	0.00013175	0.00003733	-0.00005401	0.00013647	0.00011846
DisRailway (m)	0.00000808	-0.00000152	0.00000145	-0.00001959	-0.00000694
DisRiver (m)	0.00001284	-0.00003618	-0.00003483	-0.00008011	0.00003977
DisVillage (m)	-0.00006065	-0.00001629	-0.00000988	0.00001257	-0.00003284
DisRoad(m)	-0.00014293	0.00000885	-0.00021078	0.00000247	-0.00010072
Constant	-0.32620496	-4.04933074	-0.67114000	-3.72471954	-1.72240487
ROC	0.761	0.756	0.747	0.667	0.726
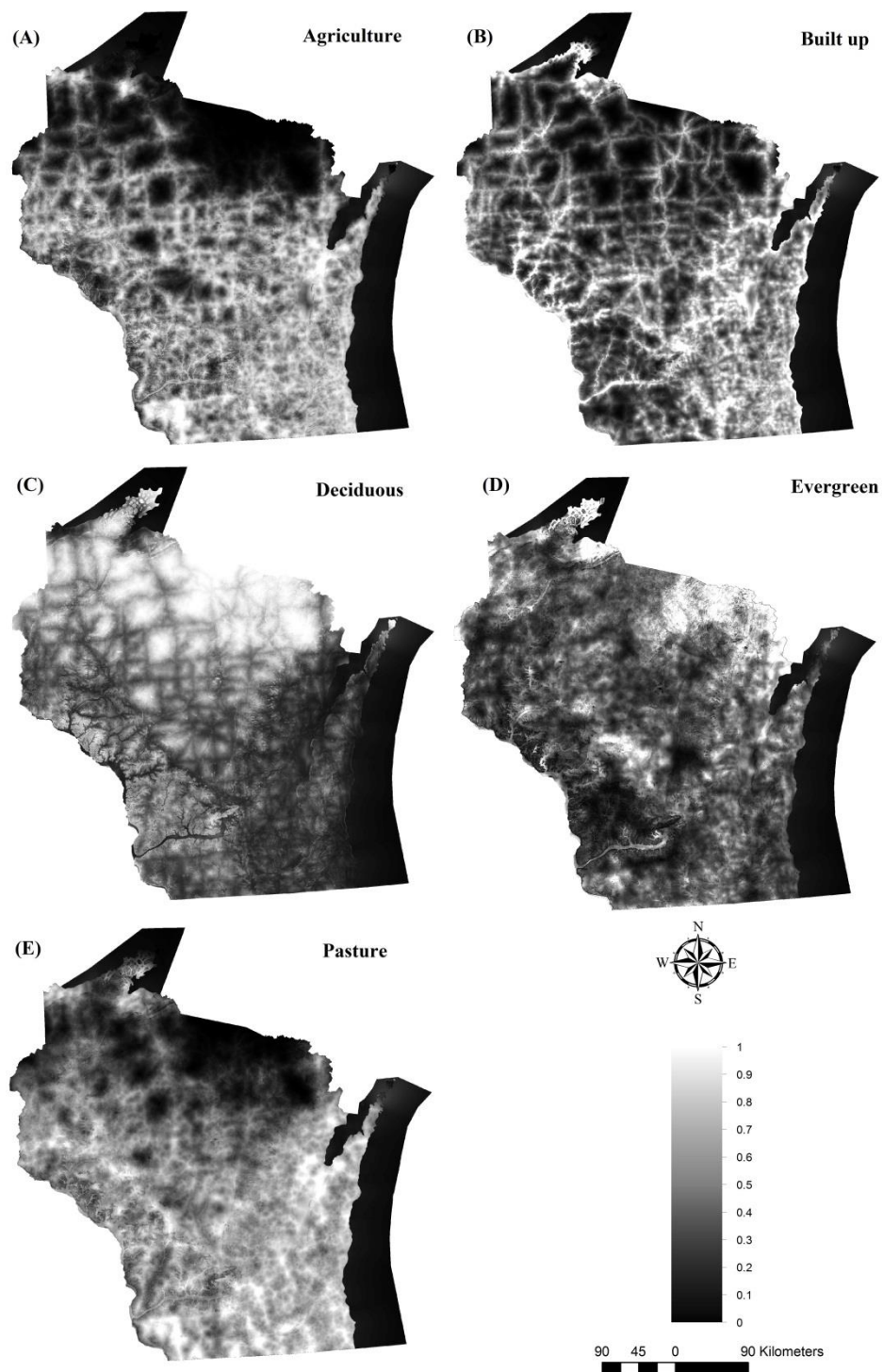
Figure 10 The spatial distribution probabilities of endmember classes

3.4.2Endmember class type identification

With the probability of each endmember class type, a classification tree model was constructed for each endmember class type to identify whether an endmember class is present or absent in a particular pixel. The rules derived from the classification tree approach are shown in Table3.Taking the agriculture land endmember class as an example, it is present in a pixel if the probability of agriculture land is higher than 14.4% and the probability of evergreen forest is lower than 5.2%, or the probability of agriculture is lower than 14.4% but the built-up probability is between 11.0% and 24.5%. The former may indicate agriculture lands in rural areas, and the later may represent agriculture lands near to built-up areas. Similarly, the built-up endmember class is present if the probability of built-up endmember class is greater than 9.3%, or the built-up endmember class probability is lower than 9.3% but the probability of evergreen class is higher than 0.6%, or the built-up class probability is lower than 7.8% but the probability of agriculture class is higher than 44.1%. With these cases, the first one indicates high density urban areas, and the second one indicates the mixture of impervious surfaces and forest, and the third one indicates the mixtures of impervious surfaces and agricultural lands. With the extracted thresholds for all endmember classes (Table 3), we can identify the types and numbers of endmember classes at each pixel for spectral unmixing. Take impervious surfaces as an example (see Figure 11), we can find that impervious surfaces are mostly distributed in the southeast part of Wisconsin.

Table 3 Rules derived from classification tree

Endmember class	Status	Agriculture	Deciduous	Evergreen	Built-up	Pasture
Agriculture	Present	>14.4%		<5.2%		
		<14.4%			11.0% - 24.5%	
	Absent	>=14.4%		>=5.2%		
		<=14.4%			>=24.5%	
		<=14.4%			<=11.0%	
Built-up (Impervious Surfaces)	Present	>44.1%			<=7.8%	
					>9.3%	
				>0.6%	<=9.3%	
	Absent	<=44.1%			<=7.78%	
				<=0.6%	<=9.3%	
Deciduous					>16.9%	
	Present		>45.3%		<=16.9%	
		>38.9%	<=45.3%		>6.5%	
	Absent	<=38.9%	<=45.3%		<=16.9%	
		>38.9%	<=45.3%		<=6.5%	
Evergreen	Present		>20.3%	>2.2%		
			>20.3%	<=2.2%		11.1% - 11.5%
	Absent		<=20.3%			
			>20.3%	<=2.2%		>11.5%
			>20.3%	<=2.2%		<=11.1%
Pasture	Present	>14.5%				>11.6%
	Absent	<=14.5%				<=11.6%
		>14.5%				
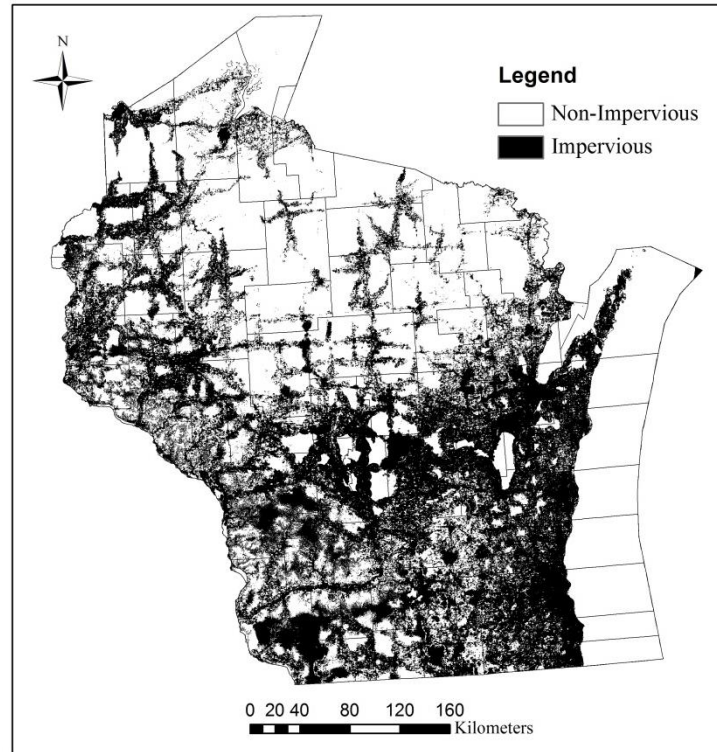
Figure 11 The spatial distribution of impervious surfaces in Wisconsin

3.4.3Temporal mixture analysis

With the identified endmember class type, number, and spectra (see Figure 12), TMA was performed using Equations 3.2 and 3.3, and the results are reported in Figure 13. A visual examination of the spatial distributions of urban impervious surfaces indicates that the patterns of impervious surface distributions are consistent with the known LULC patterns of Wisconsin. Especially, high fractional impervious surface areas are mainly located in urbanized and populated regions (e.g. southeast Wisconsin), including the metropolitan statistical area (MSA) of Milwaukee, Madison, and Green Bay, etc. In addition, very low fractional urban impervious surface areas can be found in the northern portion of Wisconsin. In addition to the visual

55

examination, the results of accuracy assessment are reported in Table 4 Results (see Table 4) indicate that the proposed LULC probability based TMA is with a reasonably well performance for estimating impervious surfaces for the study area, with an SE of 2.25% and MAE of 3.18%. With a detailed analysis, results indicate a better performance in less developed areas (e.g. an SE of 1.62% and an MAE of 2.53%) when compared to developed areas (e.g. an SE of -8.66% and MAE of 12.89%). For developed areas, in particular, the under-estimation of urban impervious surfaces is a major concern.

Table 4 Accuracy assessment of impervious surfaces with the proposed TMA, simple TMA and METMA

		Proposed TMA (%)	Simple TMA (%)	Percent difference (%)	METMA (%)	Percent difference (%)
Overall	SE	2.25	3.25	-30.8**	2.13	5.63
	MAE	3.18	4.03	-21.1*	3.36	-5.36
Developed	SE	-8.66	-8.17	6.0	-7.46	16.09
	MAE	12.89	12.15	6.1	12.16	6.00
Less developed	SE	1.62	3.43	-52.8**	2.32	-30.17*
	MAE	2.53	3.90	-35.1*	3.23	-27.67*

*significant at the 95% significance level
**significant at the 99% significance level
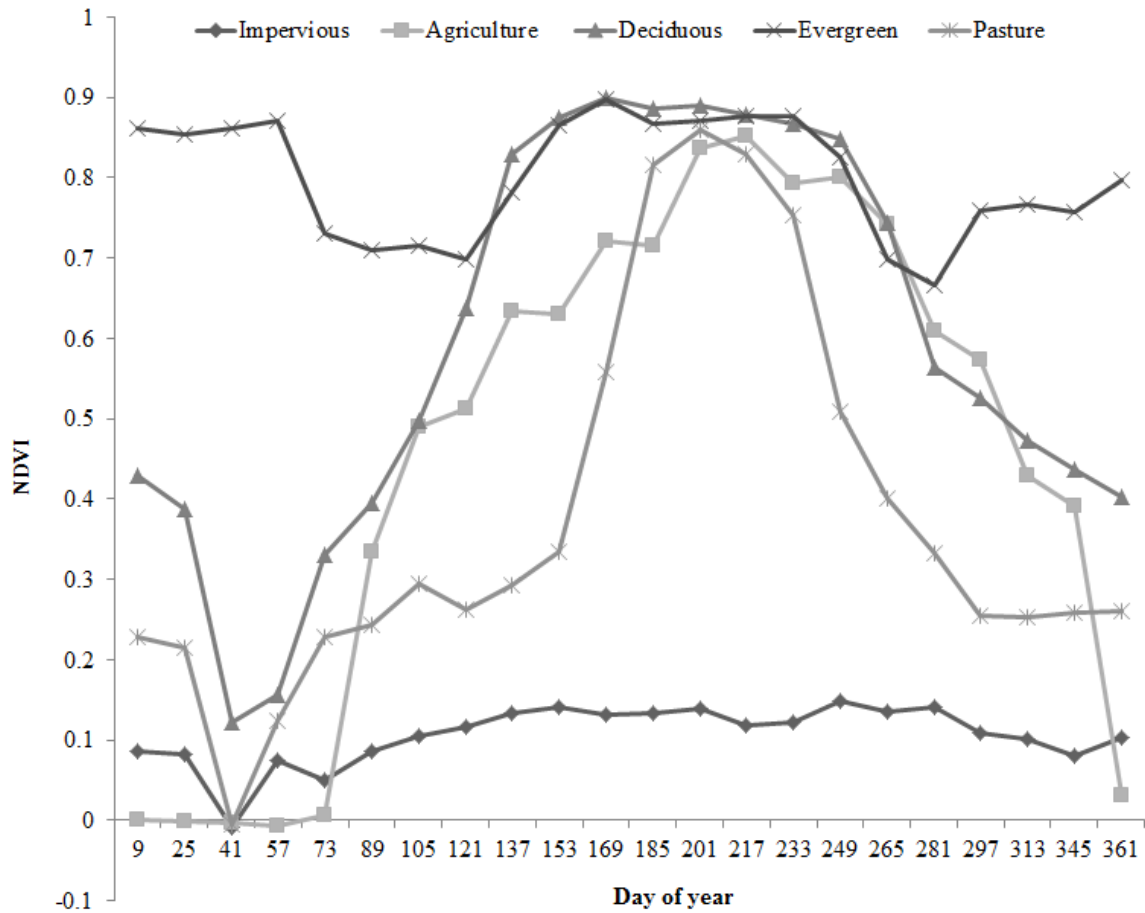
Figure 12 NDVI spectral signatures of identified endmember classes
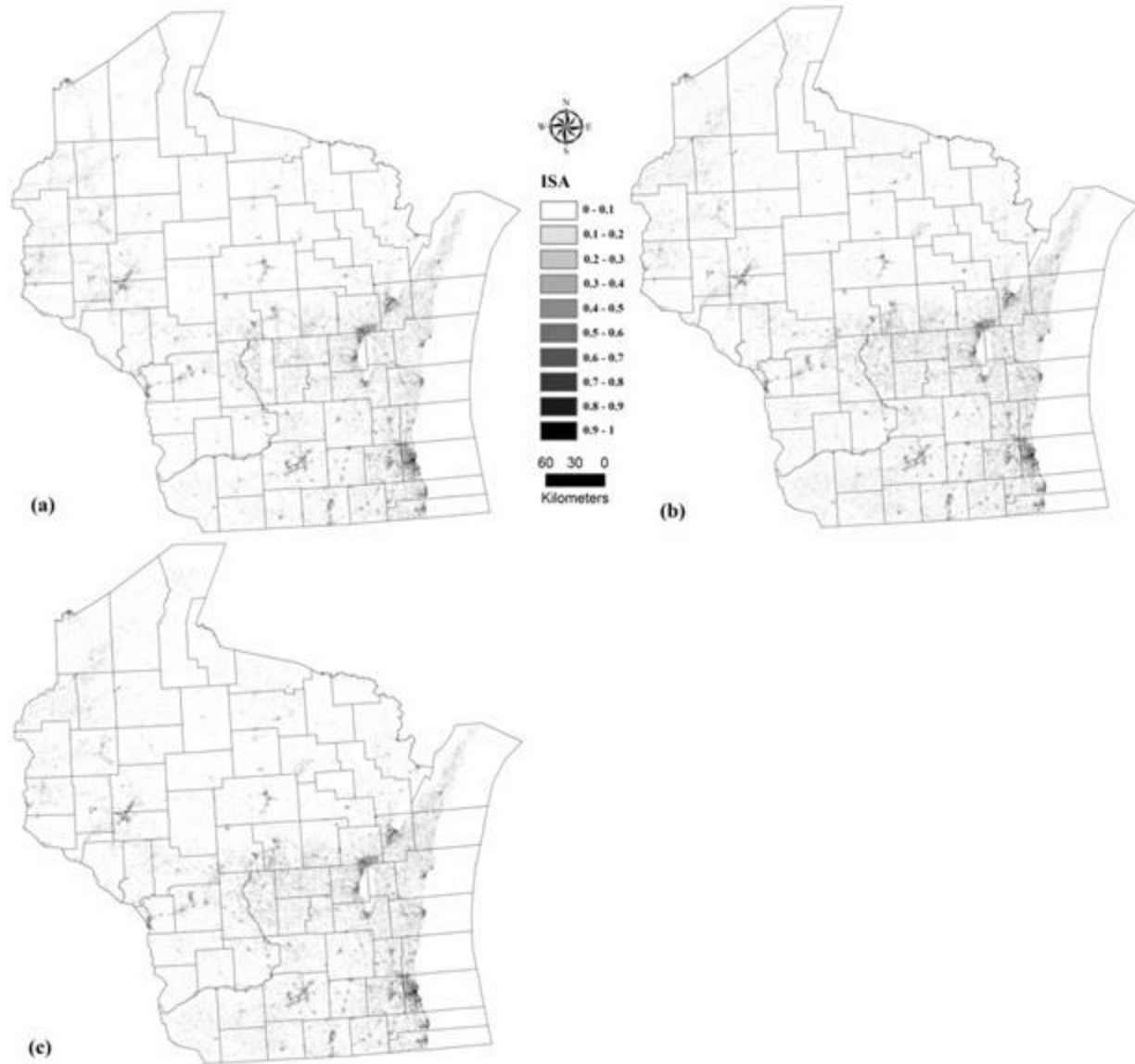
Figure 13 Impervious surfaces fraction maps generated from (a) proposed TMA method (b) simple TMA method and (c) METMA method

3.4.4 Comparative analysis and accuracy assessment

For a comparative analysis, the simple TMA and METMA were implemented and the results are reported in Figure 13 Through a visual comparison, we found that a rather similar impervious surface distribution pattern is shown in most parts of Wisconsin, with the majority of

impervious surfaces located in major cities in the southeastern portion, and lower fractional impervious surfaces were found in the northern and northwestern parts of Wisconsin. Moreover, further quantitative accuracy assessment indicates that the performance of the simple TMA is worse than that of the LULC probability based TMA method. Specifically, the overall performance of the simple TMA is worse, with an SE of 3.25% and MAE of 4.03%, both of them are significantly higher than those of the proposed TMA method (see Table 4). Further analyses indicate that a more severe over-estimation can be detected in less developed areas with significantly higher values of SE (3.43%vs. 1.62%), and MAE (3.90%vs. 2.53%). For developed areas, the performance of the simple TMA and the proposed TMA method is comparable, and a slightly better performance was achieved with the simple TMA method. When compared to the proposed LULC probability based TMA approach, METMA method also achieved a satisfactory performance for overall study area with SE of 2.13% and MAE of 3.36%. In detail, METMA performs slightly better in developed areas with a lower SE value (-7.46% vs. -8.66%) and a slightly higher MAE value (12.16% vs. 12.15%), but generate much higher errors in less developed areas with an SE of 2.32 %(vs.1.62%) and MAE of 3.23 %(vs.2.53%). In addition to the above comparisons, we also generated a scatter plot to show the relationship between the examined and observed impervious surfaces fractions using randomly selected samples. Figure14 indicates that the proposed TMA provides a better performance with a higher value of R^2.As a summary, the proposed LULC probability based TMA has a satisfied performance in the entire study area and greatly improved estimation accuracy in less developed areas, while a slightly better accuracy was achieved with the simple TMA and METMA in developed areas.
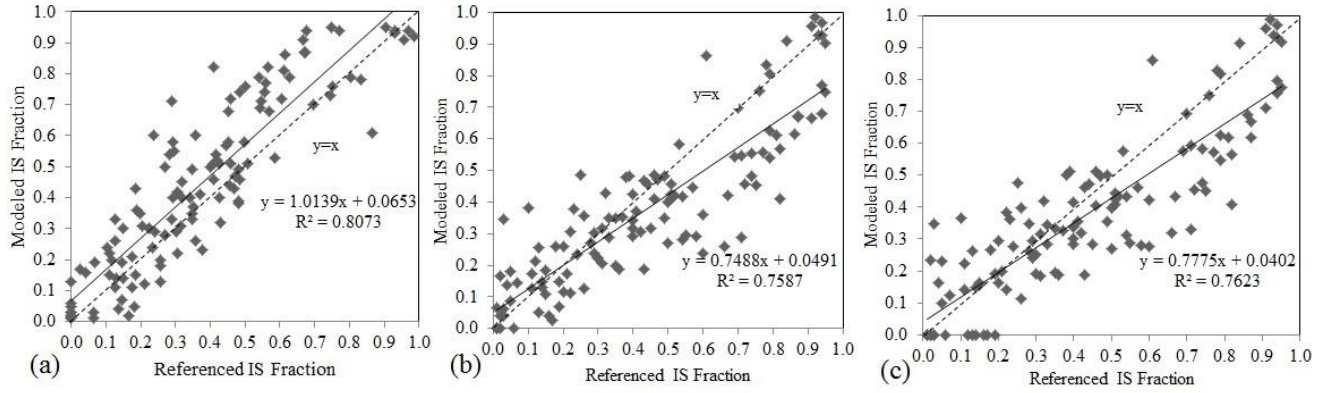
Figure 14 Accuracy assessment of the impervious surfaces estimation by (a) proposed TMA method (b) simple TMA method and (c) METMA method

3.5 Discussion

3.5.1 Endmember class variability

With SMA, the first and the most important step is the selection of endmember class type, number and spectra. While the spectra variability of endmember classes has been studied extensively (Asner and Lobell, 2000; Chang and Ji, 2006; Somers et al, 2010; Zhang, 2004; Wu, 2004), little research has been conducted in selecting endmember class type and number (Small, 2001; Somers et al, 2009b; Wu and Murray, 2003; Zhang et al., 2014). The choice of endmember classes, however, is the foundation of endmember extraction, and key to successful applications of SMA(Tompkins et al., 1997; Elmore et al., 2000). Because of the spatially heterogeneous nature of landscapes, the distribution of endmember classes tends to illustrate spatial variability. Up to now, however, endmember class types for each remote sensing image pixel are always assumed to be identical (Deng and Wu, 2013; Small and Lu, 2006; Song, 2005; Wu, 2004; Wu and Murray, 2003; Yang et al., 2012). Although the MESMA method has employed different types of endmember classes, they only used the pixel-based error terms (e.g. EAR or

60

RMSE)(Dennison and Roberts, 2003), minimum average spectral angle (MASA) (Dennison et al., 2004), or iterative endmember selection (IES)(Dennison, et al., 2011) as the criteria for endmember class selection, and neglected the physical meanings of endmember classes (Roberts et al., 1998). As a result, endmember classes may be misidentified and lead to large errors in fractional land cover estimates. The developed LULC probability based TMA might be helpful in addressing this issue. Specifically, the general spatial distribution probability can be extracted through analyzing the relationship between the sampled locations of endmember classes and their surrounding natural and socio-economic forces through a logistic regression analysis. Furthermore, a classification tree approach was developed to automatically identify the per-pixel level endmember classes based on the derived spatial distribution probabilities of all endmember classes. Consequently, the selected endmember classes with clear physical meanings can effectively improve the estimation accuracy for fractional land cover estimates. Results of this study indicate that it is highly necessary to conduct the selection of endmember class type and number prior to spectral unmixing.

3.5.2 Importance of endmember class type and number selection

Through incorporating the LULC probability information in the TMA method, we found that the accuracy of resultant impervious surface fractional estimates in less developed areas is significantly better than that with the simple TMA and MEMTA methods, while similar performance was found in developed areas (see Table 4). This observation might indicate that the selections of endmember class type and number are more essential in less developed areas when compared to developed areas. With the simple SMA model, built-up (impervious surfaces)

61

has to be an endmember for all pixels, thereby leading to remarkable overestimation of impervious surfaces in rural areas. While the METMA model considers the issue of endmember class variability, the selection of endmember classes only related to estimation residuals without any physical meanings. Therefore, it may also cause mis-identified endmember class (e.g. impervious surfaces) to be included, and finally lead to the overestimation of impervious surfaces in less developed areas. Such over-estimation, however, has been partially addressed with the LULC probability based TMA method, as urban impervious surface class has been effectively removed from the endmember class set for each rural pixel. In developed (urban) areas, the less-than-desired results of impervious surface estimates may be due to the high heterogeneity of urban environments with numerous manmade materials (e.g. asphalt, concrete, glass, metal, etc.), and endmember variability may play an essential role in the modeling accuracy of the resulting impervious surface estimates. Although several studies (Small, 2001; Somers et al, 2009b; Wu and Murray, 2003; Zhang et al., 2014) have attempted to employ different endmember class sets for urban and rural areas, this study provides a clear theoretical foundation of selecting endmember class type and number, and highlighted the importance of endmember class type selections, which has been neglected in the SMA literature.

3.6 Conclusions and future research

In this paper, we incorporated LULC probability information into the selections of endmember class type and number for TMA. In particular, logistic regression analyses were conducted to estimate the LULC probabilities of endmember classes through modeling their relationships with socio-economic and environmental drivers. Then, classification tree methods

were employed to identify the existence of each endmember class type for each remote sensing pixel. As a result, an appropriate endmember class set was determined for each image pixel. Finally, the linear TMA method was applied to estimate the impervious surface fractions for each model. This developed method was applied to the MODIS NDVI imagery of Wisconsin, United States, and comparative analysis with the simple TMA and METMA were performed.

Analysis of results indicates three major conclusions. First, the proposed LULC probability based TMA has a promising accuracy in the estimation of impervious surfaces fractions. It has an overall MAE of 3.18% and SE of 2.25%, with better performance in less developed areas than in developed areas. Further results of accuracy assessment indicate that a slight over-estimation was found in less developed areas, and under-estimation was found in developed areas. Second, comparative analysis with simple TMA and METMA indicates that the proposed TMA model has achieved comparable performance for overall study area and greatly improved the estimation accuracy of fractional impervious surface cover for the less developed areas. Specifically, when compared to simple TMA and METMA, the SE values for less developed areas have decreased 52.8% and 30.17%, and the MAE values for the less developed areas have decreased 35.1% and 27.67% respectively. Finally, for developed (urban) areas, the performance of the proposed TMA method is comparable to that of simple TMA and METMA, indicating that endmember class sections might not be as essential in heterogeneous urban environments, and endmember variability might be a more important factor.

Although a relatively satisfactory performance was achieved using the proposed LULC probability based TMA method, only the global LULC probabilities were considered for selecting endmember class type and number. Local spatial information, however, may also play an essential role in identifying endmember class types. Therefore, one research direction could

63

be incorporating local LULC probability into endmember class selections for further improving the modeling accuracy. Furthermore, in this study, only MODIS NDVI data was applied, and it is necessary to evaluate the proposed model's performance with other dataset in other study area at different scales.

CHAPTER4 A GEOSTATISTICAL TEMPORAL MIXTURE ANALYSIS APPROACH TO ADDRESS ENDMEMBER VARIABILITY FOR ESTIMATING REGIONAL IMPERVIOUS SURFACE DISTRIBUTIONS[3]

4.1 Introduction

Spectral mixture analysis (SMA) is one of the major approaches for estimating fractional land covers through modeling the relationship between the spectral signatures of a mixed pixel and those of the comprised pure land covers (also termed as endmembers) within the pixel(Keshava 2003). Because of its effectiveness in addressing the mixed pixel problem, SMA has been applied in many fields, including urban impervious surface and vegetation mapping, agricultural production assessment, terrestrial ecosystem monitoring, geological mapping, etc. (Bedini 2009; Cunningham et al. 2015; Eckmann et al. 2010; Gilabert et al. 2000; Hestir et al. 2008; Jia et al. 2006; Johnson et al. 1993; Lelong et al. 1998; Li et al. 2013; Liu et al. 2008; Rhee et al. 2014; Rosa and Wiesmann; 2013; Wu 2004; Wu and Murray 2003). When implementing SMA, the first and most important issue is the selections of endmember class types, number, and their corresponding spectra (Elmore et al. 2000; Tompkins et al. 1997). The set of corresponding spectra of endmember classes have been typically identified manually or statistically through analyzing the spectral plots. Subsequently, these endmembers were applied to each individual pixel of an image to extract areal fractions of land covers using spectral unmixing (Sabol et al. 1992). While it's straightforward, the endmember variability was ignored, and it might resulting in large estimation errors in areas with heterogeneous landscapes (Asner and Lobell 2000; Bateson et al. 2000; Bhatti and Tripathi; 2014; Herold etal. 2004; Qiu et al.2014; Roberts et al.

---

[3]Portions of this chapter have been published in the journal of *GIScience & Remote Sensing*, coauthored with Dr. Changshan Wu.

1998). As a result, endmember variability has become a profound error source and essential problem in SMA(Bateson et al. 2000).

Endmember variability can be generally categorized as intra-class variability and inter-class variability (Zhang et al. 2006). The first one refers to the relative spectral differences within a specific endmember class, and the later one is associated with spectral variations among different classes. To overcome endmember variability, several studies have been conducted in the past decades through reducing intra-class variability or enhancing inter-class variability(Somers et al. 2011). Somers et al. (2011) first reviewed and compared all the proposed techniques for addressing the issue of endmember variability, they pointed out that the first attempt should be associated with the selection of appropriate spectral features for unmixng analysis. In particular, Asner and Lobell (2000) developed an autoSWIR approach to enhance between-class spectral variations through selecting the partial shortwave infrared (SWIR) spectral region. Moreover, statistical approaches, such as principal component analysis (PCA) (Johnson et al. 1993; Miao et al. 2006), discrete cosine transform (DCT) (Li 2004), and residual analysis (Ball et al. 2007; Miao et al. 2006), have been proposed to select the best wavebands for spectral unmixing. Furthermore, Somers et al. (2010) developed a stable zone unmixing (SZU) technique to select the bands with the lowest intra-class variation according to the instability index (ISI). Other techniques include spectral weighting, spectral transformation, and spectral transfer model. Chang and Ji (2006) proposed a weighted spectral mixture analysis (WSMA) to reduce endmember variability, with which higher weights were assigned to bands with relative low endmember variability. Further, Somers et al. (2009) developed a two-step weighting SMA through considering the variations of the reflected energy associated with each band. In addition to the spectral weighting techniques, spectral transformation has also been developed for

66

mitigating within-class endmember variability.Wu (2004) developed normalized spectral mixture analysis (NSMA) to minimize the within-class endmember variability by normalizing the original spectra. This method was subsequently employed in geological applications (Zhang et al. 2005). In addition, Zhang et al. (2004) developed a derivative spectral unmixing (DSU) to address the variability issue through inputting the second-derivative endmember spectra in SMA. Although DSU is effective in solving the endmember variability issue, it also enhances high frequency noise. Thus, continuous wavelets techniques, and discrete wavelet and other wavelet analysis techniques, have been developed (Li 2004). With the wavelet analysis, transformed spectral features, instead of original reflectance features, have been employed in SMA (Li 2004; Rivard et al. 2008). Further, soil modeling mixture analysis (SMMA) was proposed to decrease within-class moisture differences for soil (Lobell et al. 2002; Somers et al. 2009).

In addition to the aforementioned techniques for addressing endmember variability, the other approach is the multiple endmember spectral mixture analysis (MESMA) method (Roberts et al. (1998), which considers all possible endmember combinations, and selects the best endmember set for each pixel. In MESMA, multiple endmembers were collected and saved in a spectra library, and numerous SMA models were constructed and tested with different combinations of types, number, and spectra of endmember classes for each individual pixel, and the best fit combination set was selected. Generally, the lowest root mean square error (RMSE) was used as the selection criterion. In addition, other selection techniques have also been developed, including count-based (COB)(Roberts et al. 2003), endmember average RMSE (EAR) (Dennison and Roberts 2003), minimum average spectral angle (MASA) (Dennison et al. 2004), and iterative endmember selection (IES) (Schaaf et al. 2011). In addition to MESMA, the endmember bundles approach proposed by Bateson and Curtiss (1996) is the other trial-and-error

67

technique for mitigating endmember variability. Specifically, instead of using only one endmember, a bundle of endmembers are collected and employed to construct endmember sets, and the minimum, mean, and maximum fractions for each land cover type are then extracted.

Although those proposed approaches have proven valuable in addressing endmember variability, there are still some challenging problems. In particular, most approaches still apply a set of fixed endmembers to extract image-wide land cover fractions. In fact, due to local variations of environmental and socio-economic factors (e.g. topography, climate, economic development, population density, and etc.), endmembers can be typically varied from location to location, and the selected endmembers may not be adequate to represent the complex conditions of a geographic area, which in turn results in erroneous estimates. While MESMA has addressed the endmember variability issue through including a variety of endmember sets, it is a pixel-based approach without considering geographic knowledge. Recently, Deng and Wu (2013) developed a spatial adaptive SMA (SASMA), with which local endmembers for a target pixel were selected within a moving window, and an inverse distance weighting approach was applied to derive the endmembers for the target pixels. SASMA, however, is a mathematical approach with empirically determined neighborhood size and distance-weighting functions (Li and Wu, 2015).

Instead of employing single-date reflectance imagery, a temporal mixture analysis (TMA) was proposed by Knight and Voth (2011) using multiple-temporal NDVI (Normalized Difference Vegetation Index) data. The results show that the 2-year NDVI temporal profiles have achieved a satisfactory performance for estimating urban imperviousness. Further, Yang (2012) applied TMA in Japan and demonstrated the ability of NDVI temporal profiles in estimating urban imperviousness at the national scale. Recently, Li and Wu (2014) proposed a phenology

based TMA and METMA (Multiple-Endmember Temporal Mixture Analysis) with the highlight of the importance of phenological information derived from NDVI temporal profiles, and they found with the extracted phenological information, one land cover type can be easily distinguished from another, and the issue of inter-class variability (such as the mixture of bare soil and impervious surface) can be effectively addressed. Furthermore, Li and Wu (2015) also successfully addressed the issue of endmember class selections through incorporating land use/land cover spatial information into TMA.

Although all proposed approaches have proven helpful for improving estimation accuracy, the issue of endmember variability has not been fully addressed. Therefore, in this study, we developed a geostatistical approach to approximate the "representative" endmembers for each individual pixel. In particular, we proposed to apply an ordinary kriging analysis method to interpolate the endmembers for each pixel. Ordinary kriging is a geostatistical approach and considered as a non-biased interpolation technique, as it can interpolate the value of a function at a given point by computing a weighted average of the known values of the function in the neighborhood of the point. It derives a best linear unbiased estimator based on assumptions on covariance and make use of Gauss-Markov theorem to prove the independence of the estimate and error, and finally generate reasonable results. Ordinary kriging has been widely applied in soil mapping, population estimation, climatology, etc. (Cressie 1993; Vauclin et al. 1983; Wu and Murray 2005). This geostatistical temporal mixture analysis (GTMA) method can be divided into three steps, including 1) identifying potential endmember candidates over the entire image using image endmember extraction and sampling, 2) calculating endmembers for each individual pixel using an ordinary kriging technique, and 3) estimating the endmember class fractions through spectral unmixing.

The rest of the paper is structured as follows. Section 4.2 describes the selected study area and data source. Section 4.3 introduces the proposed GTMA approach, including endmember extraction and sampling, per-pixel endmember estimation using ordinary kriging, and fractional land cover estimation using fully constrained linear temporal mixture analysis. The estimation results of the proposed GTMA and comparative analyses with PTMA and PMETMA are reported in Section 4.4. Finally, discussion and conclusions are provided in Sections 4.5 and 4.6.

4.2 Study area and data

States of Wisconsin, United States (U.S.) was selected as the study area for this research (see Figure15). Wisconsin is situated in the mid-western region of the U.S. with a geographic area of approximately 170,000 square kilometers and has experienced rapid urbanization during the past decades. According to 2010 U.S. census, the populations in Wisconsin was about 5.7 million, and with increments of approximately 16% from 1990 to 2010, and this trend was predicted to continue in the next decades (U.S. Census Bureau, 2014). Wisconsin is covered by a wide variety of land use/land cover types. Specifically, forest lands, including evergreen forest and deciduous forest, can be found in the northern part. Large patches of agricultural lands and pastures can be found in the southwest and northwest parts respectively. Comparatively, urban areas, including Madison, Milwaukee, and Green Bay, are majorly distributed in the southeast part of the State. As the major component of urbanized areas, impervious surfaces are composed of various manmade materials, such as asphalts for drive way, sidewalks and parking lots, concrete and cement for building rooftops, and tiles for residential house rooftops.

70
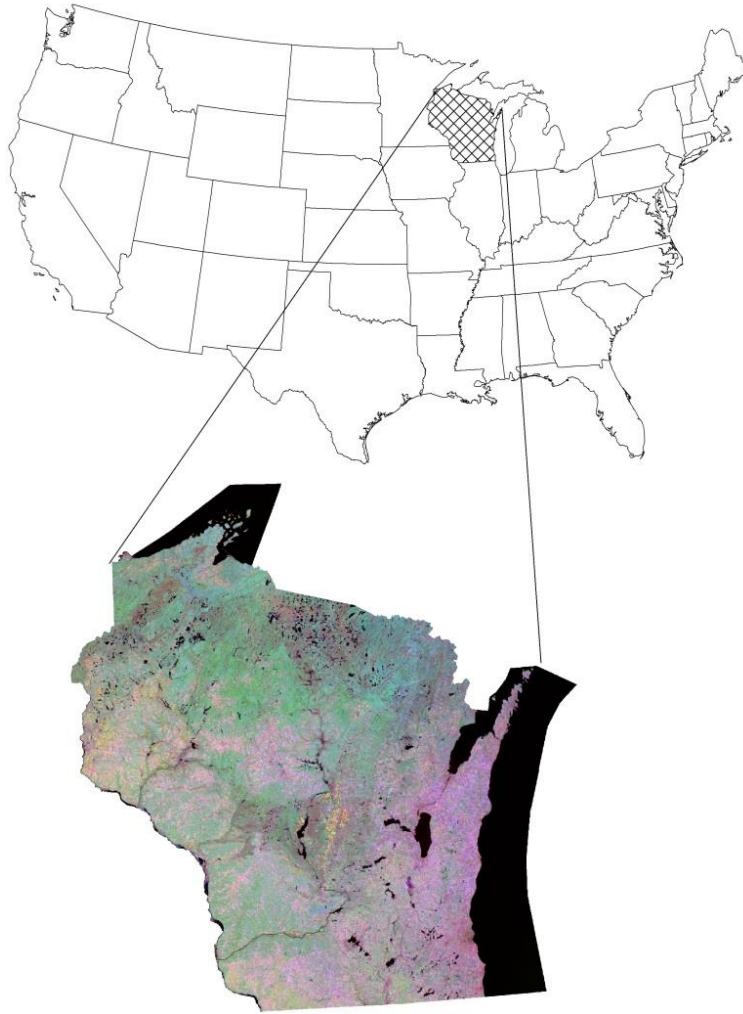
Figure 15 Study area: Wisconsin State, USA

In order to map subpixel impervious surfaces fractions in Wisconsin and North Carolina through the proposed GTMA, 44 (22 for each study area) MODIS (Moderate-resolution imaging spectroradiometer) NDVI images (1 band, Product of MOD13Q1) acquired in 2006 were employed (two images per month, except the one in late November for Wisconsin and one in late August for North Carolina as heavy cloud covered). All images were collected from the United States Geological Survey (USGS) website (www.usgs.gov) with a 0.5-pixel positional accuracy

and a spatial resolution of 250 meters. In addition to MODIS NDVI data, we also collected the

National Land Cover Data (NLCD) 2006 Percent Developed Imperviousness data from the

Multi-Resolution Land Characteristics Consortium (MRLC) website

(http://www.mrlc.gov/nlcd06_data.php) for accuracy assessment. NLCD data, generated by

USGS, is the national land cover dataset that covers the entire United States. The data was

produced based Landsat TM/ETM+ imagery at a spatial resolution of 30 meters, and updated for

every 5-10 years. For NLCD, the Anderson classification scheme was employed to classify the

image into ten major classes (see Table 5), and in this study, five land covers, including

agriculture, deciduous forest, evergreen forest, pasture, and impervious surface were considered.

Barren land and grassland were ignored due to their small areal coverages and the coarse

resolution (250m) of our remote sensing imagery. Further, water and wetlands were masked out

before spectral unmixing to mitigate spectral confusion.

Table 5 Land covers types in the study areas

Land cover type	Description
Urban	Areas with constructed materials and high number of impervious surfaces
Deciduous forest	Forest with trees losing the foliage seasonally
Evergreen forest	Forest with trees keeping leaves in all seasons
Pasture	Vegetation planted for livestock grazing
Grassland	Vegetation covered mainly by gramanoid or herbaceous, not subject to any intensive management
Agriculture	Areas for annual crops production
Barren land	Areas of glacial debris, sand, mines, bedrock, slides, desert pavement
Water	Areas of river, lake, reservoirs, streams
Wetland	Areas of forest or shrubland vegetation saturated with or covered with water

4.3 Methodology

To implement the proposed GTMA approach, three major steps were carried out, including endmember candidate extraction and sampling, spatially varying per-pixel endmember extraction using kriging, and fully constrained linear temporal mixture analysis. The details of these three steps are described as follows.

4.3.1 Endmember candidate extraction and sampling

Endmember selection is the first and the most important step for successful spectral unmixing. Typically, principal component analysis (PCA) or minimum noise fraction (MNF) transformation is employed to guide the selection of endmembers. Due to the ability of ordering components on the basis of signal to noise ratios, MNF was applied in this study to remove noise and guide endmember selection. In this study, several feature spaces were generated using the first several MNF components, and finally we found all expected endmembers could be identified from scatterplots of the first three MNF components (see Figure 16). With the 2-dimentional scatter plots generated using the first three MNF components; the vertices of these plots were selected as endmembers after verification with ground observations. These endmembers include agriculture, impervious surface, deciduous forest, evergreen forest, and pasture. Based on the pure spectra sets of endmembers chosen from the 2-dimentional scatter plot, a stratified random sampling was applied for each class to collect endmembers for each class, and 200 endmember samples were selected for agriculture, deciduous forest, evergreen forest, and pasture respectively, and 50 samples were chosen for impervious surfaces (as limited quantity of "pure" impervious surfaces exist) (see Figure 17). In order to show the spatial

73

variation of the collected endmember samples, the NDVI temporal profiles of endmembers (calculated by averaging all samples of each endmember) including the first standard deviation were quantified and showed in figure 18.
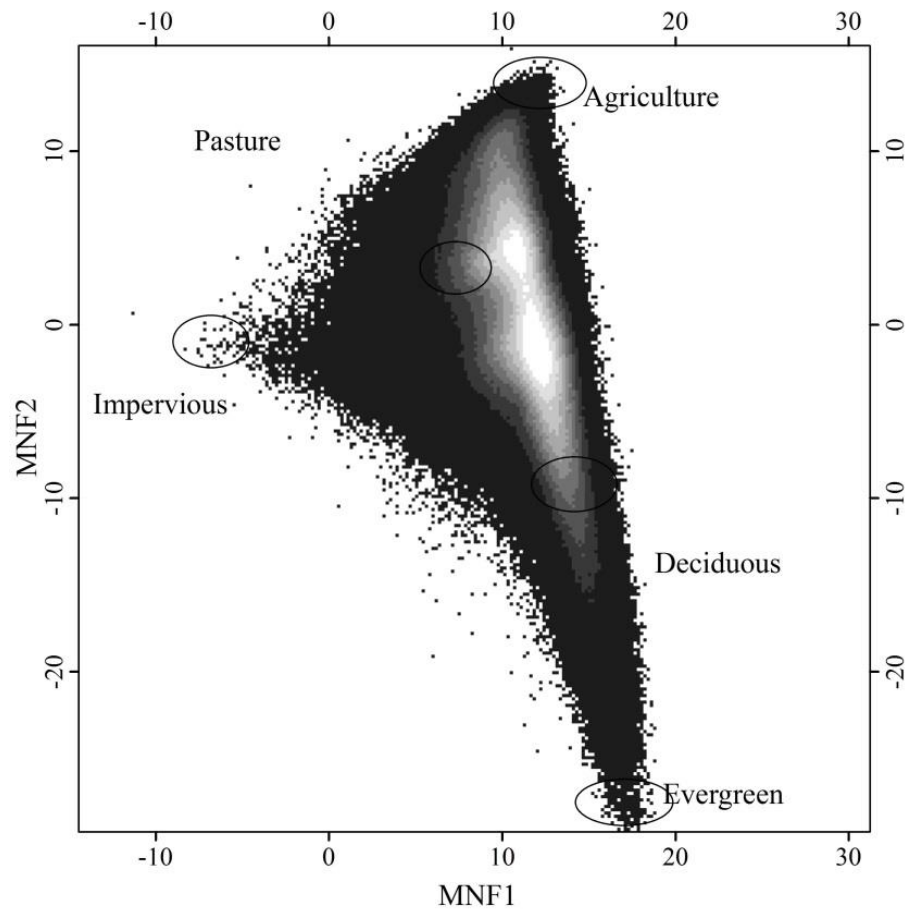
Figure 16 2-dimentional scatter plot generated from MNF components
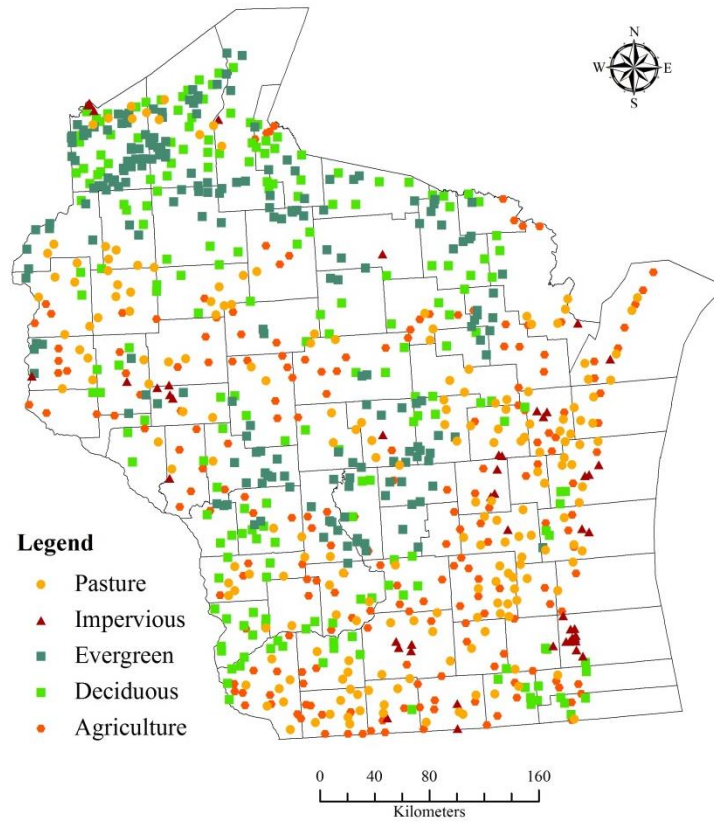
Figure 17 Spatial distribution of endmember class samples
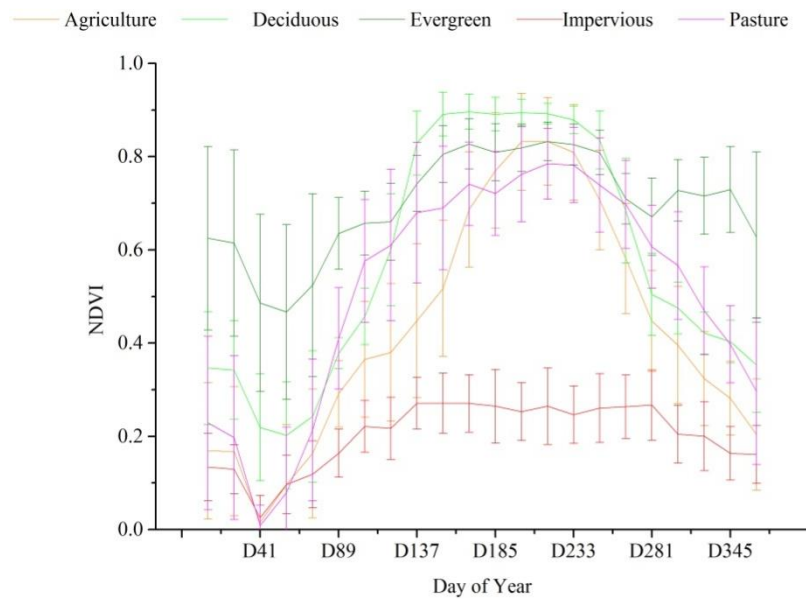
Figure 18 NDVI temporal profiles of selected endmember classes (including the 1st standard deviation)

4.3.2 Per-pixel endmember estimation using ordinary kriging

In order to apply ordinary kriging method to estimate the endmember for each class at per image pixel, a second moment stationary hypothesis (the correlation of two variables only associated with the spatial distance between them, and is not related to their location) test was conducted. The test results show that no significant variation can be detected and ordinary kriging analysis can be applied in further study. As the temporal profiles of each class include 22 NDVI bands in the stacked MODIS image, the ordinary kriging analysis needs to be implemented 22 times, each of which is to estimate the NDVI value for a particular band. The ordinary kriging was implemented with three major steps, including 1) estimating the experimental variogram of an NDVI value of a specific band for a particular endmember class using collected samples, 2) fitting the estimated experimental variogram into a mathematical model, and 3) interpolating the NDVI value of the specific band for the endmember at each pixel. In this study, we identified five endmember classes (e.g. agriculture, impervious surface, deciduous forest, evergreen forest, and pasture) and each of them has 22-band NDVI temporal profiles. Therefore, this ordinary kriging process needs to be replicated for 110 times to derive the per-pixel endmembers for all endmember classes.

The details of this ordinary kriging process for estimating NDVI value for band b ($1 <= b <= 22$) of endmember class i are shown as follows. The first step is to estimate the experimental variogram using Equation (4.1).

$$\hat{\gamma}(d) = \frac{1}{2n(d)} \sum_{d_{jk}=d} (NDVI_{i,b,j} - NDVI_{i,b,k})^2 \qquad (4.1)$$

Where, $\hat{\gamma}(d)$ is the experimental variogram with a lag of d, $NDVI_{i,b,j}$ and $NDVI_{i,b,k}$ are the NDVI values of endmember samples j and k, and d_{jk} is the distance between samples j and k. In this study, the variogram was derived by using the mean value of all directions. With the knowledge of the spatial structure extracted from the experimental variogram, several theoretical mathematical models including circular, spherical, exponential, Gaussian, and linear models were applied to fit the experimental variogram, and the one with the highest R^2 was selected as the best-fit model. Following the guidance provided by Curran and Atkinson(1998)and McBratney and Webster(1986), a weighted least square fitting method was applied to derive the mathematical function of $\gamma(d)$. With an appropriate mathematical expression of $\gamma(d)$, kriging attempts to minimize the squares of the difference between the estimated and the reference NDVI values, expressed in Equation (4.2).

Minimize
$$E\{[N\hat{D}VI_{i,b,s} - NDVI_{i,b,s}]^2\}$$
(4.2)
$$= 2\sum_{j=1}^{n} w_j \gamma(d_{js}) - \sum_{j=1}^{n}\sum_{k=1}^{n} w_j w_k \gamma(d_{jk})$$

Subject to $\sum_{j=1}^{n} w_j = 1$

$$N\hat{D}VI_{i,b,s} = \sum_{j=1}^{n} w_j NDVI_{i,b,j}$$

where $N\hat{D}VI_{i,b,s} = \sum_{j=1}^{n} w_j NDVI_{i,b,j}$ is the estimated value of NDVI of band b of endmember class i at pixel s, $NDVI_{i,b,s}$ and $NDVI_{i,b,j}$ are the NDVI value for band b of endmember i at pixels s and j, and w_j and w_k are the weights of pixels j and k. To solve this optimization problem, a Lagrangian relaxation method was applied to derive the weights, as well as the NDVI value for pixel s. In this study, the experimental variograms and fitted mathematic model were calculated using

GS+7.0, and ArcGIS10 was employed subsequently to implement the ordinary kriging for deriving the per-pixel endmember.

4.3.3 Fully constrained linear temporal mixture analysis

With the identified endmember classes and the corresponding endmembers derived from the ordinary kriging, a fully constrained linear TMA was conducted. The formulation of the TMA and the associated constraints are listed as follows:

$$NDVI_b = \sum_{i=1}^{N} f_i \times NDVI_{i,b} + e_b \tag{4.3}$$

Subject to $\sum_{i=1}^{N} f_i = 1$ and $f_i \geq 0$

Where $NDVI_b$ is the NDVI value for each band b, N is the total number of endmember classes (5), fi is the fraction of endmember class i, NDVIi,bis the NDVI value for band b of endmember i, and eb is the residual. The TMA was carried out based on the assumption that the NDVI temporal profile of a mixed pixel (NDVIb) is a linear combination of the estimated NDVI temporal profiles of all quantified endmember classes (NDVIi,b), and the areal abundances (fi) of all identified endmember classes can be extracted through implementing an inverse least squares deconvolution model. In order to present the physical meanings of the TMA results, the sum-to-one and non-negativity constraints were applied.

In order to assess the model fitness, the e_b and RMS error were applied. RMS error is typically used to measure the differences (also called residual) between predicted and observed values. RMS error can be expressed as follows:

78

$$\text{RMS} = \left(\frac{\sum_{b=1}^{B} e_b^2}{B}\right)^{1/2} \tag{4.4}$$

Where B is the number of bands (22) of the MODIS NDVI image.

4.3.4 Comparative analysis and accuracy assessment

For comparative purposes, Phenology based TMA (PTMA) and Phenology based METMA (PMETMA) have also been implemented in this study. With PTMA, instead of using the localized endmembers derived from kriging analysis, a mean endmember set was calculated through averaging the collected endmembers, and this mean endmember set was subsequently applied for the whole image to estimate impervious surfaces fractions using the fully constrained linear temporal mixture analysis. Different from PTMA, PMETMA allows the use of a variety of endmember set combinations, and selects the one with the best model fit. For details of the PTMA and PMETMA models, readers can refer to (Li and Wu, 2014).

To assess the performance of the proposed GTMA, as well as those of PTMA and PMETMA, the NLCD 2006 Percent Developed Imperviousness data from USGS was applied in this study as the ground truth data, and a pixel by pixel comparison was conducted. Two widely used accuracy assessment metrics, systematic error (SE, Equation 4.5) and mean absolute error (MAE, Equation 4.6), were calculated respectively to evaluate the performance of these three models. Specifically, SE quantifies the systematic bias (overestimation or underestimation), while MAE measure the overall precision.

$$SE = \frac{\sum_{j=1}^{N}(\bar{f}_j - f_j)}{N} \tag{4.5}$$

$$MAE = \frac{\sum_{j=1}^{N}|f_j - \bar{f}_j|}{N} \tag{4.6}$$

Where $\bar{f}_i$ is the estimated impervious surface fraction for pixel j, f_j is the referenced impervious surface fraction value collected from NLCD 2006 impervious surfaces fractions for pixel j, and N is the total number of pixels.

4.4 Results

4.4.1 Spatially varying endmember estimation using ordinary kriging

For estimating spatially varying per-pixel endmember for each endmember class, the ordinary kriging method was applied. Through analyzing the spatial variation structure of sampled endmembers for each class, we found that there is no significant anisotropy, and the variograms can be considered as isotropic. Results of experimental variograms and fitted exponential models of early August NDVI image (NDVI band 14), as an example, are illustrated in Figure 19. This result proves the existence of endmember variability, as well as the spatial autocorrelation of these endmembers. That is, the endmember of a pixel is likely to be similar to that of its neighbouring pixels, and significantly different from those of pixels farther away. With the experimental variograms and fitted mathematical models, the endmember of each land cover type, e.g. agriculture, deciduous forest, evergreen forest, impervious surface, and pasture, was interpolated for each image pixel. Taking impervious surfaces as examples, Figure 20 indicates that the estimated endmember is with significant spatial variations. For example, a relatively high NDVI values (e.g. 0.34) in early August were found in the northern part of Wisconsin, and a rather low NDVI values (e.g. 0.20) were discerned in the southern portion. In order to further illustrate the spatial variability of endmembers derived from the ordinary kriging, 10 samples

were randomly selected in the study area, and the corresponding endmembers for impervious surfaces in Wisconsin are shown in Figure 20B. These results further prove the existence of spatial variations of endmembers, and endmember variability should be carefully examined before spectral unmixing. Artifacts of the impervious surface endmember distribution, however, do exist in Figure 20. In particular, it appears that low NDVI values are found in or around urban areas, and significant higher NDVI values exist in rural areas (see Figure 20). This may be due to the lack of impervious surface endmember samples, as well as their uneven spatial distributions. Further improvements, may include the adoption of a more quantitative approach for selecting a larger number and evenly distributed endmembers. This, however, might be difficult to achieve due to the scarce of potential impervious surfaces endmember candidates.
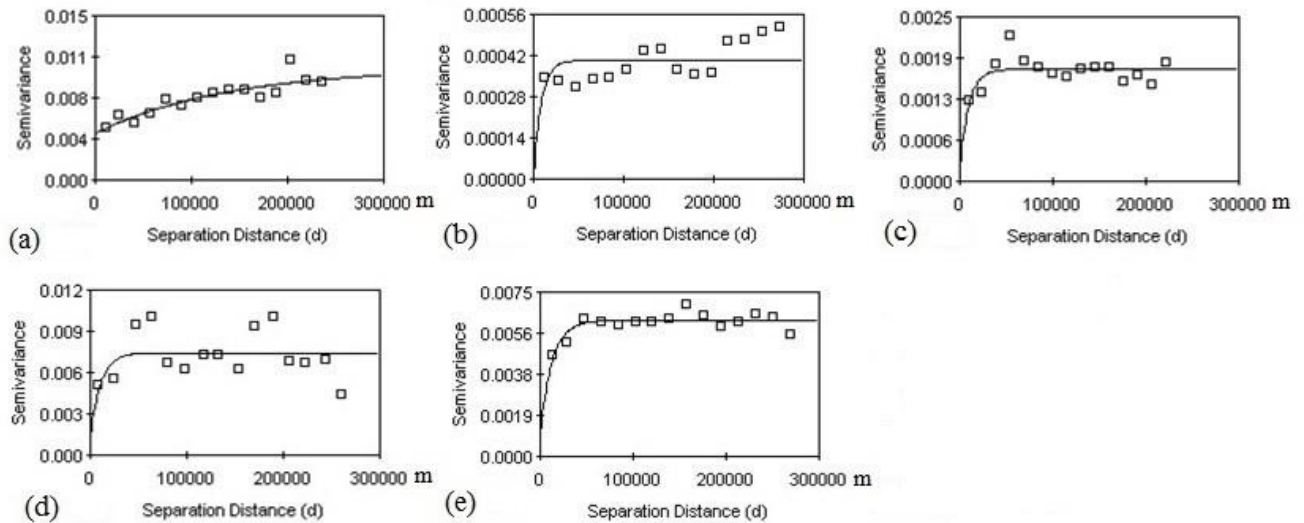
Figure 19 Variograms of pure spectra of (a) Agriculture (b) Deciduous forest (c) Evergreen forest (d) Impervious surface and (e) Pasture (Take early August as an example)

81
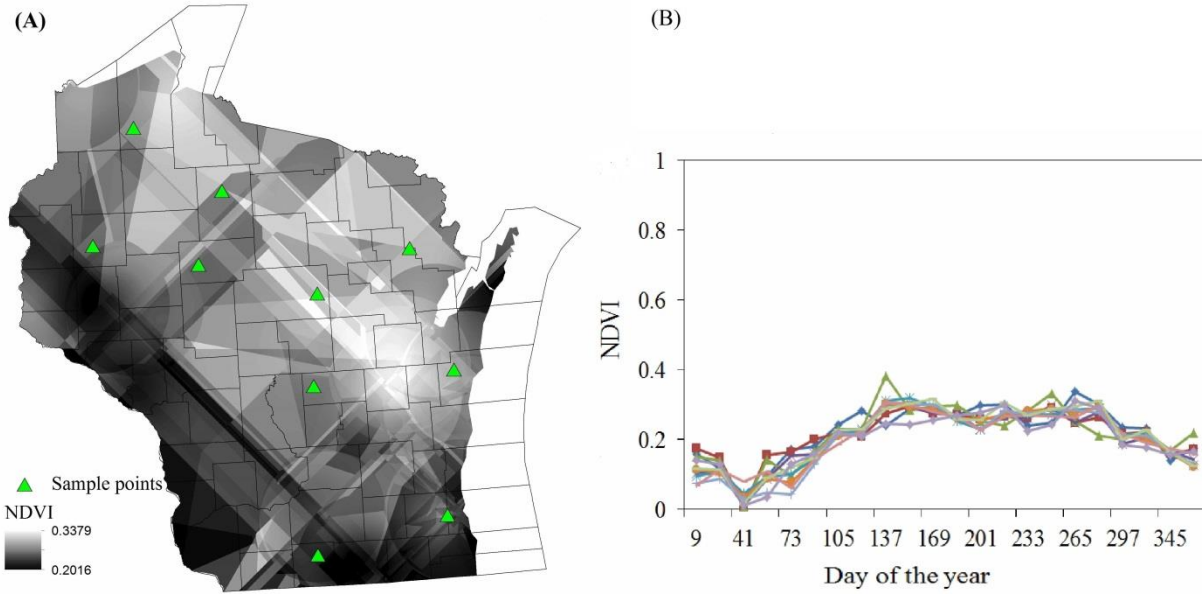
Figure 20 Interpolated impervious surface spectra using ordinary kriging and sampled NDVI temporal profile (Take early August as an example, colored lines are impervious surfaces temporal profiles from 10 sampling locations)

4.4.2 Fully constrained linear temporal mixture analysis

With the identified endmember classes and spatially varying per-pixel endmembers, we implemented the fully constrained linear temporal mixture analysis to extract the fractional land covers for each endmember class. Results (see Figure 21) illustrate that the spatial pattern of the modelled impervious surfaces corresponds well with our local knowledge of the study areas. In particular, high impervious surface fractions (ISF: 70-100%) are mainly located in the downtown area of urbanized areas such as Madison City (the state capital of Wisconsin) and Milwaukee City (the largest city of Wisconsin). Further, medium impervious surface fractions (ISF: 30-70%) are majorly distributed in the suburban areas such as Mequon, Grafton, and Oak Creek in Wisconsin which can be commonly categorized as residential areas. In addition, low impervious surface fractions (ISF: 0-30%) can be easily found in the northern and western parts of the Wisconsin which are majorly covered by vegetation. In addition to the visual examination, a

82

quantitative analysis was also conducted for the whole study area, developed areas (ISF>=30%) and less developed areas (<30%). The 30% of ISA threshold is selected based on the definition of developed lands of the NLCD (http://www.epa.gov/mrlc/definitions.html). Results (see Table6) indicate that the proposed GTMA has achieved a promising accuracy in modelling the impervious surface fractions. Specifically, the overall study area was with an SE of 2.98%and MAE of 3.83%. Detailed analysis indicate that GTMA performs better in less developed areas (MAE=3.71%) than developed areas (MAE=9.36%), and a slightly overestimation (SE=3.07%) for less developed areas and underestimation (SE=-1.49%) for developed areas have been detected.
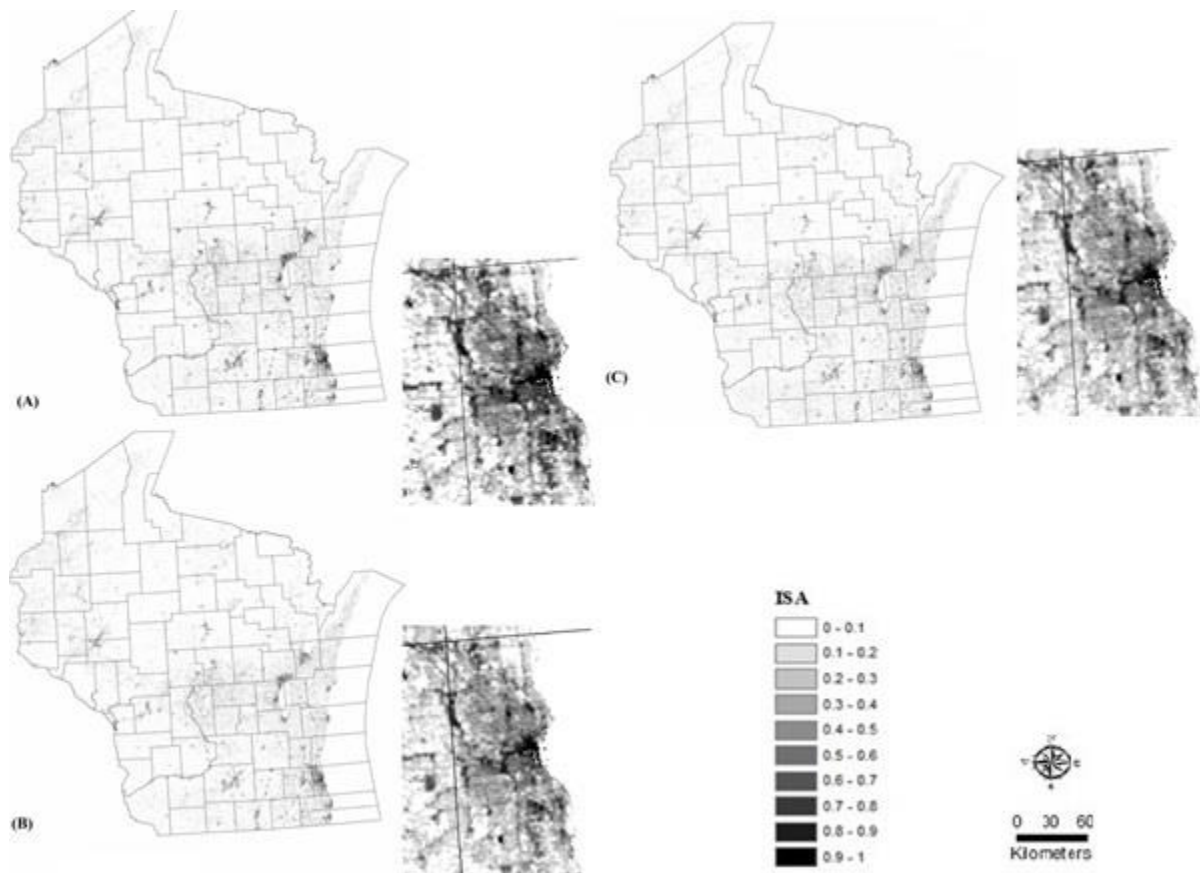
Figure 21 Estimated impervious surface fraction maps from (A) GTMA, (B) PTMA, (C) PMETMA

Table 6 Accuracy assessment of impervious surfaces with GTMA, PTMA, and PMETMA

			SE (%)	MAE (%)
	GTMA	Overall	2.98	3.83
		Developed	-1.49	9.36
		Less developed	3.07	3.71
	PTMA	Overall	3.25	4.03
Wisconsin		Developed	-8.17	12.15
		Less developed	3.43	3.9
	PMETMA	Overall	2.13	3.36
		Developed	-7.46	12.16
		Less developed	2.32	3.23

4.4.3 Comparative analysis

The estimation results (see Figure 21) indicate that impervious surface fraction maps generated from GTMA, PTMA, and PMETMA are with similar spatial distribution patterns. In particular, higher impervious surface fraction values can be found in the southeast Wisconsin (e.g. Milwaukee City), and significantly lower impervious surface fraction values are located in the western and northern Wisconsin, covered by wetlands, agriculture, and forest. Although with similar spatial patterns, one noticeable difference can be found in urban areas. That is, with PTMA and PMETMA, impervious surface fraction estimates in urban areas are much lower than those estimated with GTMA. In order to illustrate the improvement in developed areas, Milwaukee, the largest city in Wisconsin was selected and comparative maps were shown in Figure 21. It indicates that obvious underestimation can be detected with PTMA and PMETMA, and this problem has been effectively addressed with GTMA. Further quantitative analysis

84

confirms these visual observations. For the entire study area, as well as less developed areas, the performances of PTMA and PMETMA are comparable to that of GTMA. That is, these three models are with similar SE and MAE values. In urban areas, however, the performances of PTMA and PMETMA are significantly worse than that of GTMA. For instance, in urban areas, SE values of PTMA and PMETMA are (-8.17%) and (-7.46%) respectively, significantly higher than that of GTMA (-1.49%). Moreover, in urban areas, MAE values of PTMA and PMETMA are 12.15% 12.16% and 11.62% respectively, much higher than those of GTMA (9.36%). Moreover, in order to illustrate the relationship between the modelled and referenced impervious surfaces fractions, a scatter plot was also created through stratified randomly selected samples (see Figure 22). Figure 22 shows that with the proposed GTMA, the underestimation in the developed areas has been highly addressed, and generally, the proposed GTMA has achieved a better performance with a higher R^2. In summary, when compared to PTMA and PMETMA, the proposed GTMA has achieved a comparable performance for the whole study area and less developed areas, and a much better performance for developed areas.
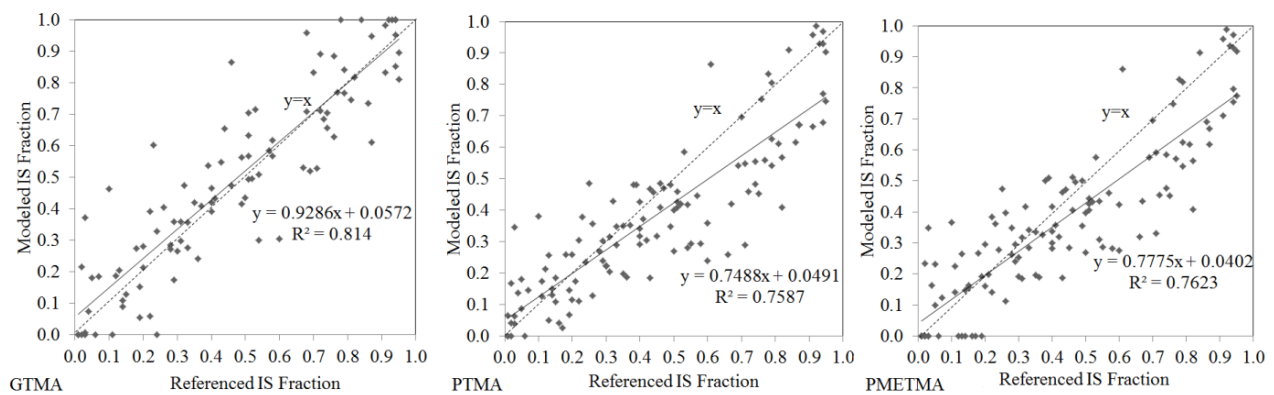
Figure 22 Accuracy assessment of the impervious surfaces estimation by the GTMA, PTMA, and PMETMA

4.5 Discussion

4.5.1 Estimating spatially varying per-pixel endmembers using geostatistical techniques

Endmember selection has been widely considered as a key step of spectra unmixing, and exerts significant impact on the estimation accuracy of fractional land covers. Specifically, as environmental factors vary spatially, endmember spectra tend to be different across space. However, derived endmember spectra are often considered identical and applied to all the pixels in a remote sensing image. While MESMA accommodates endmember variability through employing a variety of endmember sets, it only employs pixel-based spectral information, without considering spatial knowledge. Recently, the SASMA proposed by Deng and Wu (2013) attempted to address endmember variability through deriving endmembers for a particular pixel through applying an inverse distance weighting (IDW) approach using all endmember candidates in a moving window. This approach, however, only employs the distance for generating weights, and the statistical meanings of the spatial variations of endmembers have been neglected. As a consequence, inappropriate endmembers may be selected and applied in SMA and result in erroneous estimations. The proposed GTMA is able to address the aforementioned issues. In particular, a spatially varying per-pixel endmember was calculated for each image pixel using a rigorous geostatistical technique, ordinary kriging interpolation technique.

4.5.2 Endmember variability in developed and less-developed areas

Compared with the results we derived from PTMA and PMETMA (Li and Wu, 2014), the performance of GTMA is comparable in the whole study area and less developed areas. The improvements in developed areas (see Figure 21), however, are much more significant (SE of -

1.49% vs. -8.17% and-7.46%, and MAE of 9.36% vs. 12.15% and 12.16%) when compared to less-developed areas. These results might indicate that endmember variability play an even more important role in developed areas than in less-developed areas. This may be due to the complexity and heterogeneity of urban landscapes. That is, unlike less-developed areas with relatively homogenous land cover types and corresponding spectral signatures, developed areas are covered by heterogeneous and anthropogenic materials with different physical and chemical compositions. For instance, impervious surfaces may be comprised by several different materials for different purposes, such as asphalts for drive way, sidewalks, and parking lot, concrete and cement for building rooftop, and tiles for residential house rooftops. In addition, the same building materials with different ages may also show quite different spectral responses. As a result, endmember variability may play a more essential role in developed areas when compared to less-developed areas. The advantages of the proposed GTMA approach, therefore, are to better approximate the spatially varying per-pixel endmembers, especially for developed areas with heterogeneous and anthropogenic materials.

4.6 Conclusions and future research directions

This study developed a GTMA approach to address the endmember variability issue for estimating regional impervious surface distributions using time-series MODIS NDVI imagery acquired in Wisconsin, United States. In particular, an ordinary kriging interpolation technique was employed to extract spatially varying pixel specific endmembers. Consequently, a fully constrained linear temporal mixture analysis with spatially varying endmember was developed to quantify impervious surface distributions.

Analysis of results suggests several conclusions. First, the proposed GTMA has achieved a satisfactory performance for examining the fractions of impervious surfaces in the entire study area of Wisconsin with an SE of 2.98% and MAE of 3.83%. Detailed analysis indicates that a better performance has been achieved in less developed areas than developed areas, and slightly underestimation and overestimation has been detected in developed areas and less developed areas respectively. Second, for a comparative purpose, PTMA and PMETMA have been implemented and the comparative analysis results indicate that the proposed GTMA has achieved a comparable performance with PTMA and PMETMA in the overall area and less developed area. However, a significant improvement has been found in developed areas of Wisconsin with the SE of -1.49% (vs. -8.17% and -7.46%) and MAE of 9.36% (vs.12.15% and 12.16%).

Although the proposed GTMA has achieved a promising accuracy for estimating impervious surfaces fractions through addressing endmember variability, endmember class variability has not been fully considered in this study. In fact, the selection of endmember classes is the foundation of endmember extraction, and it may play a very important role in successfully spectral unmixing. Therefore, one future research could be considering both endmember class variability and endmember variability through constructing an integrated temporal mixture analysis model to improve the estimation accuracy. In addition, in this study, only local spatial information has been incorporated in spectral unmixing analysis, and regional spatial information has been more or less neglected. However, such information may also be helpful in addressing the endmember variability issue. Therefore, another future research direction could be incorporating both regional and local spatial information into temporal mixture analysis.

CHAPTER5 CONCLUSIONS

5.1 Summary

Spectral mixture analysis (SMA) has been considered as a powerful and widely used technique for estimating fractional land covers (e.g. impervious surfaces). For impervious surface estimation, though, effects of temporal and spectral variability of endmembers have not been successfully addressed. In particular, impervious surface estimation is likely to vary in different seasons, majorly due to shadowing effects of vegetation canopy in summer and the confusion between impervious surfaces and soil in winter. Moreover, endmember variability and multi-collinearity have adversely impacted the accurate estimation of impervious surface distribution with coarse resolution remote sensing imagery. To address these issues, this study incorporated phenology, spatial information, as well as geostatistic method into SMA to derive improved impervious surfaces fractions at a large-scale. Specifically, three new approaches have been developed in the dissertation to improve the large-scale impervious surface estimation accuracy. On one hand, phenological information of all endmembers have been extracted and applied in unmxing analysis for addressing the issue of seasonal sensitivity and spectral confusion using one-year continuous MODIS NDVI data. On the other hand, a logistic regression analysis was conducted in this study to analyze the spatial relationship between endmembers and surrounding environmental and socio-economic factors in support of the selection of appropriate number and types of endmember classes for handling the endmember class variability issue. Finally, with the identified per-pixel level endmember classes, the selection of the corresponding pure endmember spectra has become a key step of SMA. In order to consider the endmember spectra spatial variation, a geostatistic method, ordinary kriging

interpolation technique, has been applied in this study to generate per-pixel spatially varied endmember spectra for overcoming the issue of endmember variability.

5.2 Contributions

The first contribution of this research is the successful incorporation of phenology information into SMA for addressing the challenging issue of seasonal variations of vegetation and spectral confusion between impervious surfaces and bare soil. With a single date remote sensing imagery, impervious surface is sensitive to the seasonal change and easy to be mis-estimated largely due to the obstruction by large tree crowns in summer and the confusion with soil in winter. With the developed phenology based method, temporal mixture analysis, can partially address the seasonal variability problem by adopting one-year multi-temporal NDVI data with four integral phenological phases (i.e., dormancy, green-up, maturity, senescence). Specifically, urban impervious surfaces only experience the dormancy phenophase, with low NDVI values throughout the year. Bare soil experiences dormancy in winter (e.g. with low NDVI values), green-up in spring (with elevated NDVI values associated with the growth of vegetation), maturity in summer (with high NDVI values), and senescence in autumn (with decreasing NDVI values due to the harvest of agricultural lands). Consequently, the significant phenophase difference between impervious surfaces and soil facilitates their discrimination with phenology-based approaches.

The second contribution of this research is that the spatial information has been successfully incorporated into SMA to handle the issue of endmember class variability. With SMA, the choice of endmember classes is the foundation of endmember extraction and key to the

successfully application of SMA. Due to the spatial variation of the natural landscapes, the distribution of endmember classes tends to illustrate spatial variability. With the simple SMA model, the same endmember class set of each individual pixel is applied for the whole image, and neglects their spatial distributions. In this research, a logistic regression model was applied to estimate the distribution probability of a land use land cover (LULC) type through analyzing the relationships among LULCs and their socio-economic and environmental factors, such as distance to the nearest city, distance to water, elevation, slope, etc. And then we incorporated LULC probability information into the selections of endmember class type and number, and further inputted to spectral unmixing for better derivation of impervious surface estimates. The selected endmember classes with clear physical meanings can effectively improve the estimation accuracy for fractional land cover estimates. Results of this study indicate that it is highly necessary to conduct the selection of endmember class type and number prior to spectral unmixing.

The third contribution of this research is the application of geostatistic method in SMA to overcome the endmember spectra variability issue. Endmember spectra selection has been widely considered as a key step of spectra unmixing, and exerts significant impact on the estimation accuracy of fractional land covers. Specifically, as environmental factors vary spatially, endmember spectra tend to be different across space. However, derived endmember spectra are often considered identical and applied to all the pixels in a remote sensing image. As a consequence, inappropriate endmembers may be selected and applied in SMA and result in erroneous estimations. In this dissertation research, a geostatistic approach, ordinary kriging interpolation technique, has been employed to address the aforementioned issues. In particular, a

spatially varying per-pixel endmember was derived for each image pixel using a rigorous geostatistical technique, ordinary kriging interpolation technique.

5.3 Future research

Future research will be focusing on two aspects. First, it is necessary to further improve the performance of the unmixing analysis model and impervious surface estimation accuracy through simulation techniques and other mathematical methods. Until now, the model performance of unmixing analysis is highly associated with the selected study area and the quality of the remote sensing image. Therefore, it's difficult to make consistent and confident conclusions for comparing different unmixing methods. Moreover, in most studies, endmembers are assumed to be with equal probability at the per-pixel level without a prior assumptions about the spatial distribution. However, dissertation research demonstrates that the distribution probability of land use land covers varies spatially. Multiple mathematical methods such as Bayesian and Markov chain may serve as a better alternative to consider that a prior knowledge in SMA for improving the model performance. Second, with the improved modeling performance and estimation accuracy, another future research direction would be how to apply the proposed methods in associated application studies such as population estimation, environmental evaluation, public transportation optimization, etc.

REFERENCES

Arnold, C.L., & Gibbons, C.J. (1996). Impervious surface coverage - The emergence of a key environmental indicator. *Journal of the American Planning Association, 62*, 243-258.

Asner, G.P., & Lobell, D.B. (2000). A biogeophysical approach for automated SWIR unmixing of soils and vegetation. *Remote Sensing of Environment, 74*, 99-112.

Ball, J.E., Bruce, L.M., & Younan, N.H. (2007). Hyperspectral pixel unmixing via spectral band selection and DC-insensitive singular value decomposition. *Ieee Geoscience and Remote Sensing Letters, 4*, 382-386.

Bateson, A., & Curtiss, B. (1996). A method for manual endmember selection and spectral unmixing. *Remote Sensing of Environment, 55*, 229-243.

Bateson, C.A., Asner, G.P., and Wessman, C.A. (2000). Endmember bundles: a new approach to incorporating endmember variability into spectral mixture analysis. *IEEE Transactions on Geoscience and Remote Sensing* 38, 1083-1094.

Bauer, M.E., Heinert, J.J., Doyle, J.K., & Yuan, F. (2004). Impervious surface mapping and change monitoring using Landsat remote sensing. In, *ASPRS annual conference proceedings*. Denver,Colorado

Bedini, E. (2009). Mapping lithology of the Sarfartoq carbonatite complex, southern West Greenland using HyMap imaging spectrometer data. *Remote Sensing of Environment*, *113*, 1208-1219.

Ben-Dor, E., Irons, J.R., & Epema, G. (1999). Soil reflectance. In A.N. Rencz, & R.A. Ryerson (Eds.), *Manual of Remote Sensing, Volume 3, Remote Sensing for the Earth Sciences* (pp. 111-188). New York: John Wiley & Sons

Ben-Dor, E., Levin, N., & Saaroni, H. (2001). A spectral based recognition of the urban environment using the visible and near-infrared spectral region (0.4-1.1 mu m). A case study over Tel-Aviv, Israel. *International Journal of Remote Sensing, 22*, 2193-2218.

Bhatti, S. and Tripathi, N. (2014). Built-up area extraction using Landsat 8 OLI imagery.*GIScience & Remote Sensing 51*, 445-467.

Brabec, E., Schulte, S., & Richards, P.L. (2002). Impervious surfaces and water quality: A review of current literature and its implications for watershed planning. *Journal of Planning Literature, 16*, 499-514.

Brun, S.E., & Band, L.E. (2000). Simulating runoff behavior in an urbanizing watershed. *Computers, Environment and Urban Systems, 24*, 5-22.

Chang, C.I., & Ji, B.H. (2006). Weighted abundance-constrained linear spectral mixture analysis. *Ieee Transactions on Geoscience and Remote Sensing, 44*, 378-388.

Cressie, N. 1993. *Statistics for spatial data*. (Revised edition ed.). New York: Wiley

Cunningham, S., Rogan, J., Martin, D., Delauer, V., McCauley, S. and Shatz, A.(2015) Mapping land development through periods of economic bubble and bust in Massachusetts using Landsat time series data.*GIScience & Remote Sensing 52*, 397-415.

Curran, P.J., and Atkinson, P.M. (1998). Geostatistics and remote sensing. *Progress in Physical Geography 22*, 61-78.

Demarchi, L., Canters, F., Chan, J.C.-W., & Van de Voorde, T. (2012). Multiple Endmember Unmixing of CHRIS/Proba Imagery for Mapping Impervious Surfaces in Urban and Suburban Environments. *Ieee Transactions on Geoscience and Remote Sensing, 50*, 3409-3424.

Dendoncker, N., Rounsevell, M., & Bogaert, P. (2007). Spatial analysis and modelling of land use distributions in Belgium. *Computers Environment and Urban Systems, 31*, 188-205.

Deng, C., & Wu, C. (2013). A spatial adaptive spectral mixture analysis of mapping subpixel urban impervious surface distribution. *Remote Sensing of Environment 133, 62-70.*

Dennison, P.E., Halligan, K.Q., & Roberts, D.A. (2004). A comparison of error metrics and constraints for multiple endmember spectral mixture analysis and spectral angle mapper. *Remote Sensing of Environment, 93*, 359-367.

Dennison, P.E., & Roberts, D.A. (2003). Endmember selection for multiple endmember spectral mixture analysis using endmember average RMSE. *Remote Sensing of Environment, 87*, 123-135.

Dennison, P.E. Fryer, G., Roth, K. Roberts, D.A., (2011). Mapping plant functional types at multiple spatial resolutions using imaging spectrometer data. *GIScience & Remote Sensing 48*, 324-344.

Dobigeon, N., Moussaoui, S., Coulon, M., Tourneret, J.-Y., & Hero, A.O. (2009). Joint Bayesian Endmember Extraction and Linear Unmixing for Hyperspectral Imagery. *IEEE Transactions on Signal Processing, 57*, 4355-4368.

Dobigeon, N., Tourneret, J.-Y., & Chang, C.-I. (2008). Semi-supervised linear spectral unmixing using a hierarchical Bayesian model for hyperspectral imagery. *IEEE Transactions on Signal Processing, 56*, 2684-2695.

Eches, O., Dobigeon, N., & Tourneret, J.-Y. (2011). Enhancing Hyperspectral Image Unmixing With Spatial Correlations. *Ieee Transactions on Geoscience and Remote Sensing, 49*, 4239-4247.

Eckmann, T.C., Still, C.J., Roberts, D.A., Michaelsen, J.C., (2010). Variations in Subpixel Fire Properties with Season and Land Cover in Southern Africa. *Earth Interactions 14(6)*, 1-29.

Elmore, A.J., Mustard, J.F., Manning, S.J., Lobell, D.B., (2000). Quantifying Vegetation Change in Semiarid Environments: Precision and Accuracy of Spectral Mixture Analysis and the Normalized Difference Vegetation Index. *Remote Sensing of Environment 73*, 87-102.

Elvidge, C.D., Tuttle, B.T., Sutton, P.S., Baugh, K.E., Howard, A.T., Milesi, C., Bhaduri, B.L., & Nemani, R. (2007). Global distribution and density of constructed impervious surfaces. *Sensors, 7*, 1962-1979.

Foody, G.M., & Cox, D.P. (1994). Sub-pixel land-cover composition estimation using a linear mixture model and fuzzy membership functions. *International Journal of Remote Sensing, 15*, 619-631.

Franke, J., D. A. Roberts, K. Halligan, and G. Menz. (2009). Hierarchical Multiple Endmember Spectral Mixture Analysis (MESMA) of hyperspectral imagery for urban environments.*Remote Sensing of Environment113 (8)*:1712-23.

Fry, J. A., G. Xian, S. Jin, J. A. Dewitz, C. G. Homer, L. Yang, C. A. Barnes, N. D. Herold, and J. D. Wickham. (2012). Completion of the 2006 National Land Cover Database Update for the Conterminous United States. *Photogrammetric Engineering and Remote Sensing*, *77*, 858-864.

Gilabert, M.A., García-Haro, F.J., and Meliá, J. (2000). A Mixture Modeling Approach to Estimate Vegetation Parameters for Heterogeneous Canopies in Remote Sensing. *Remote Sensing of Environment 72*, 328-345.

Gillies, R.R., Box, J.B., Symanzik, J., & Rodemaker, E.J. (2003). Effects of urbanization on the aquatic fauna of the Line Creek watershed, Atlanta - a satellite perspective. *Remote Sensing of Environment, 86*, 411-422.

Gluch, R., Quattrochi, D.A., & Luvall, J.C. (2006). A multi-scale approach to urban thermal analysis. *Remote Sensing of Environment, 104*, 123-132.

Goetz, S., & Fiske, G. (2008). Linking the diversity and abundance of stream biota to landscapes in the mid-Atlantic USA. *Remote Sensing of Environment, 112*, 4075-4085.

Goetz, S.J., Jantz, P., & Jantz, C.A. (2009). Connectivity of core habitat in the Northeastern United States: Parks and protected areas in a landscape context. *Remote Sensing of Environment, 113*, 1421-1429.

Goodwin, N., N. C. Coops, and C. Stone. (2005). Assessing plantation canopy condition from airborne imagery using spectral mixture analysis and fractional abundances. *International Journal of Applied Earth Observation and Geoinformation* 7 (1):11-28..

Green, A. A., M. Berman, P. Switzer, and M. D. Craig. (1988). A transformation for ordering multispectral data in terms of image quality with implications for noise removal. *IEEE Transactions on Geoscience and Remote Sensing* 26 (1):65-74.

Grubler, A. (1994). Technology and global change: Land-use, past and present. Edited by W.B. Merye and B.L. Turner, *Changes in Land Use and Land Cover: A Global Perspective*. London, UK: Cambridge University Press.

Guttikunda, S. K., G. R. Carmichael, G. Calori, C. Eck, and J. H. Woo. 2003. "The contribution of megacities to regional sulfur pollution in Asia." Atmospheric Environment 37 (1):11-22.

Herold, M., Roberts, D.A., Gardner, M.E., & Dennison, P.E. (2004). Spectrometry for urban area remote sensing - Development and analysis of a spectral library from 350 to 2400 nm. *Remote Sensing of Environment, 91*, 304-319.

Hestir, E.L., Khanna, S., Andrew, M.E., Santos, M.J., Viers, J.H., Greenberg, J.A., Rajapakse, S.S., and Ustin, S.L. (2008). Identification of invasive vegetation using hyperspectral remote sensing in the California Delta ecosystem.*Remote Sensing of Environment 112*, 4034-4047.

Hu, X., & Weng, Q. (2009). Estimating impervious surfaces from medium spatial resolution imagery using the self-organizing map and multi-layer perceptron neural networks. *Remote Sensing of Environment, 113*, 2089-2102.

Hu, X., & Weng, Q. (2011). Estimating impervious surfaces from medium spatial resolution imagery: a comparison between fuzzy classification and LSMA. *International Journal of Remote Sensing, 32*, 5645-5663.

Huang, C., & Townshend, J.R.G. (2003). A stepwise regression tree for nonlinear approximation: applications to estimating subpixel land cover. *International Journal of Remote Sensing, 24*, 75-90.

Hurd, J.D., & Civo, D.L. (2004). Temporal characterization of impervious surfaces for the State of Connecticut. In, *ASPRS Annual Conference Proceeddings*. Denver, Colorado.

Imhoff, M.L., Zhang, P., Wolfe, R.E., & Bounoua, L. (2010). Remote sensing of the urban heat island effect across biomes in the continental USA. *Remote Sensing of Environment, 114*, 504-513.

Irons, J.R., Weismiller, R.A., & Petersen, G.W. (1989). Soil reflectance. In G. Asrar (Ed.), *Theory and Application of Optical Remote Sensing*. New York, NY: John Wiley and Sons.

Jantz, C. A., S. J. Goetz, and M. K. Shelley. (2004). Using the SLEUTH urban growth model to simulate the impacts of future policy scenarios on urban land use in the Baltimore - Washington metropolitan area.*Environment and Planning B: Planning and Design 31 (2)*:251-71.

Jia, G.J., Burke, I.C., Goetz, A.F.H., Kaufmann, M.R., Kindel, B.C., (2006). Assessing spatial patterns of forest fuel using AVIRIS data. *Remote Sensing of Environment 102*, 318-327.

Johnson, P.E., Smith, M.O., Taylorgeorge, S., & Adams, J.B. (1993). A semiempirical method for analysisi of the reflectance spectra of binary mineral mixtures. *Journal of Geographical Research, 88*, 3557-3561

Keshava, N. (2003). Survey of spectral unmixing algorithms.*Lincoln Laboratory Journal 14*, 55-78.

Knight, J., & Voth, M. (2011). Mapping Impervious Cover Using Multi-Temporal MODIS NDVI Data. *Ieee Journal of Selected Topics in Applied Earth Observations and Remote Sensing, 4*, 303-309.

Lee, S., and R. G. Lathrop. (2006). Subpixel analysis of Landsat ETM+ using Self-Organizing Map (SOM) neural networks for urban land cover characterization. I*EEE Transactions on Geoscience and Remote Sensing 44 (6)*:1642-54.

Lelong, C.C.D., Pinet, P.C., and Poilvé, H. (1998). Hyperspectral Imaging and Stress Mapping in Agriculture: A Case Study on Wheat in Beauce (France). *Remote Sensing of Environment 66*, 179-191. d

Li, G., Lu, D., Moran, E. and Hetrick, S.(2013). Mapping impervious surface area in the Brazilian Amazon using Landsat Imagery. *GIScience & Remote Sensing 50*, 172-183.

Li, J. (2004). Wavelet-based feature extraction for improved endmember abundance estimation in linear unmixing of hyperspectral signals. *IEEE Transactions on Geoscience and Remote Sensing, 42*, 644-649.

Li, W., Wu, C., (2013). A spatially explicit method to examine the impact of urbanisation on natural ecosystem service values. *Journal of Spatial Science 58(2)*, 275-289.

Li, W., Wu, C., (2014). Phenology-based temporal mixture analysis for estimating large-scale impervious surfaces distributions. *International Journal of Remote Sensing 35(2)*, 779-795.

Li, W., and Wu, C. (2015). Incorporating land use land cover probability information into endmember class selections for temporal mixture analysis.*ISPRS Journal of Photogrammetry and Remote Sensing 101*, 163-173.

Li, W., Wu, C., Zang, S., (2014). Modeling urban land use conversion of Daqing City, China: a comparative analysis of "top-down" and "bottom-up" approaches. *Stochastic Environmental Research and Risk Assessment*, 817-828.

Lin, G. C. S., and S. P. S. Ho. (2003). China's land resources and land-use change: insights from the 1996 land survey.*Land Use Policy* 20 (2):87-107.

Liu, T., Yang, X., (2013). Mapping vegetation in an urban area with stratified classification and multiple endmember spectral mixture analysis. *Remote Sensing of Environment 133*, 251-264.

Liu, J., Miller, J.R., Haboudane, D., Pattey, E., and Hochheim, K. (2008). Crop fraction estimation from casi hyperspectral data using linear spectral unmixing and vegetation indices.*Canadian Journal of Remote Sensing 34*, S124-S138.

Lobell, D.B., Asner, G.P., Law, B.E., & Treuhaft, R.N. (2002). View angle effects on canopy reflectance and spectral mixture analysis of coniferous forests using AVIRIS. *International Journal of Remote Sensing, 23*, 2247-2262.

Lu, D., Moran, E., & Hetrick, S. (2011). Detection of impervious surface change with multitemporal Landsat images in an urban-rural frontier. *ISPRS J Photogramm Remote Sens, 66*, 298-306.

Lu, D., & Weng, Q. (2006). Use of impervious surface in urban land-use classification. *Remote Sensing of Environment, 102*, 146-160.

Lu, D., & Weng, Q. (2009). Extraction of urban impervious surfaces from an IKONOS image. *International Journal of Remote Sensing, 30*, 1297-1311.

Lu, D.S., & Weng, Q.H. (2004). Spectral mixture analysis of the urban landscape in Indianapolis with landsat ETM plus imagery. *Photogrammetric Engineering and Remote Sensing, 70*, 1053-1062.

Madhavan, B.B., Kubo, S., Kurisaki, N., & Sivakumar, T. (2001). Appraising the anatomy and spatial growth of the Bangkok Metropolitan area using a vegetation-impervious-soil model through remote sensing. *International Journal of Remote Sensing, 22*, 789-806.

Maselli, F. (2001). Definition of spatially variable spectral endmembers by locally calibrated multivariate regression analyses. *Remote Sensing of Environment, 75*, 29-38.

McBratney, A.B., and Webster, R. (1986). Choosing functions for semi-variograms of soil properties and fitting them to sampling estimates.*Journal of Soil Science 37*, 617-639.

Miao, X., Gong, P., Swope, S., Pu, R., Carruthers, R., Anderson, G.L., Heaton, J.S., & Tracy, C.R. (2006). Estimation of yellow starthistle abundance through CASI-2 hyperspectral imagery using linear spectral mixture models. *Remote Sensing of Environment, 101*, 329-341.

Michishita, R., Jiang, Z., & Xu, B. (2012). Monitoring two decades of urbanization in the Poyang Lake area, China through spectral unmixing. *Remote Sensing of Environment, 117*, 3-18.

Mohapatra, R.P., & Wu, C. (2010). High Resolution Impervious Surface Estimation: An Integration of Ikonos and Landsat-7 ETM+ Imagery. *Photogrammetric Engineering and Remote Sensing, 76*, 1329-1341.

Newman, P., and J.R. Kenworthy. (1999). Sustainability and cities: overcoming automobile dependence. Washington D.C.: Island Press.

Overmars, K.P., de Koning, G.H.J., & Veldkamp, A. (2003). Spatial autocorrelation in multi-scale land use models. *Ecological Modelling, 164*, 257-270.

Pauleit, S., and F. Duhme. (2000). Assessing the environmental performance of land cover types for urban planning.*Landscape and Urban Planning 52 (1)*:1-20.

Phinn, S., Stanford, M., Scarth, P., Murray, A.T., & Shyy, P.T. (2002). Monitoring the composition of urban environments based on the vegetation-impervious surface-soil (VIS) model by subpixel analysis techniques. *International Journal of Remote Sensing, 23*, 4131-4153.

Pielke, R. A. (2005). Land use and climate change.*Science 310 (5754)*:1625-6.

Plaza, A., Martinez, P., Perez, R., & Plaza, J. (2002). Spatial/spectral endmember extraction by multidimensional morphological operations. *Ieee Transactions on Geoscience and Remote Sensing, 40*, 2025-2041.

Plaza, A., Martinez, P., Perez, R., & Plaza, J. (2004). A quantitative and comparative analysis of endmember extraction algorithms from hyperspectral data. *Ieee Transactions on Geoscience and Remote Sensing, 42*, 650-663.

Pontius Jr, R.G., Schneider, L.C., (2001). Land-cover change model validation by an ROC method for the Ipswich watershed, Massachusetts, USA. *Agriculture, Ecosystems & Environment 85(1-3)*, 239-248.

Powell, R.L., Roberts, D.A., Dennison, P.E., & Hess, L.L. (2007). Sub-pixel mapping of urban land cover using multiple endmember spectral mixture analysis: Manaus, Brazil. *Remote Sensing of Environment, 106*, 253-267.

Pu, R., P. Gong, R. Michishita, and T. Sasagawa. (2008). Spectral mixture analysis for mapping abundance of urban surface components from the Terra/ASTER data.*Remote Sensing of Environment 112 (3)*:939-54.

Qiu, X. Wu, S. and Miao, X. (2014). Incorporating road and parcel data for object-based classification of detailed urban land covers from NAIP images.*GIScience & Remote Sensing 51*, 498-520.

Ramsey, M.S. Christensen, P.R. (1998). Mineral abundance determination: quantitative deconvolution of thermal emission spectra. *Journal of Geophysical Research, Solid Earth 103*, 577-596.

Rashed, T., Weeks, J.R., Gadalla, M.S., & Hill, A.G. (2001). Revealing the Anatomy of Cities through Spectral Mixture Analysis of Multispectral Satellite Imagery: A Case Study of the Greater Cairo Region, Egypt. *Geocarto International, 16*, 7-18.

Rhee, J., Park, S. and Lu, Z. (2014). Relationship between land cover patterns and surface temperature in urban areas.*GIScience & Remote Sensing 51*, 521-536.

Ridd, M.K. (1995). Exploring a V-I-S (Vegetation-Impervious surface-Soil) model for urban ecosystem analysis through remote sensing-comparative anatomy for cities. *International Journal of Remote Sensing, 16*, 2165-2185.

Rivard, B., Feng, J., Gallie, A., & Sanchez-Azofeifa, A. (2008). Continuous wavelets for the improved use of spectral libraries and hyperspectral data. *Remote Sensing of Environment, 112*, 2850-2862.

Roberts, D.A., Dennison, P.E., Gardner, M.E., Hetzel, Y., Ustin, S.L., & Lee, C.T. (2003). Evaluation of the potential of Hyperion for fire danger assessment by comparison to the Airborne Visible/Infrared Imaging Spectrometer. *Ieee Transactions on Geoscience and Remote Sensing, 41*, 1297-1310.

Roberts, D.A., Gardner, M., Church, R., Ustin, S., Scheer, G., & Green, R.O. (1998). Mapping chaparral in the Santa Monica Mountains using multiple endmember spectral mixture models. *Remote Sensing of Environment, 65*, 267-279.

Roessner, S., Segl, K., Heiden, U., & Kaufmann, H. (2001). Automated differentiation of urban surfaces based on airborne hyperspectral imagery. *IEEE Transactions on Geoscience and Remote Sensing, 39*, 1525-1532.

Rogge, D.M., Rivard, B., Zhang, J., Sanchez, A., Harris, J., & Feng, J. (2007). Integration of spatial-spectral information for the improved extraction of endmembers. *Remote Sensing of Environment, 110*, 287-303.

Rosa, D. and Wiesmann, D. (2013). Land cover and impervious surface extraction using parametric and non-parametric algorithms from the open-source software R: an application to sustainable urban planning in Sicily.*GIScience & Remote Sensing 50*, 231-250.

Rosso, P. H., S. L. Ustin, and A. Hastings. (2005). Mapping marshland vegetation of San Francisco Bay, California, using hyperspectral data.*International Journal of Remote Sensing 26* (23):5169-91.

Sabol, D.E., Adams, J.B., and Smith, M.O. (1992). Quantitative subpixel spectral detection of targets in multispectral images. *Journal of Geophysical Research: Planets 97*, 2659-2672.

Samanta, A., S. Ganguly, E. Vermote, R. R. Nemani, and R. B. Myneni. (2012). Interpretation of variations in MODIS-measured greenness levels of Amazon forests during 2000 to 2009.*Environmental Research Letters 7* (2): 024018.

Schaaf, A., Dennison, P., Fryer, G., Roth, K., & Roberts, D. (2011). Mapping Plant Functional Types at Multiple Spatial Resolutions Using Imaging Spectrometer Data. *GIScience & Remote Sensing, 48*, 324-344.

Schueler, T.R. (1994). The importance of imperviousness. *Watershed Protection Techniques, 1*, 100-111.

Sexton, J.O., Song, X.-P., Huang, C., Channan, S., Baker, M.E., & Townshend, J.R. (2013). Urban growth of the Washington, D.C.–Baltimore, MD metropolitan region from 1984 to 2010 by annual, Landsat-based estimates of impervious cover. *Remote Sensing of Environment, 129*, 42-53.

Small, C., (2001). Estimation of urban vegetation abundance by spectral mixture analysis. *International Journal of Remote Sensing 22(7)*, 1305-1334.

Small, C., Lu, J.W., (2006). Estimation and vicarious validation of urban vegetation abundance by spectral mixture analysis. *Remote Sensing of Environment 100*, 441-456.

Smith, M.O., Ustin, S.L., Adams, J.B., Gillespie, A.R., (1990). Vegetation in deserts: I. A regional measure of abundance from multispectral images. *Remote Sensing of Environment 31*, 1-26.

Somers, B., Asner, G.P., Tits, L., & Coppin, P. (2011). Endmember variability in Spectral Mixture Analysis: A review. *Remote Sensing of Environment, 115*, 1603-1616.

Somers, B., Delalieux, S., Stuckens, J., Verstraeten, W.W., Coppin, P., (2009a). A weighted linear spectral mixture analysis approach to address endmember variability in agricultural production systems. *International Journal of Remote Sensing 30(1)*, 139-147.

Somers, B., Delalieux, S., Verstraeten, W.W., Verbesselt, J., Lhermitte, S., Coppin, P., (2009b). Magnitude- and Shape-Related Feature Integration in Hyperspectral Mixture Analysis to Monitor Weeds in Citrus Orchards. *IEEE Transactions on Geoscience and Remote Sensing 47(11)*, 3630-3642.

Somers, B., Verbesselt, J., Ampe, E.M., Sims, N., Verstraeten, W.W., & Coppin, P. (2010). Spectral mixture analysis to monitor defoliation in mixed-aged Eucalyptus globulus Labill plantations in southern Australia using Landsat 5-TM and EO-1 Hyperion data. *International Journal of Applied Earth Observation and Geoinformation, 12*, 270-277.

Song, C.H. (2005). Spectral mixture analysis for subpixel vegetation fractions in the urban environment: How to incorporate endmember variability? *Remote Sensing of Environment, 95*, 248-263.

Stevens, D., S. Dragicevic, and K. Rothley. (2007). City: A GIS-CA modelling tool for urban planning and decision making. Environmental *Modelling & Software 22 (6)*:761-73.

Sung, C.Y., & Li, M.-H. (2012). Considering plant phenology for improving the accuracy of urban impervious surface mapping in a subtropical climate regions. *International Journal of Remote Sensing, 33*, 261-275.

Sunshine, J.M. Pieters, C.M. (1993). Estimating modal abundances from the spectra of natural and laboratory pyroxene mixtures using the modified Gaussian model. *Journal of Geophysical Research, Planets 98*, 9075-9987.

Tompkins, S., Mustard, J.F., Pieters, C.M., Forsyth, D.W., (1997). Optimization of endmembers for spectral mixture analysis. *Remote Sensing of Environment 59*, 472-489.

United Nations (2012). Department of Economic and Social Affairs, Population Division. *World Urbanization Prospects: The 2011 Revision*, CD-ROM Edition.

U.S. Census Bureau. (2014). National Population Projections. http://www.census.gov/population/projections/data/national/

Van Metre, P. C., and B. J. Mahler. (2005). Trends in hydrophobic organic contaminants in urban and reference lake sediments across the United States, 1970-2001. *Environmental Science & Technology 39 (15)*:5567-74.

Vauclin, M., Vieira, S.R., Vachaud, G., and Nielsen, D.R. (1983). The Use of Cokriging with Limited Field Soil Observations.*Soil Science Society of America Journal 47*, 175-184.

Verburg, P.H., van Eck, J.R.R., de Nijs, T.C.M., Dijst, M.J., & Schot, P. (2004). Determinants of land-use change patterns in the Netherlands. *Environment and Planning B-Planning & Design, 31*, 125-150.

Ward, D., Phinn, S.R., & Murray, A.T. (2000). Monitoring growth in rapidly urbanizing areas using remotely sensed data. *Professional Geographer, 52*, 371-386.

Weng, Q. (2012). Remote sensing of impervious surfaces in the urban areas: Requirements, methods, and trends. *Remote Sensing of Environment, 117*, 34-49.

Weng, Q., & Hu, X. (2008). Medium spatial resolution satellite imagery for estimating and mapping urban impervious surfaces using LSMA and ANN. *IEEE Transactions on Geoscience and Remote Sensing, 46*, 2397-2406.

Weng, Q., Hu, X., & Liu, H. (2009). Estimating impervious surfaces using linear spectral mixture analysis with multitemporal ASTER images. *International Journal of Remote Sensing, 30*, 4807-4830.

Weng, Q., Hu, X., & Lu, D. (2008). Extracting impervious surfaces from medium spatial resolution multispectral and hyperspectral imagery: a comparison. *International Journal of Remote Sensing, 29*, 3209-3232.

Weng, Q.H. (2001). Modeling urban growth effects on surface runoff with the integration of remote sensing and GIS. *Environmental Management, 28*, 737-748.

Weng, Q.H. (2007). Remote sensing of impervious surfaces: An overview. In Q.H. Weng (Ed.), *Remote sensing of impervious surfaces* (pp. XV-XXVI). Boca Raton: CRC Press.

Wu, C. (2009). Quantifying high-resolution impervious surfaces using spectral mixture analysis. *International Journal of Remote Sensing, 30*, 2915-2932.

Wu, C., & Murray, A.T. (2005). A cokriging method for estimating population density in urban areas. *Computers, Environment and Urban Systems, 29*, 558-579.

Wu, C., & Yuan, F. (2007). Seasonal sensitivity analysis of impervious surface estimation with satellite imagery. *Photogrammetric Engineering and Remote Sensing, 73*, 1393-1401.

Wu, C.S. (2004). Normalized spectral mixture analysis for monitoring urban composition using ETM plus imagery. *Remote Sensing of Environment, 93*, 480-492.

Wu, C.S., & Murray, A.T. (2003). Estimating impervious surface distribution by spectral mixture analysis. *Remote Sensing of Environment, 84*, 493-505.

Wu, J. (2010). Urban sustainability: an inevitable goal of landscape research. *Landscape Ecology 25 (1)*:1-4.

Wu, J., G. D. Jenerette, A. Buyantuyev, and C. L. Redman. (2011). Quantifying spatiotemporal patterns of urbanization: The case of the two fastest growing metropolitan regions in the United States.*Ecological Complexity* 8 (1):1-8.

Xian, G., & Crane, M. (2005). Assessments of urban growth in the Tampa Bay watershed using remote sensing data. *Remote Sensing of Environment, 97*, 203-215.

Xian, G., & Homer, C. (2010). Updating the 2001 National Land Cover Database Impervious Surface Products to 2006 using Landsat Imagery Change Detection Methods. *Remote Sensing of Environment, 114*, 1676-1686.

Xu, H. (2013). Rule-based impervious surface mapping using high spatial resolution imagery. *International Journal of Remote Sensing, 34*, 27-44.

Yang, F., Matsushita, B., & Fukushima, T. (2010). A pre-screened and normalized multiple endmember spectral mixture analysis for mapping impervious surface area in Lake Kasumigaura Basin, Japan. *Isprs Journal of Photogrammetry and Remote Sensing, 65*, 479-490.

Yang, F., Matsushita, B., Fukushima, T., & Yang, W. (2012). Temporal mixture analysis for estimating impervious surface area from multi-temporal MODIS NDVI data in Japan. *Isprs Journal of Photogrammetry and Remote Sensing, 72*, 90-98.

Yang, L.M., Huang, C.Q., Homer, C.G., Wylie, B.K., & Coan, M.J. (2003a). An approach for mapping large-area impervious surfaces: synergistic use of Landsat-7 ETM+ and high spatial resolution imagery. *Canadian Journal of Remote Sensing, 29*, 230-240.

Yang, L.M., Xian, G., Klaver, J.M., & Deal, B. (2003b). Urban land-cover change detection through sub-pixel imperviousness mapping using remotely sensed data. *Photogrammetric Engineering and Remote Sensing, 69*, 1003-1010.

Yang, L., L. Jiang, H. Lin, and M. Liao. 2009. "Quantifying Sub-pixel Urban Impervious Surface through Fusion of Optical and InSAR Imagery." Giscience & Remote Sensing 46 (2):161-71. doi: 10.2747/1548-1603.46.2.161.

Yang, X., & Liu, Z. (2005). Use of satellite-derived landscape imperviousness index to characterize urban spatial growth. *Computers, Environment and Urban Systems, 29*, 524-540

Yang, X.J. (2006). Estimating landscape imperviousness index from satellite imagery. *Ieee Geoscience and Remote Sensing Letters, 3*, 6-9.

Yu, D., & Wu, C. (2004). Understanding Population Segregation from Landsat ETM+ Imagery: A Geographically Weighted Regression Approach. *GIScience & Remote Sensing, 41*, 187-206.

Yu, D.L., & Wu, C.S. (2006). Incorporating remote sensing information in modeling house values: A regression tree approach. *Photogrammetric Engineering and Remote Sensing, 72*, 129-138.

Yuan, F., & Bauer, M.E. (2007). Comparison of impervious surface area and normalized difference vegetation index as indicators of surface urban heat island effects in Landsat imagery. *Remote Sensing of Environment, 106*, 375-386.

Yuan, F., Bauer, M.E., Heinert, N.J., & Holden, G.R. (2005). Multi-level Land Cover Mapping of the Twin Cities (Minnesota) Metropolitan Area with Multi-seasonal Landsat TM/ETM+ Data. *Geocarto International, 20*, 5-13.

Yuan, F., Wu, C., & Bauer, M.E. (2008). Comparison of spectral analysis techniques for impervious surface estimation using Landsat imagery. *Photogrammetric Engineering and Remote Sensing, 74*, 1045-1055.

Zang, S., C. Wu, H. Liu, and X. Na. (2011). Impact of urbanization on natural ecosystem service values: a comparative study. *Environmental Monitoring and Assessment 179 (1-4)*:575-88.

Zhang, J., Rivard, B., Sanchez-Azofeifa, A., & Castro-Esau, K. (2006). Intra and inter-class spectral variability of tropical tree species at La Selva, Costa Rica: Implications for species identification using HYDICE imagery. *Remote Sensing of Environment, 105*, 129-141.

Zhang, J., He, C., Zhou, Y., Zhu, S., Shuai, G., (2014). Prior-knowledge-based spectral mixture analysis for impervious surface mapping. *International Journal of Applied Earth Observation and Geoinformation 28*, 201-210.

Zhang, J.K., Rivard, B., & Sanchez-Azofeifa, A. (2004). Derivative spectral unmixing of hyperspectral data applied to mixtures of lichen and rock. *IEEE Transactions on Geoscience and Remote Sensing, 42*, 1934-1940.

Zhang, J.K., Rivard, B., & Sanchez-Azofeifa, A. (2005). Spectral unmixing of normalized reflectance data for the deconvolution of lichen and rock mixtures. *Remote Sensing of Environment, 95*, 57-66.

Zhou, L. M., R. E. Dickinson, Y. H. Tian, J. Y. Fang, Q. X. Li, R. K. Kaufmann, C. J. Tucker, and R. B. Myneni. (2004).Evidence for a significant urbanization effect on climate in China.*Proceedings of the National Academy of Sciences of the United States of America* 101 (26):9540-4.

Zortea, M., & Plaza, A. (2009). Spatial Preprocessing for Endmember Extraction. *Ieee Transactions on Geoscience and Remote Sensing, 47*, 2679-2693.

CURRICULUM VITAE

EDUCATION

2016   **Ph.D. Geography, University of Wisconsin-Milwaukee**
Dissertation title: *Large-scale Urban Impervious Surfaces Estimation through Incorporating Temporal and Spatial Information into Spectral Mixture Analysis*
Adviser: Dr. Changshan Wu

2010   **M.S. Physical Geography, Harbin Normal University, China**
Thesis title: *Dynamic Simulation on the Spatial-temporal Patterns of Land Use Change in Hadaqi Industrial Corridor, China*
Advisers: Dr. ShuyingZang and Dr. Lijuan Zhang

2007   **B.S. Geography, Harbin Normal University, China**

PUBLICATIONS

Peer-reviewed journal articles:

2016   **Wenliang Li**, Changshan Wu. A geostatistical temporal mixture analysis approach to address endmember variability for estimating regional impervious surface distributions. *GIScience &Remote Sensing*. 53(1):102-121.

2015   Lijuan Zhang, **Wenliang Li**, Chunyan Jiang, Shuying Zang. Examining the century dynamic change of forest oxygen production in Heilongjiang Province, China. *International Journal of Environmental Science and Technology*.12:4005-4016.

2015   Xiaodong Na, Shuying Zang, Changshan Wu, **Wenliang Li**. Mapping forested wetlands in the Great Zhan River Basin through integrating optical radar and topographical data classification techniques. *Environmental Monitoring and Assessment*. 187:696.

2015   Xiaodong Na, Shuying Zang, Yuhong Zhang, **Wenliang Li**. Assessing breeding habitat suitability for the endangered red-crowned crane (Grus Japonensis) based on multi-source remote sensing data. *Wetlands*. 35(5):955-967.

2015   **Wenliang Li**, Changshan Wu. Incorporating land use land cover probability information into endmember class selections for temporal mixture analysis. *ISPRS Journal of Photogrammetry and Remote Sensing*. 101:163-173.

2014   **Wenliang Li**, Changshan Wu. Phenology-based temporal mixture analysis for estimating large-scale impervious surface distributions. *International Journal of Remote Sensing*.35(2):779-795.

2014   **Wenliang Li**, Changshan Wu, ShuyingZang.Modeling urban land use conversion of Daqing City, China: a comparative analysis of "Top-Down" and "Bottom-Up" Approaches.*Stochastic Environmental Research and Risk Assessment*.28(4):817-828.

2013   **Wenliang Li**, Changshan Wu.A spatially explicit method to examine the impact of urbanization on natural ecosystem service values.*Journal of Spatial Science*. 58(2):275-289.

2009   **Wenliang Li**, Lijuan Zhang, Hong Chen, etal. The Integrated Risk Assessment and zoning of Meteorological Disaster in Heilongjiang Province of China.*Sciences in Cold and Arid Regions*. 1(6):531-540.

PRESENTATIONS

Conference presentations

2016   **Wenliang Li**, Changshan Wu. Geographic information assisted temporal mixture analysis for urban impervious surface estimation. *Annual Meeting of the Association of American Geographers*, San Francisco, CA, March 29 - April2.

2015   **Wenliang Li**, Changshan Wu. A geostatistical temporal mixture analysis approach to address endmember variability for estimating regional impervious surface distributions. *Annual Meeting of the Association of American Geographers*, Chicago, IL, April 21-24.

2014   **Wenliang Li**, Changshan Wu. Incorporating land use land cover probability information into endmember class selections for temporal mixture analysis.*Annual Meeting of the Association of American Geographers*, Tampa, FL, April 8-12.

2013   **Wenliang Li**, Changshan Wu.Incorporating phenological information to large scale impervious surface estimation: a comparative analysis of SMA and MESMA techniques.*Annual Meeting of the Association of American Geographers*, Los Angeles, CA, April 9-13.

2012   **Wenliang Li**, Changshan Wu.Modeling Urban Land Use Conversion of Daqing City, China: A Comparative Analysis of "Top-Down" and "Bottom-Up" Approaches.*Annual Meeting of the Association of American Geographers*, New York, NY, February 24-28.

2011   **Wenliang Li**. Dynamic Simulation on the Spatio-temporal Patterns of Land Use Change in Hadaqi Industrial Corridor. *Annual Meeting of the Association of American Geographers*, Seattle, WA, April 12-16.

Invited presentations

2016   **Wenliang Li.** Analyzing urbanization using remote sensing and GIS techniques. *Department of Atmospheric Science, University of Alabama in Huntsville*, Huntsville, Alabama May 19

2016   **Wenliang Li**. Analyzing urbanization using remote sensing and GIS techniques. *Department of Geography, University of Mary Washington*, Fredericksburg, Virginia, February 18

2015   **Wenliang Li**. Large-scale urban impervious surfaces estimation through incorporating temporal and spatial information into spectral mixture analysis. *Deaprtment of Marine Sciences, Texas A&M University at Galveston*, Texas, February 9.

2014   **Wenliang Li**. Phenology based temporal mixture analysis for estimating large-scale impervious surface distributions. *Key Laboratory of Remote Sensing Monitoring of Geographic Environment, College of Heilongjiang Province, Harbin Normal University*, Harbin, Heilongiang Province, China, May 26.

2014   **Wenliang Li**. Incorporating temporal information into spectral mixture analysis for estimating impervious surface distribution. *GEOG403 Remote sensing: environmental and land use analysis, Department of Geography, UWM*, March 25.

2012   **Wenliang Li**. Modeling the urbanization process of the resource based city: a case study of Daqing city, China. *GEOG247 Quantitative analysis in geography, Department of Geography, UWM*, November 27.

RESEARCH EXPERIENCES

2013-2014 **Research Assistant**, Department of Geography, UWM
Impacts of climatic and land use changes on stream flow and water quality in the Milwaukee River basin, WI Groundwater Coordinating Council, United States Geological Survey, PI: Professor Woonsup Choi, Co-PI: Professor Changshan Wu.

2012-2013 **Research Assistant**, Department of Geography, UWM
Urban impervious surface estimation using remote sensing techniques: a simulation approach, University of Wisconsin-Milwaukee Research Growth Initiative Grant, PI: Professor Changshan Wu.

2007-2010 **Research Assistant**, Department of Geography, Harbin Normal University, China
The process, mechanisms and environmental effects of Land use and land cover change in Hadaqi industrial corridor, China, National Science Foundation of China (No.40771195), PI: Professor Shuying Zang.

RESEARCH GRANT AWARDED

2009-2010 Spatial-temporal dynamic simulation of Hadaqi Industrial Corridor in Heilongjiang Province, China. Graduate Students Innovative Programs Foundation of Heilongjiang Province (YJSCX2009-258HLJ), Department of Education, Heilongjiang Province, China, PI, CNY10000.

TEACHING EXPERIENCES

2015-2016 **Instructor**, Department of Geography, UWM
Fall & Spring: GEOG120: Our Physical Environment

2014-2015 **Instructor**, Department of Geography, UWM
Fall: GEOG625: Intermediate Geographic Information Science
Spring: GEOG403: Remote Sensing: Environmental and Land Use Analysis

2013-2014 **Lab Instructor**, Department of Geography, UWM
Fall:GEOG625: Intermediate Geographic Information Science
Spring:GEOG525: Geographic Information Science

2012-2013   **Lab Instructor**, Department of Geography, UWM
          Fall: GEOG625: Intermediate Geographic Information Science
          Spring: GEOG525: Geographic Information Science

2011-2012   **Lab Instructor**, Department of Geography, UWM
          Fall: GEOG525: Geographic Information Science
                  GEOG547: Spatial Analysis
          Spring: GEOG403: Remote Sensing: Environmental and Land Use Analysis

2010-2011   **Lab Instructor**, Department of Geography, UWM
          Fall: GEOG120: Our Physical Environment
          Spring: GEOG403: Remote Sensing: Environmental and Land Use Analysis

PROFESSIONAL MEMBERSHIPS

2014-Present   American Society for Photogrammetry and Remote Sensing (ASPRS)
2010-Present   Association of American Geographers (AAG)
2010-Present   Student Chapter of ASPRS at UWM
2014-Present   GIS Clubat UWM

HONORS AND AWARDS

2014-2016   Graduate Student Travel Award, Graduate School, UWM
2014   Finalist, Student Honors Paper Competition, Remote Sensing Specialty
             Group, Association of American Geographers
2014   Student Travel Scholarship, Western Great Lakes Region, ASPRS
2013   First Place, Student GIS Project Competition, GIS Council, UWM
2013-2014   Clinton Edwards Grad Research Award, Geography, UWM
2013-2014   Finalist, Chancellor's Golda Meir Library Scholar Award, UWM
2013-2014   Mary Jo Read Fellowship, Department of Geography, UWM
2012-2013   Chancellor's Graduate Student Award, UWM
2010-2016   Mary Jo Read Travel Award, Department of Geography, UWM
2010-2011   Mary Jo Read Dissertation Travel Award, Geography, UWM
2010-2011   Chancellor's Graduate Student Award, UWM
2010   Outstanding Master Thesis Award, Harbin Normal University, China
2010   Distinguished Graduate Students Award, Department of Education,
             Heilongjiang Province, China

PROFESSIONAL SERVICES

Journal article peer reviewer
ISPRS Journal of Photogrammetry and Remote Sensing
GIScience & Remote Sensing
International Journal of Applied Geospatial Research

University-wide services

2015-2016	Secretary of the GIS Club at UWM
2012-2016	President of Student Chapter of ASPRS at UWM
2013-2016	P.A. of Undergraduate Committee, Department of Geography, UWM
2014	Panelist of Graduate Students Professional Workshop-Publication, Department of Geography, UWM
2015	Panelist of Graduate Students Professional Development Workshop-Job Searching, Department of Geography, UWM

Others

2016	Co-organizer of the sessions "Global Urban Observation: Towards Sustainable Cities (III) - Natural and Human Ecosystems" & (IV)-Innovative Methods and Indicators" in *2016 Annual Meeting of Association of AmericanGeographers*, San Francisco, CA, March 29-April 2.
2015	Co-organizer of the session "Global Urban Observation (V): Remote Sensing of Urban and Suburban Environments" in *2015 Annual Meeting of Association of American Geographers*, Chicago, IL, April 21-25.